



# CHALMERS

## Chalmers Publication Library

**Data for Evaluation of Crash Test Dummies and Human Body Models: New and past Post Mortem Human Subject Data from Groupement d'Intérêt Economique de Recherches et Etudes PSA-RENAULT; and Volunteer shoulder range-of-motion and stiffness**

This document has been downloaded from Chalmers Publication Library (CPL). It is the author's version of a work that was accepted for publication in:

**Citation for the published paper:**

Erwan, L. ; Davidsson, J. (2013) "Data for Evaluation of Crash Test Dummies and Human Body Models: New and past Post Mortem Human Subject Data from Groupement d'Intérêt Economique de Recherches et Etudes PSA-RENAULT; and Volunteer shoulder range-of-motion and stiffness".

Downloaded from: <http://publications.lib.chalmers.se/publication/192432>

Notice: Changes introduced as a result of publishing processes such as copy-editing and formatting may not be reflected in this document. For a definitive version of this work, please refer to the published source. Please note that access to the published version might require a subscription.

Chalmers Publication Library (CPL) offers the possibility of retrieving research publications produced at Chalmers University of Technology. It covers all types of publications: articles, dissertations, licentiate theses, masters theses, conference papers, reports etc. Since 2006 it is the official tool for Chalmers official publication statistics. To ensure that Chalmers research results are disseminated as widely as possible, an Open Access Policy has been adopted. The CPL service is administrated and maintained by Chalmers Library.

(article starts on next page)

**EUROPEAN COMMISSION  
DG RTD**

SEVENTH FRAMEWORK PROGRAMME  
THEME 7  
TRANSPORT - SST  
SST.2007.4.1.2: Human physical and behavioral components  
GA No. 218516



**THORAX**  
**Thoracic injury assessment for improved vehicle safety**

<b>Deliverable No.</b>	THORAX D2.2
<b>Deliverable Title</b>	DATA FOR EVALUATION OF CRASH TEST DUMMIES AND HUMAN BODY MODELS - New and past Post Mortem Human Subject data from Groupement d'Intérêt Economique de Recherches et Etudes PSA-RENAULT - Volunteer shoulder range-of-motion and stiffness
<b>Dissemination level</b>	Public
<b>Written By</b>	E Lecuyer (GieRePSA) J Davidsson (Chalmers)
<b>Checked by</b>	
<b>Approved by</b>	
<b>Issue date</b>	2013-04-09

## Executive summary

Vehicle accident related injuries to the thorax have been reduced significantly. However, these injuries are still common and rank second as source of fatalities and serious injuries. In order to develop improved restraints there is a need for improved tools, such as crash test dummies and Human Body Models (HBM). These models should, when used to study vehicle crash performance, preferably interact with the restraints and respond as would a human. For assessment of their performance and for the development of injury risk functions there is a need for additional biofidelity data. In this report two types of data are made available: Part A - post mortem human subject exposed to various restraints in simulated frontal collisions; Part B – volunteer shoulder range-of-motion for improved shoulder design of future crash test dummies and human body models.

### **Part A - New and past Post Mortem Human Subject Data from Groupement d'Intérêt Economique de Recherches et Etudes PSA-RENAULT for the THORAX project**

Test series LAB-2002:

Load-limiting belt restraints have been present in French cars since 1995. An accident study showed the greater effectiveness in thorax injury prevention using a 4 kN load limiter belt with an airbag than using a 6 kN load limiter belt without airbag.

To improve the understanding of thoracic tolerance, frontal sled crashes were performed using PMHS. Restraint conditions evaluated are 6 kN load-limiting belt and 4 kN load-limiting belt with an airbag. Loads between the occupant and the sled environment were recorded. Various measurements characterize the PMHS behaviour and injuries were noted.

This study presents results that can be used to evaluate the ability of a crash test dummy to discriminate both restraint types and dummy measurement ability to be representative of thoracic injury risk for all restraint types.

Test series LAB-2005:

Many studies have reported multiple rib fractures sustained by an Out-of-Position (OOP) driver subjected to a frontal airbag deployment. Until this study was carried out in 2005 the injury mechanisms and thresholds remained unclear. Two successive phases occur during the bag deployment: punch-out loading of the thorax, followed by a membrane effect. The aim of this study was to investigate the thoracic injuries generated by each phase separately.

Tests of nine post-mortem human surrogates were carried out on a static test bench using a driver side airbag module. The steering wheel was replaced by a plate in order to increase the loading generated by the airbag. Three loading configurations were performed: membrane only, punch-out only, and both types combined. The membrane-only tests were performed with the thorax initially positioned at 13, 78 and 128 mm from the plate in order to vary the load magnitude. The punch-out and the combined tests were performed with the thorax initially 8 mm from the module. Accelerometers and angular rate sensors were fixed on the sternum and on the first, fourth, and eighth thoracic vertebrae of the PMHS. Ribs 2 to 6 were instrumented with strain gauges. The reaction force of the bag on the plate was measured using four 2-axis load cells.

Results showed that both pure punch-out and pure membrane loading can result in thoracic injuries. However, the rib fracture locations seemed to differ from one type of

loading to the other. Moreover, for the same initial distance between the airbag module and the thorax, the injuries were more severe in the combined effect tests than in the pure punch-out or pure membrane. This report makes this data available for injury risk construction and for assessment of future injury mechanisms.

#### Test series LAB-2008:

In 2008 the behaviour of the rib cage during frontal loading was not well documented. Rib strains during a crash remained unknown. In order to address this issue, a test protocol was developed, where the ribs of 8 PMHS were equipped with up to 96 strain gauges. In a first series of 3 tests, the subjects were seated upright and their chests were loaded by a 23.4 kg impactor propelled at 4.3 m/s in pure frontal, oblique and pure lateral directions. In a second series of 3 tests, the subjects were loaded by the deployment of an unfolded airbag in the same 3 directions. This report presents the detailed results of these tests. The data can be used for injury risk developments and for assessing the performance of the ribcage.

## **Part B - Volunteer shoulder range-of-motion and stiffness – Data for evaluation of crash test dummies and human body models**

Until recently the shoulder complex has received rather low priority in the development of frontal impact crash test dummies and HBM. The shoulder complex, including the shoulder girdle and the clavicle, is rarely exposed to injuries in life-threatening frontal and oblique frontal collisions, but influence the belt interaction and as such the thorax compression and head kinematics. Therefore, the purpose of this study was to establish response requirements for the shoulder complex in terms of range-of-motion and stiffness.

Six male volunteers of average size were seated in a rigid seat that simulated a car driver's posture whilst in a special designed test rig. Loads to the shoulders were applied through the arms, by means of brackets fastened to the elbows, loads rearward were applied by means of a strap around the shoulder complex. Torso movement was blocked by two pre-tensed diagonal belts that were routed close to the neck to avoid excessive clavicle interaction. Both shoulders were statically loaded with increasing load from 0–200 N/shoulder at 50 N increments. A test series included four load series: shoulders pulled straight forward, forward-upward, upward and rearward. Throughout the tests the arms were resting on supports adjusted to match these loading conditions. Each volunteer was exposed to three tests for assessment of repeatability and habituation.

Shoulder positions relative to the spine were obtained from film analysis of images captured with three cameras: from above, right and left hand sides. Photo markers were mounted on the volunteer's skin: head, posterior tip of acromion process, chest, T1 and T4. The right and left acromion relative to T1 displacements were used to calculate the shoulder range-of-motion in three directions. Belt loads and seat back loads were recorded.

Average resultant volunteers' acromion relative to T1 range-of-motion, at the maximum load, was 55 mm for forward loads, 69 mm for forward-upward loads, 73 mm for upward loads and 50 mm for rearward loads (200 N/shoulder, 18 tests for each average). The volunteers provided measurements with reasonable repeatability; pooled CV for maximum resultant acromion relative to T1 range-of-motion varied from 6 to 13%.

The volunteers curved their spines only slightly when shoulder loads were applied. Hence, shoulder complex motion was successfully isolated and results reflect pure

shoulder relative to chest motions. As such the data is suitable for dummy and HBM evaluations. The results could to some degree be a function of preferred initial shoulder position in each loading condition. However, the preferred initial starting position of the acromion process varied only slightly between the four load conditions and was compensated for in eth data analysis.

The applied loads were lower than those commonly seen in frontal crashes, however the shoulder is highly mobile and its response to loads is largely dependent on muscle characteristics. As such studies using volunteers may be complimentary to tests with post mortem human subjects.

## Contents

<b>Executive summary</b> .....	<b>2</b>
<b>Contents</b> .....	<b>5</b>
<b>1 Introduction</b> .....	<b>7</b>
1.1 Background.....	7
<b>2 Aims</b> .....	<b>8</b>
<b>3 Thorax Test: LAB-2002</b> .....	<b>9</b>
3.1 Context of the study .....	9
3.2 Test set-up.....	9
3.3 Test Matrix .....	9
3.4 PMHS anthropometry.....	9
3.5 Results.....	11
3.5.1 Time history response.....	11
3.5.2 Injury details of the LAB 2001 surrogates.....	14
<b>4 Thorax Test: LAB-2005</b> .....	<b>17</b>
4.1 Context of the study .....	17
4.2 Test set-up.....	17
4.3 Test Matrix .....	17
4.4 PMHS anthropometry.....	18
4.5 Results.....	19
4.5.1 Membrane configuration .....	19
4.5.2 Punch out and combined configuration .....	26
4.5.3 Injury details for LAB 2005 surrogates.....	32
<b>5 Thorax Test: LAB-2008</b> .....	<b>36</b>
5.1 Context of the study .....	36
5.2 Test set-up.....	36
5.3 Test Matrix .....	37
5.4 PMHS anthropometry.....	37
5.5 Results.....	38
5.5.1 Data processing .....	38
5.5.2 Impactor test results.....	43
5.5.3 Conclusions on impactor loading.....	50
5.5.4 Airbag test results .....	50
5.5.5 Conclusions on airbag loading .....	59
5.5.6 Belt test results .....	60
5.5.7 Conclusions on belt loading .....	65
5.5.8 Harness test results .....	66
5.5.9 Conclusions on harness loading.....	73
<b>6 LAB references</b> .....	<b>74</b>

<b>7</b>	<b>Appendices.....</b>	<b>75</b>
7.1	Appendix: LAB data file organization.....	75
7.2	Appendix: LAB setup and sensor drawings .....	76
<b>1</b>	<b>Introduction .....</b>	<b>78</b>
1.1	Background.....	78
1.1	Belt to shoulder interaction – Implications for dummy shoulder design.....	78
1.2	Belt-to-clavicle interaction – Implications on dummy design .....	79
1.3	Need for shoulder response data for evaluation of models of humans .....	79
<b>2</b>	<b>Aims .....</b>	<b>81</b>
<b>3</b>	<b>Method .....</b>	<b>82</b>
3.1	Test rig.....	82
3.2	Instrumentation .....	86
3.3	Volunteers.....	88
3.4	Test procedure.....	88
3.5	Data processing .....	88
<b>4</b>	<b>Results .....</b>	<b>90</b>
4.1	Belt and seat back loads and directions of the applied shoulder loads .....	90
4.2	Shift of torso angle .....	92
4.3	Shift in position of the acromion at zero shoulder load .....	92
4.4	Range-of-motion .....	93
4.5	Stiffness .....	96
4.6	Repeatability .....	96
<b>5</b>	<b>Discussion.....</b>	<b>99</b>
5.1	Range-of-motion .....	99
5.2	Isolation of volunteer shoulder complex responses .....	99
5.3	Usefulness of the data provided .....	99
5.4	Stiffness .....	99
5.5	Repeatability .....	100
5.6	Sources of error .....	100
<b>6</b>	<b>Conclusions .....</b>	<b>101</b>
6.1	Range-of-motion .....	101
6.2	Repeatability .....	101
6.3	Stiffness .....	101
<b>7</b>	<b>References.....</b>	<b>102</b>

## Part A

### 1 Introduction

#### 1.1 Background

It has been shown, by analysing accident data, that the probability of thoracic injury with a 4 kN load limiting belt and air bag was lower compared with a 6 kN load limiting belt without air bag. This observation can be used as the basis for evaluating the appropriateness of dummy thoracic criteria. The risks associated to both restraint types must be differentiated by the criteria, as they are on the road. In order to study this further, sled tests were performed with Post Mortem Human Subject (Test: LAB-2002), with the two restraint systems and a representative crash pulse. The appropriateness of the laboratory reconstruction was evaluated by comparing PMHS injuries to those observed in accident studies. The PMHS data can be used to assess biofidelity of crash test dummies, the developed laboratory test can be used to assess potential injury criterion and for development of injury risk functions.

The use of airbags in automobiles has improved occupant protection in many collisions. Nevertheless, fatal thoracic injuries due to airbag loading in Out-of- Position (OOP) situations have been observed. It has been identified that two thoracic loading phases during an OOP airbag deployment, either of which may cause injury: first, the punch-out effect and second, the membrane effect. The punch-out effect can be related to both the high-speed impact of the fabric onto the thorax, and to the contact force on the thorax resulting from the gas pressure in the partially folded bag. The punch-out effect generates a concentrated and brief thoracic load with a high rate. The membrane effect occurs later in the loading process when the bag is unfolded. A large airbag surface loads the thorax while the inflator continues to produce gas. This phenomenon results in a distributed and relatively long-duration thoracic load with a lower rate.

The literature clearly shows that either phase has the potential to generate thoracic injuries. However, the relative importance of the two phases and the cumulative effect of the two successive loading phases were not investigated. Thorax Test: LAB-2005 was designed to investigate the thoracic injury potential of punch-out and membrane loading singly and in combination by conducting a series of well-defined OOP PMHS tests. The purpose was also to establish validation data for finite element human models and dummies. The validation of such models would allow for further analysis of thoracic injury mechanism and thresholds in the OOP airbag loading environment. For that purpose, nine PMHS were tested under OOP conditions. Three different airbag deployments were performed: punch-out only, membrane only, and a combined condition that involved a membrane loading phase following punch-out.

Rib fractures are the most frequent types of AIS3+ chest injuries, followed by injuries to the organs with the ribcage. They have been addressed by several injury criteria like the thoracic acceleration, the average spine acceleration, the deflection, the combined thoracic criterion CTI or the compression. However, these criteria have, when applied to a Hybrid III crash test dummy, limited ability to differentiate between restraints with documented differences in real life accident performance. In Thorax Test: LAB-2008 study it was decided to measure directly the strains of the ribs in multiple locations in order to understand the rib cage patterns of deformation and the rib fracture sequence as a function of the loading configuration and time.

## 2 Aims

The purpose of this study was twofold:

To establish new post mortem human subject data for studied of rib strain pattern when subjected to frontal impact loadings; airbag, impactor, diagonal belt and harness.

To post process and make past post mortem human subject test data form two test series available for crash test dummy and human body model evaluations. First a series designed to enable an evaluation of dummies ability to discriminate between restraints. Second a series of tests designed to study effect of airbag-to-ribcage interaction when the subject was positioned at close to the airbag at the time of deployment; membrane only, punch-out only, and both types combined.

### 3 Thorax Test: LAB-2002

#### 3.1 Context of the study

Thorax test LAB-2002 is based on the data of Petitjean et al 2002 where frontal sled crashed was performed with Hybrid III, THOR and four PMHS (ref 1).

Two configuration were tested:

- 6 kN load-limiting belt without airbag
- 4 kN load-limiting belt with airbag

The purpose of the study was to evaluate dummies ability to discriminate both restraint types.

Reference: *Laboratory Reconstructions of Real World Frontal Crash Configurations using the Hybrid III and THOR Dummies and PMHS — Stapp 2002 — Audrey Petitjean, Matthieu Lebarbe, Pascal Potier, Xavier Trosseille*

#### 3.2 Test set-up

The test configuration is representative of a real-world car crash event: deceleration pulse, type of restraint, and environment geometry.

The restraint system involves seat, belt with pretensioning devices, steering wheel with airbag and knee bolsters.

PMHS tests with the 6 kN load limiting belt were performed without the steering wheel to avoid any thoracic contact.

#### 3.3 Test Matrix

For each configuration, two PMHS were tested.

To facilitate the description of the tests and the reading of the tables, each PMHS number is attached to a test code that indicates the configuration.

For example SL4\_1 stands for (4kN limiter + airbag ) , first PMHS tested.

**Table 1 Test matrix**

Loading type	Test code	PMHS number	LAB reference
4 kN + AB	SL4_1	536	UTA01272C05C
	SL4_2	542	UTA01740C22c
6 kN	SL6_1	539	UTA04446C17C
	SL6_2	543	UTA01740C23c

#### 3.4 PMHS anthropometry

Main anthropometry and characteristics of the subjects are summarized in the following table.

**Table 2 PMHS main characteristics**

	SL4_1	SL4_2	SL6_1	SL6_2
--	-------	-------	-------	-------

PMHS code	536	542	539	543
Sex	F	M	M	M
Age (year)	78	76	81	75
Mass (kg)	70	67	60	70
Height (cm)	169	174	172	169
Chest height (cm)	87	92	86	69
Tight length (cm)	50	45	48	43

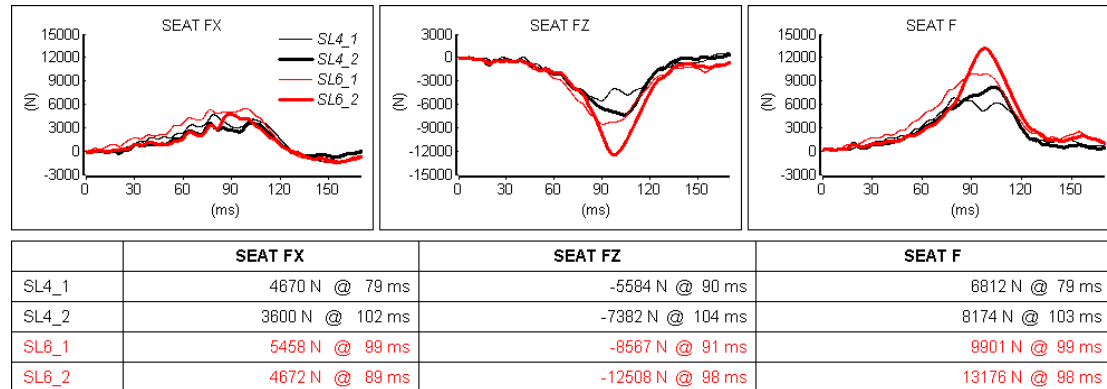
### 3.5 Results

#### 3.5.1 Time history response

The dispersion in PMHS positioning and morphological characteristics generated response corridors that are relatively wide. Thus, PMHS results were presented individually in order to better appreciate the behavior of each subject.

Red curves correspond to 4kN with airbag configuration while black ones represent the 6kN configuration.

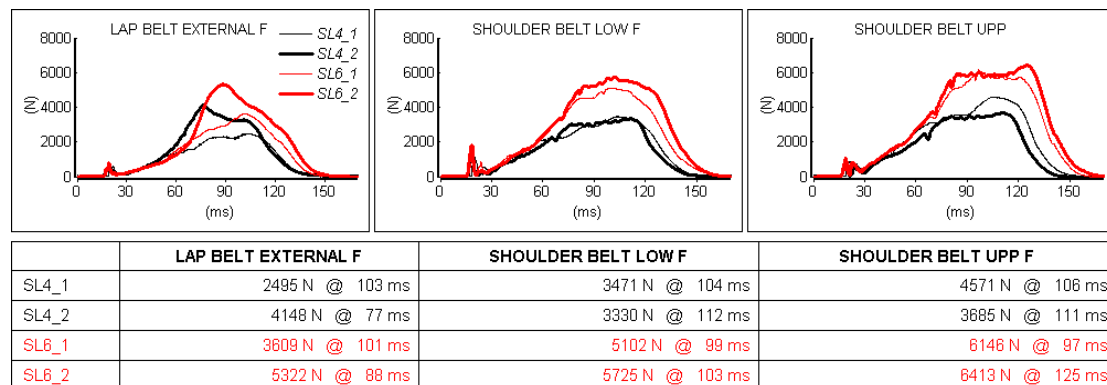
**Table 3 Seat contact forces**



Seat forces:

- CFC 60 filtered and the initial offset was removed
- inertially compensated with a mass of 15kg
- projected in the sled referential (seat sensor were oriented at 4degrees wrt to the sled)

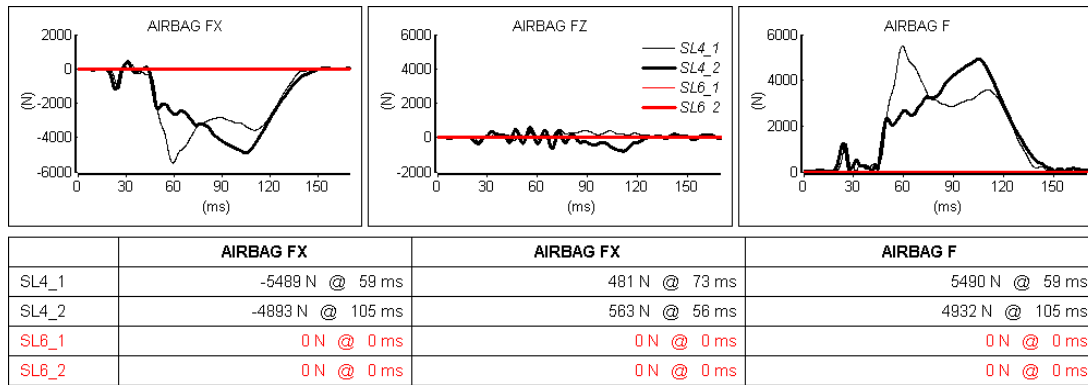
**Table 4 Belt forces**



Belt forces

- CFC 1000 filtered and the initial offset was removed

**Table 5 Airbag contact forces**

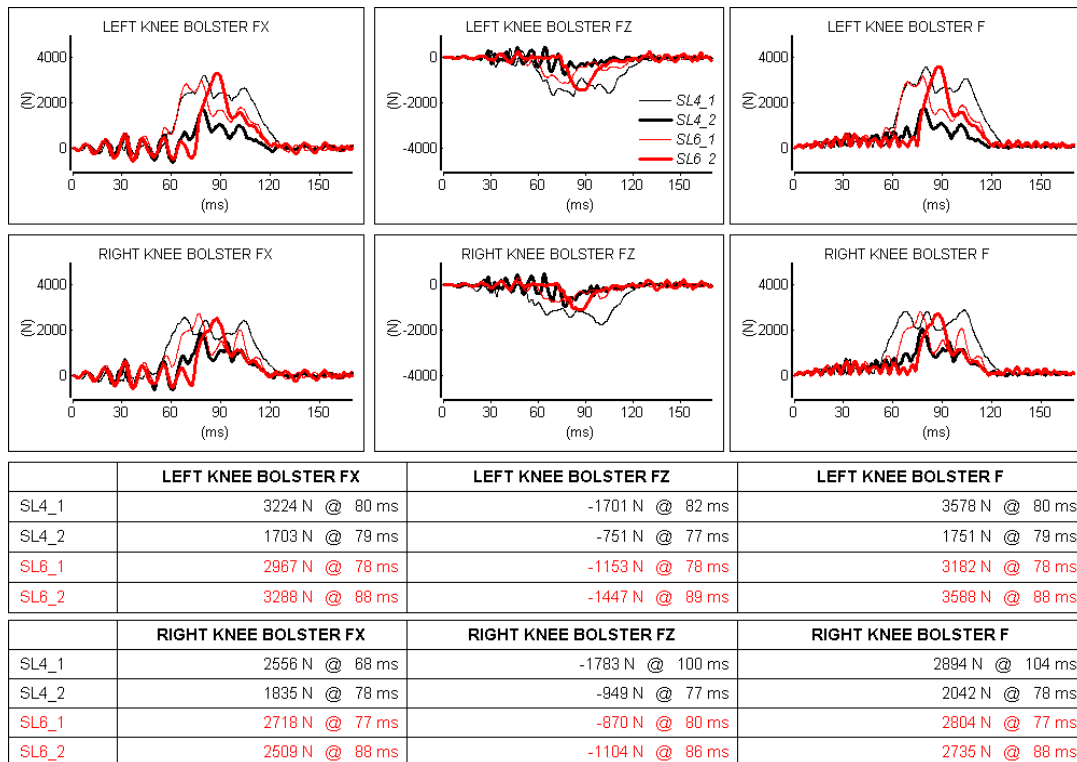


Airbag forces:

- CFC 60 filtered and the initial offset was removed
- Inertia compensated with a mass of 2.6kg
- Projected in the sled referential (the airbag sensor were oriented at 26.5 degrees wrt to the sled)

The airbag was used only for the test SL4\_1 and SL4\_2.

**Table 6 Knee bolster contact forces**

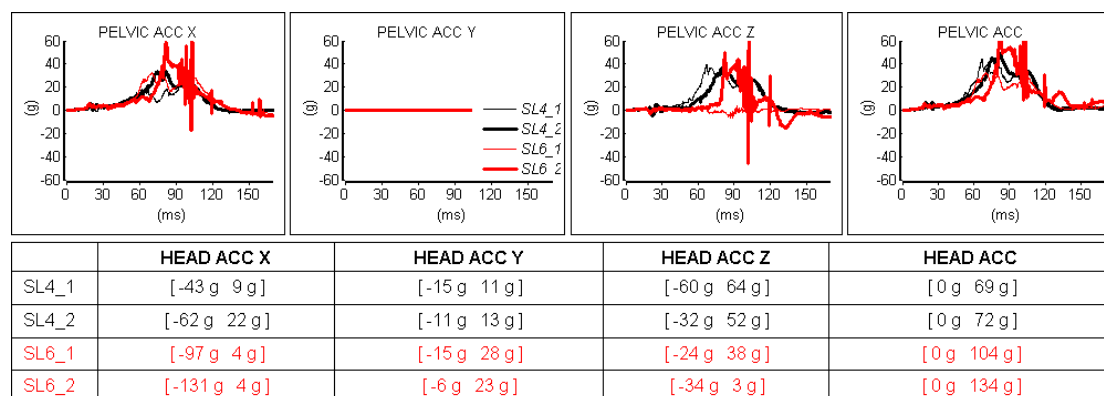


Knee bolster forces:

- CFC180 filtered and the initial offset was removed
- Inertia compensated with a mass of 2.2kg
- Projected in the sled referential (the padding sensor were oriented at -22 degrees wrt to the sled).

Knee time contact is influenced by the surrogate anthropometry and positioning.

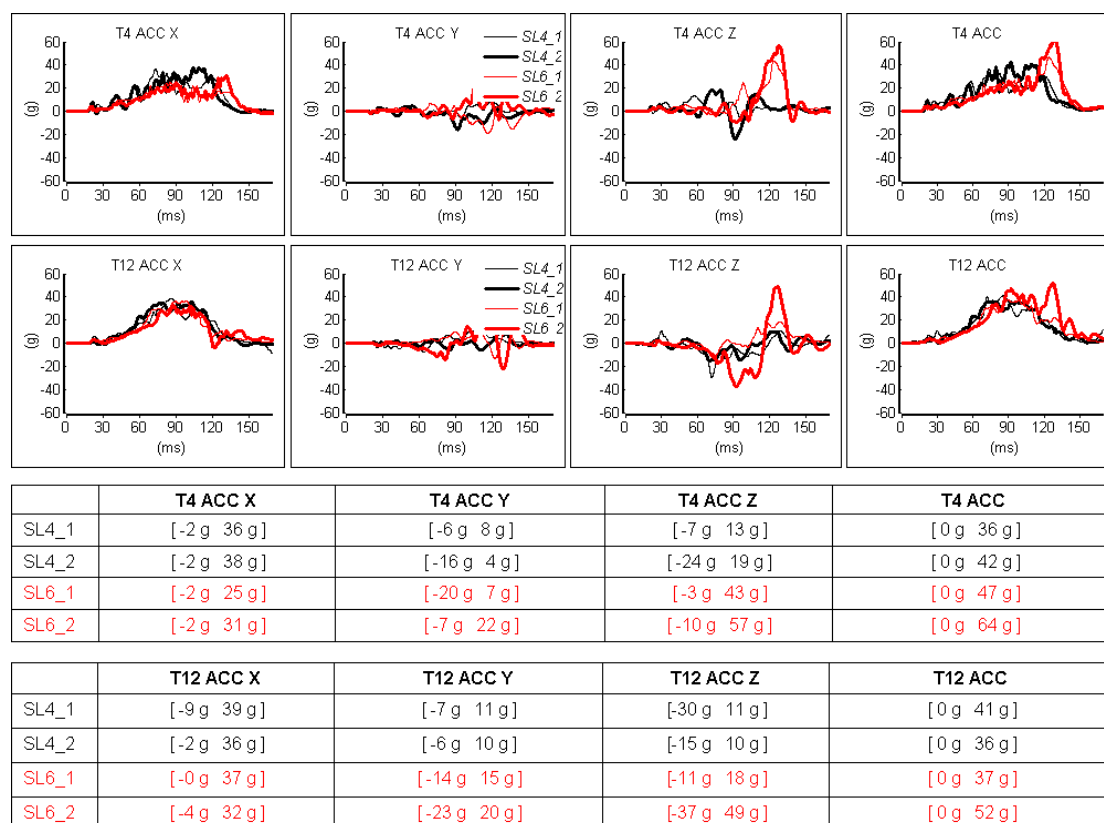
**Table 7 Sacrum acceleration**



Sacrum accelerations:

- CFC 1000 filtered and the initial offset was removed
- expressed in local sensor frame
- Y component was not measured
- sensor location and orientation are comparable in PMHS and H3

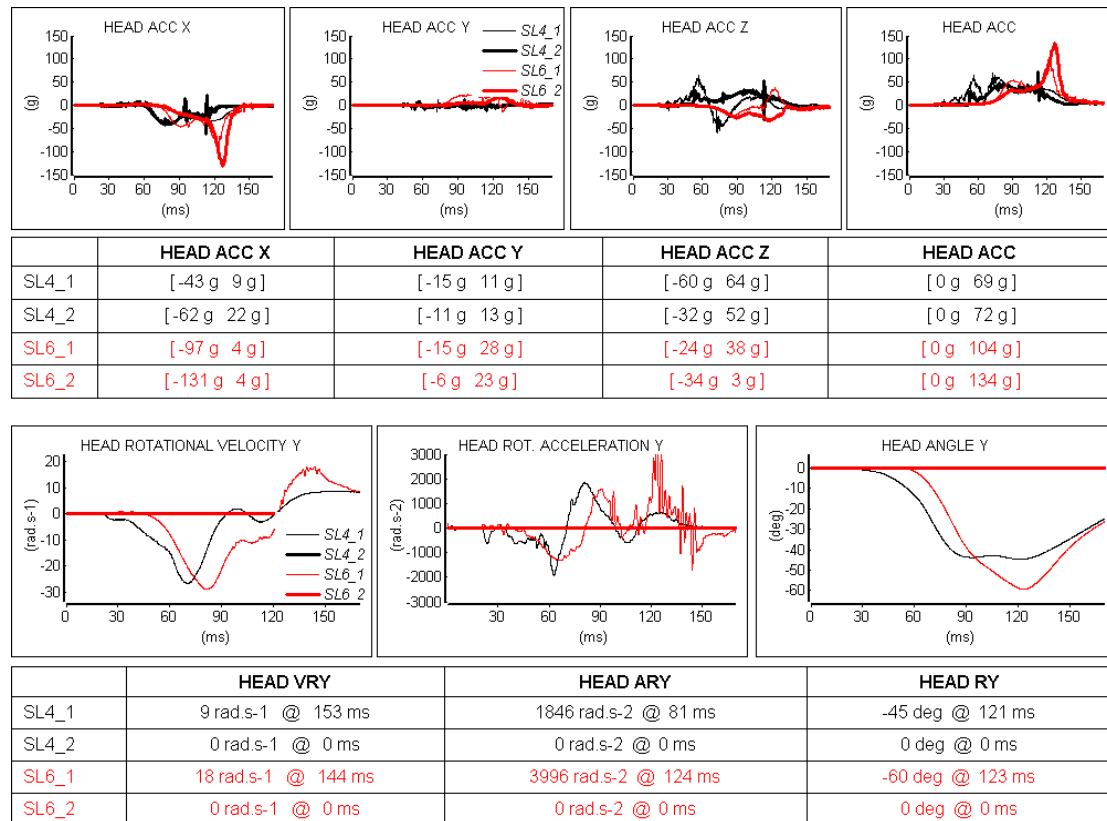
**Table 8 Spine acceleration**



Spine accelerations:

- CFC180 filtered and the initial offset was removed
- expressed in the sensor local frame

**Table 9 Head acceleration**



Head linear accelerations:

- CFC 1000 filtered and the initial offset was removed
- Expressed in local sensor frame.
- Note that the sensor is not located at head CG

Head angular velocity Y:

- CFC 1000 filtered and the initial offset is removed
- The sensor didn't work properly for SL4\_2 and SL6\_2

### 3.5.2 Injury details of the LAB 2001 surrogates

Soft tissue injuries:

For SL6\_1 the right lung was found to be crushed. The subject also sustained an abrasion of the splenic capsule along the posterior side.

No other soft tissue injury were found on the other pmhs

Rib Fracture injury

In contrast to the published stapp paper (reference 1) the cartilage fracture are not considered.

The following table presents the rib fracture detail and AIS figures. Note that AIS outcome takes into account soft tissue injury.

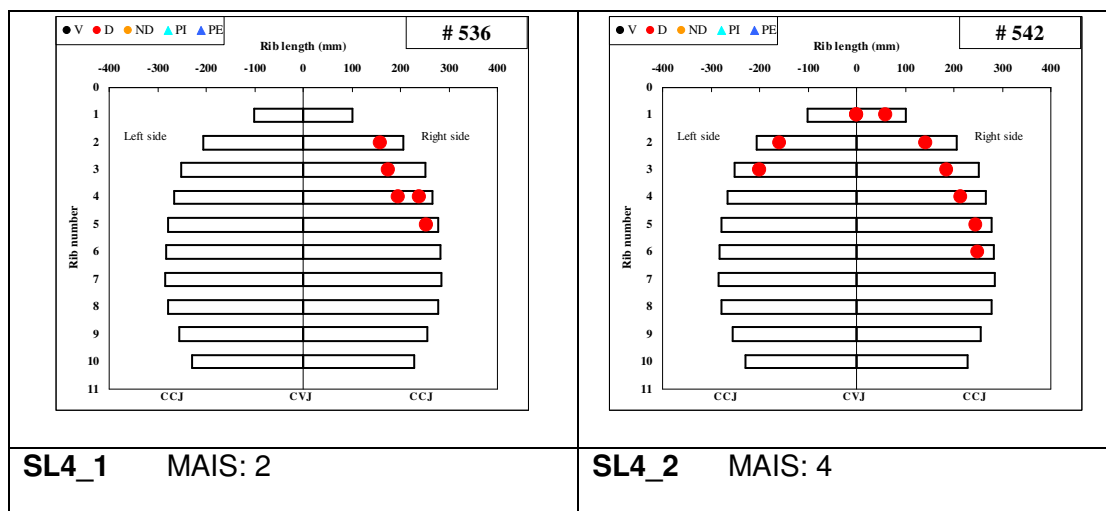
**Table 10 Rib fracture detail**

Test reference	SL4_1	SL4_2	SL6_1	SL6_2
PMHS code	536	542	539	543
MAIS	2	4	5	4
Total number of rib fractures	5	9	14	9
Nb of separated rib fractures	5	9	14	8
Total number of sternum fractures	0	1	4	2

The rib fractures localizations are shown below and a description of the symbols used is given in the following table.

Skeletal thoracic AIS (STAIS) and total rib fracture number are reminded for each test.

●	complete with displacement (D)
●	complete without displacement (ND)
▲	partial with rupture of the external cortical bone (PE)
▲	partial with rupture of the internal cortical bone (PI)
●	vertebral (V)



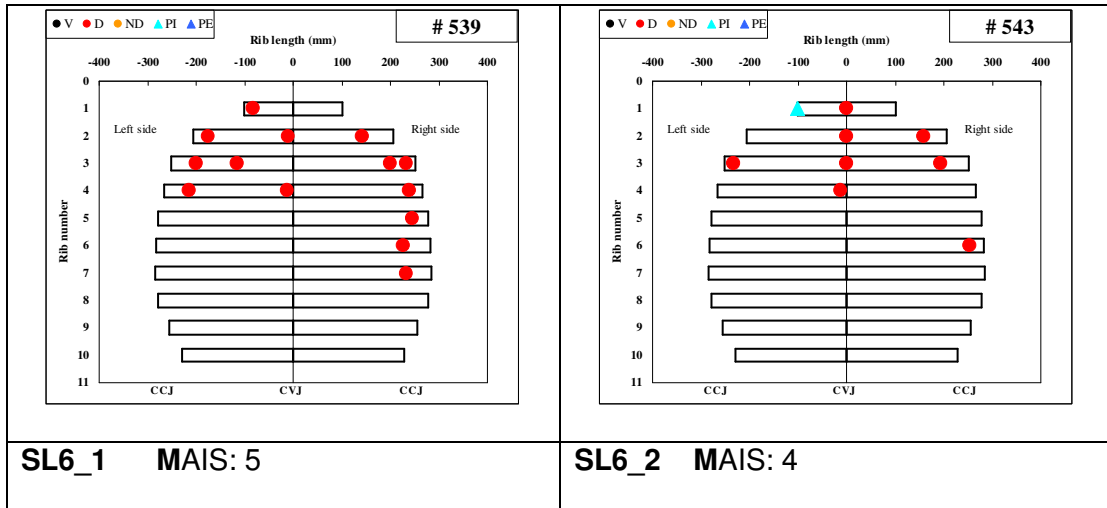


**Figure 1 Rib fracture schematic localization**

## 4 Thorax Test: LAB-2005

### 4.1 Context of the study

Thorax test LAB-2005 is based on the data of Lebarbé et al where subjects are submitted to a frontal airbag deployment in out of position configuration.

Two successive phases occur during the bag deployment: punch-out loading of the thorax, followed by a membrane effect (Horsch et al. 1990). The aim of this study was to investigate the thoracic injuries generated by each phase separately.

Tests of nine PMHS were carried out on a static test bench using a driver airbag module described by Petit et al. (2003). Three loading configurations were performed: membrane only, punch-out only, and both types combined.

Reference: *Thoracic Injury Investigation using PMHS in Frontal Airbag Out-of-Position Situations – Stapp 2005* – Matthieu Lebarbé, Pascal Potier and Pascal Baudrit.

### 4.2 Test set-up

The steering wheel was replaced by a plate in order to increase the loading generated by the airbag.

The pelvis was firmly attached to a rigid seat. The only unconstrained degree of freedom for the rigid seat during the test was the Y-axis rotation.

For the membrane-only tests, the entire cover of the module was removed and the fabric was totally unfolded out of the module.

For the punch-out-only tests, large vent holes were such that they opened after the punch-out had occurred and prior to the membrane loading phase. The size of the vent holes was chosen such that once they were opened the pressure in the bag remained low and the bag could not load the thorax significantly.

The sternum was positioned so that the sternum plane was parallel to the rigid plate; the center of the sternum body was aligned with the center of the airbag module in the  $Y_P-Z_P$  plane; the distance between the sternum and the plate was in agreement with the test matrix; the plane of the sternum was the most anterior part of the trunk with respect to the  $Y_P-Z_P$  plane. For that purpose, the rigid seat was tilted so that the abdomen remained behind the plane of the sternum.

**Table 11 Airbag characteristics**

Peak pressure*	kPa	225
Peak pressure onset rate*	kPa/ms	7
Volume of the bag	liter	45
Diameter of the vent hole	mm	38
Venting pressure	bars	0.45
Radius of the bag	mm	357

\*60 liter tank test

### 4.3 Test Matrix

The membrane-only tests were performed with the thorax initially positioned at 13, 78 and 128 mm from the plate in order to vary the load magnitude. The punch-out and the combined tests were performed with the thorax initially 8 mm from the module. The characteristics of the driver airbag module are given in table 8.

To facilitate the description of the tests and the reading of the tables, each PMHS number is attached to a test code that indicates the configuration. For instance M13\_1 stands for membrane-only loading on the thorax initially positioned 13 mm from the plate, first PMHS tested.

**Table 12 Test matrix**

Test code	Loading type	Thorax-plate distance	Thorax-module distance	PMHS number	LAB reference
M13_1	Membrane	13	/	554	PCH1597
M13_2	Membrane	13	/	555	PCH1598
M78_1	Membrane	78	/	559	PCH1624
M78_2	Membrane	78	/	561	PCH1658
M128_1	Membrane	128	/	560	PCH1625
P52_1	Punch-Out	52	8	557	PCH1622
P52_2	Punch-Out	52	8	558	PCH1623
C52_1	Combined	52	8	562	PCH1667
C52_2	Combined	52	8	565	PCH1722

#### 4.4 PMHS anthropometry

**Table 13 PMHS main characteristics and anthropometry**

PMHS code	Sex	Age	Height (m)	Total weight (kg)	Weight before test (kg)**	Thorax depth* (m)	Thorax width** (m)	Torso height*** (m)	Thorax circumference* (m)
M13_1	M	76	1.70	77	63.8	0.235	0.33	0.67	0.96
M13_2	M	67	1.75	65	51.5	0.22	0.325	0.64	0.94
M78_1	M	73	1.74	67	53.5	0.205	0.305	0.67	0.90
M78_2	M	72	1.73	83	69.5	0.235	0.33	0.695	0.99
M128_1	F	74	1.60	73	55.2	0.195	0.29	0.63	0.85
P52_1	M	79	1.66	70	56.5	0.19	0.33	0.65	0.93
P52_2	F	80	1.58	64	55	0.20	0.30	0.595	0.88
C52_1	M	80	1.67	62	50	0.20	0.32	0.66	0.915
C52_2	M	72	1.70	60	48.1	0.225	0.31	0.615	0.935
<b>Mean values</b>	/	<b>74.8</b>	<b>1.68</b>	<b>69</b>	<b>55.4</b>	<b>0.212</b>	<b>0.316</b>	<b>0.647</b>	<b>0.922</b>

\* Without legs

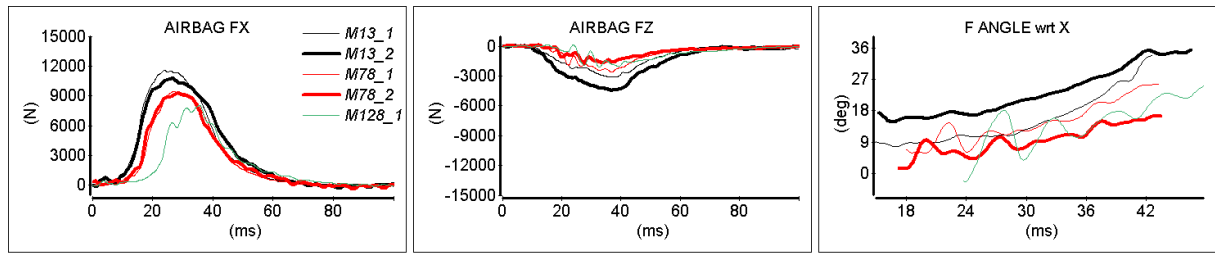
\*\* At the level of the xyphoid process

\*\*\* From the seat to the top of the shoulder

## 4.5 Results

### 4.5.1 Membrane configuration

**Table 14 Airbag forces in membrane configuration: Fx / Fz balance**



	AIRBAG FX	AIRBAG FZ	F ANGLE wrt X [min mean max]
M13_1	11561 N @ 24 ms	-3081 N @ 36 ms	[ 8 15 34 ]
M13_2	10793 N @ 27 ms	-4446 N @ 37 ms	[ 15 23 36 ]
M78_1	9435 N @ 27 ms	-2596 N @ 37 ms	[ 6 15 26 ]
M78_2	9258 N @ 28 ms	-1685 N @ 27 ms	[ 1 10 17 ]
M128_1	8044 N @ 36 ms	-2093 N @ 33 ms	[ -2 15 25 ]

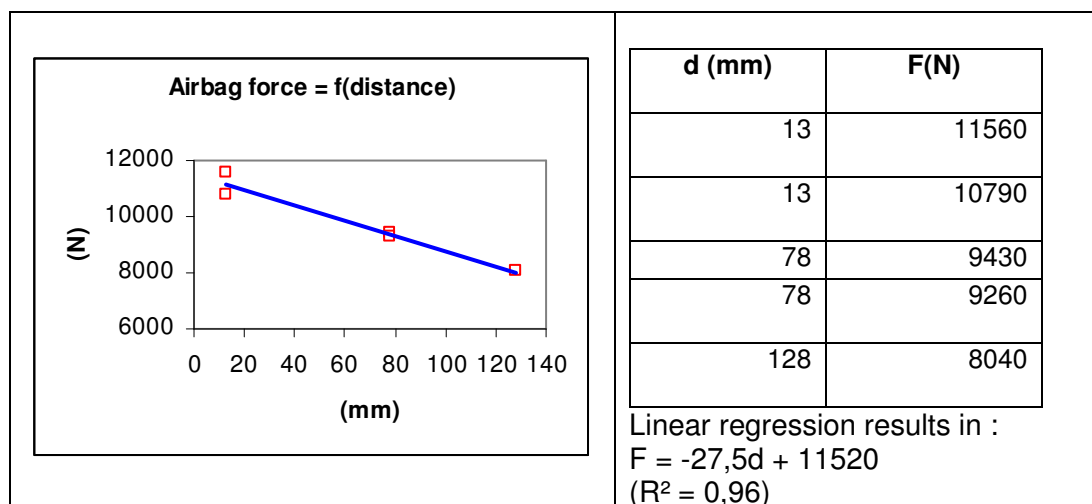
Airbag forces:

- CFC 180 filtered and the initial offset is removed
- Expressed in the airbag plate frame

For a given distance, airbag forces responses are very similar.

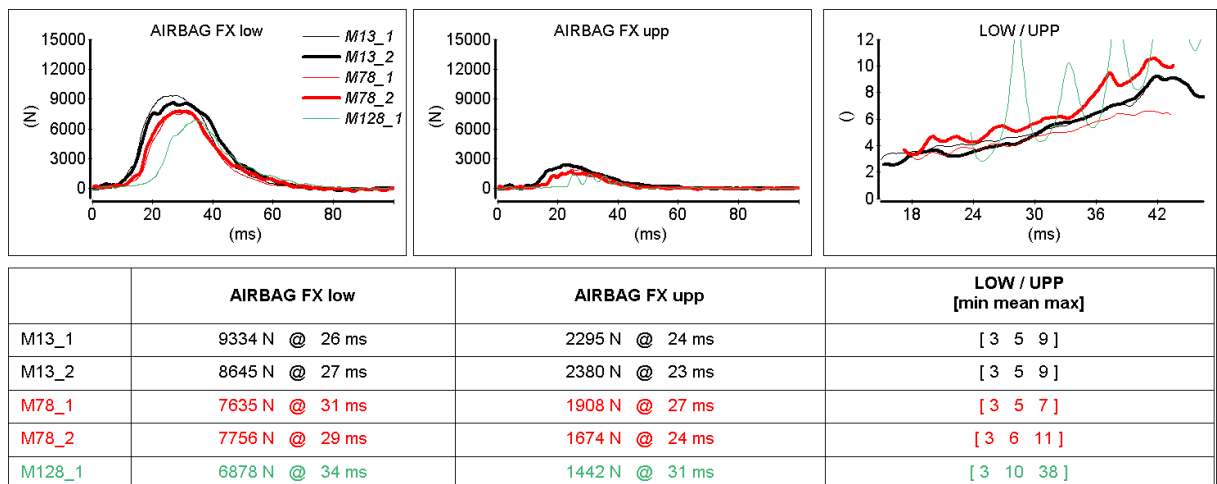
The airbag mainly acts in X-plate direction. A few part of the airbag force is applied in Z-plate direction due to contact with the upper part of the tights. This contact also leads to negative seat angular velocity for the closest test (M13).

**Table 15 Airbag forces in membrane configuration: distance effect**



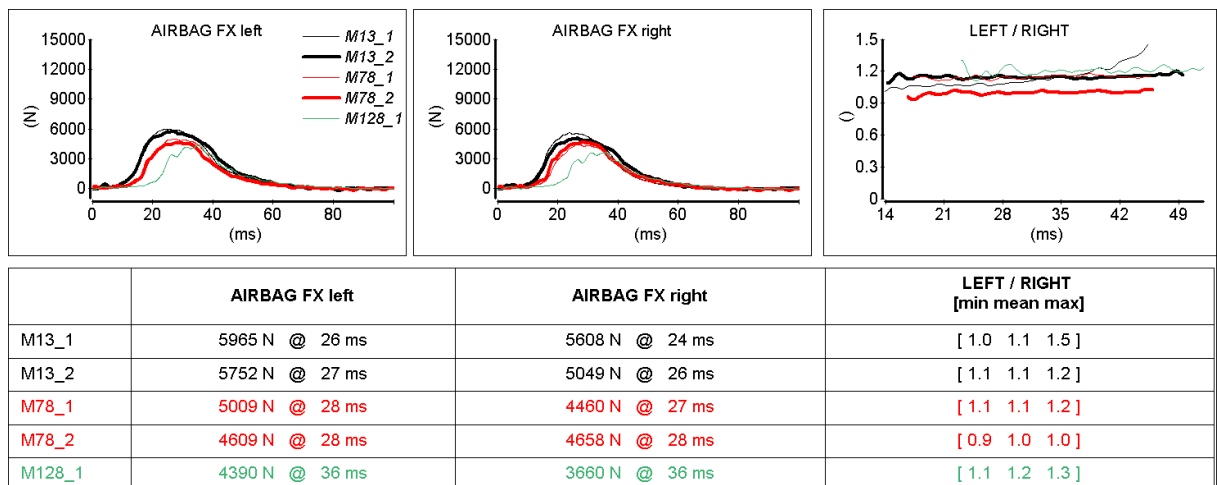
The maximum load value shows little dependency to the mass of the subject but decreased as the distance increased.

**Table 16 Airbag forces in membrane configuration: upp / low balance**



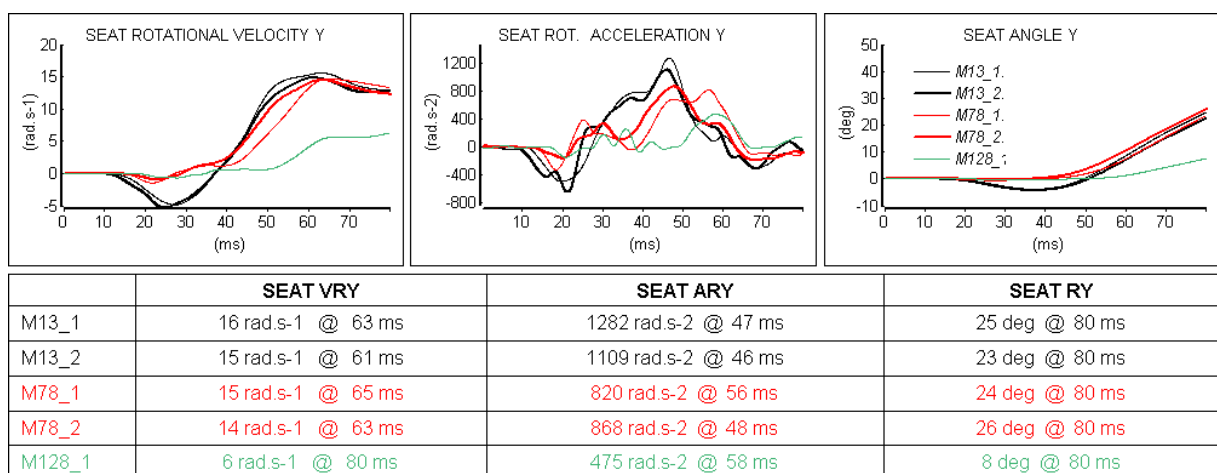
For all distances, the Fx airbag loading is mainly applied to the lower part of the plate. The ratio Fx low/ Fx upp is increasing from 3 up to 11. This reflects the general rotating kinematics of the surrogate.

**Table 17 Airbag forces in membrane configuration: left / right balance**



For all distances, the airbag loading is symmetrical with regard to X-Z plane.

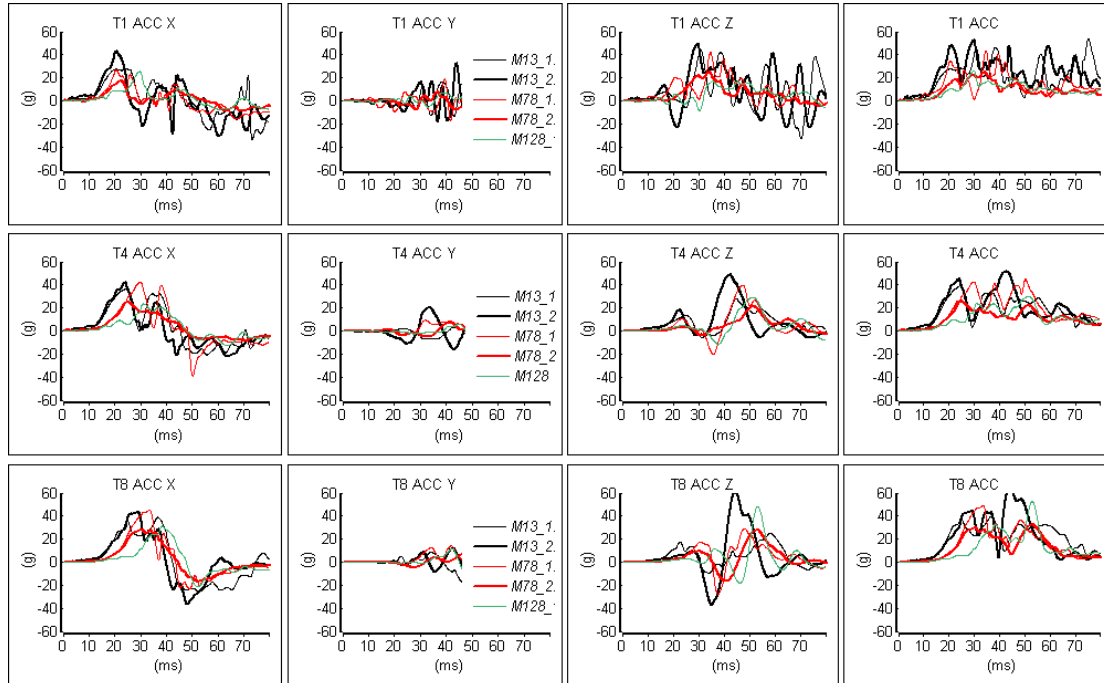
**Table 18 Rigid seat kinematics in membrane configuration: all distances**



Angular Y velocity is CFC 60 filtered and the initial offset is removed

In the case of the closest distance 13mm, the airbag force applied to the thighs results in negative angular velocity at the first stage of the loading.

**Table 19 Spine accelerations in membrane configuration: all distances CFC180**



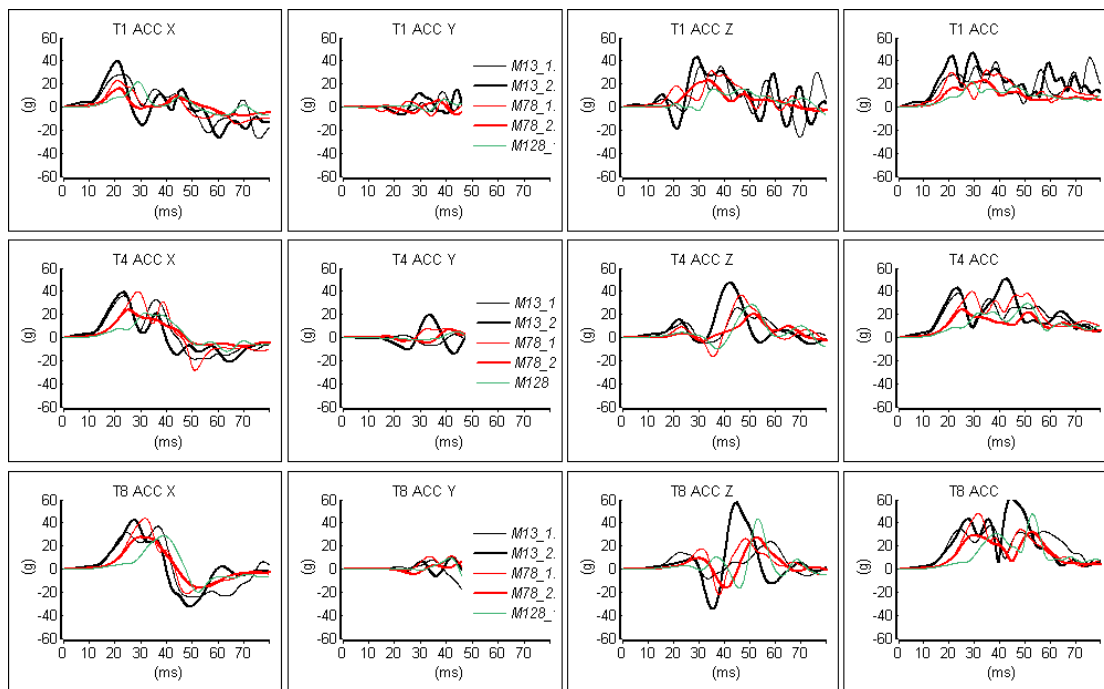
	T1 ACC X	T1 ACC Y	T1 ACC Z	T1 ACC
M13_1	[-34 g 28 g]	[-19 g 32 g]	[-32 g 44 g]	[0 g 54 g]
M13_2	[-30 g 43 g]	[-18 g 33 g]	[-23 g 49 g]	[0 g 53 g]
M78_1	[-15 g 26 g]	[-18 g 19 g]	[-5 g 42 g]	[0 g 43 g]
M78_2	[-9 g 17 g]	[-8 g 8 g]	[-5 g 25 g]	[0 g 25 g]
M128_1	[-8 g 25 g]	[-5 g 7 g]	[-9 g 17 g]	[0 g 26 g]
	T4 ACC X	T4 ACC Y	T4 ACC Z	T4 ACC
M13_1	[-21 g 37 g]	[-9 g 9 g]	[-6 g 28 g]	[0 g 39 g]
M13_2	[-22 g 42 g]	[-16 g 20 g]	[-6 g 49 g]	[0 g 51 g]
M78_1	[-39 g 42 g]	[-11 g 9 g]	[-21 g 40 g]	[0 g 45 g]
M78_2	[-8 g 25 g]	[-5 g 8 g]	[-4 g 21 g]	[0 g 26 g]
M128_1	[-13 g 24 g]	[-6 g 6 g]	[-11 g 29 g]	[0 g 30 g]
	T8 ACC X	T8 ACC Y	T8 ACC Z	T8 ACC
M13_1	[-25 g 39 g]	[-22 g 12 g]	[-10 g 25 g]	[0 g 39 g]
M13_2	[-36 g 43 g]	[-10 g 12 g]	[-37 g 62 g]	[0 g 65 g]
M78_1	[-23 g 45 g]	[-15 g 14 g]	[-28 g 29 g]	[0 g 49 g]
M78_2	[-17 g 28 g]	[-8 g 7 g]	[-17 g 28 g]	[0 g 33 g]
M128_1	[-21 g 31 g]	[-15 g 12 g]	[-18 g 48 g]	[0 g 52 g]

Spine accelerations are CFC 180 filtered and the initial offset is removed

In order to ease the reading of the curves, the graph below show the same curves processed with a CFC 60 filter.

Note that in the provided iso files the computed accelerations are CFC 180 filtered.

**Table 20 Spine accelerations in membrane configuration: all distances CFC60**



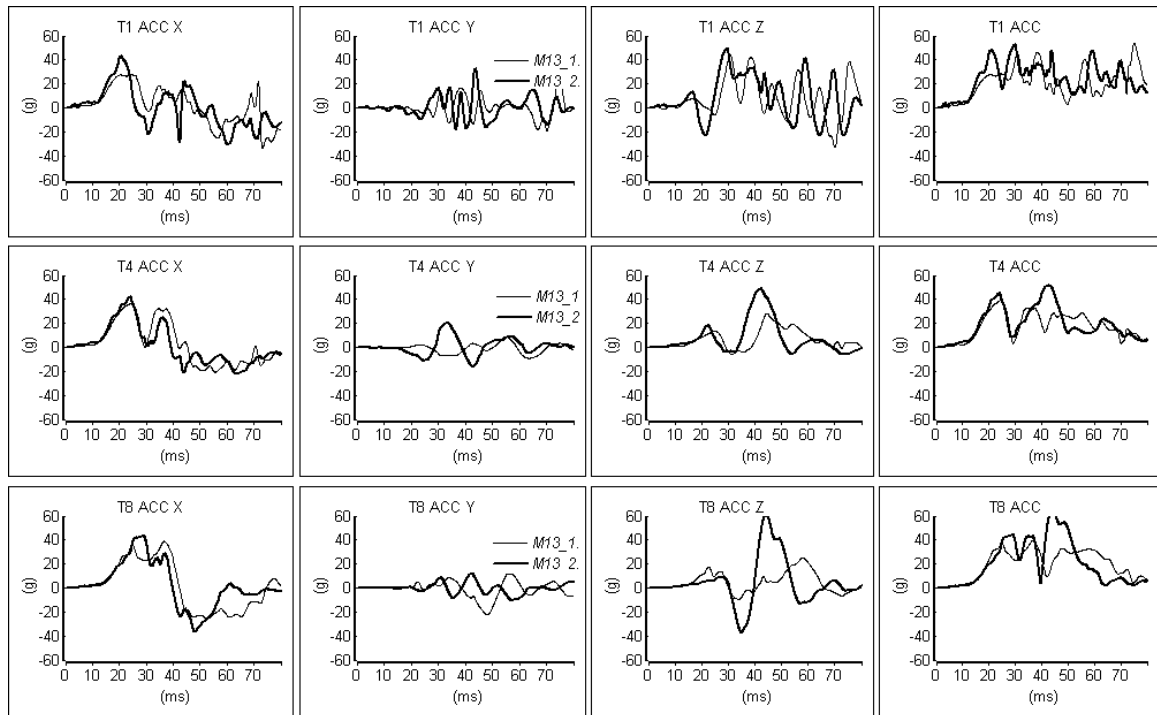
	T1 ACC X	T1 ACC Y	T1 ACC Z	T1 ACC
M13_1	[-27 g 28 g]	[-15 g 18 g]	[-26 g 35 g]	[0 g 43 g]
M13_2	[-27 g 40 g]	[-13 g 15 g]	[-19 g 44 g]	[0 g 47 g]
M78_1	[-15 g 23 g]	[-8 g 7 g]	[-3 g 31 g]	[0 g 32 g]
M78_2	[-8 g 16 g]	[-7 g 5 g]	[-4 g 23 g]	[0 g 23 g]
M128_1	[-7 g 22 g]	[-4 g 6 g]	[-7 g 16 g]	[0 g 22 g]

	T4 ACC X	T4 ACC Y	T4 ACC Z	T4 ACC
M13_1	[-19 g 36 g]	[-9 g 8 g]	[-5 g 26 g]	[0 g 38 g]
M13_2	[-21 g 39 g]	[-14 g 20 g]	[-6 g 47 g]	[0 g 51 g]
M78_1	[-28 g 40 g]	[-11 g 8 g]	[-17 g 37 g]	[0 g 40 g]
M78_2	[-8 g 24 g]	[-5 g 7 g]	[-3 g 20 g]	[0 g 24 g]
M128_1	[-12 g 21 g]	[-6 g 5 g]	[-10 g 29 g]	[0 g 29 g]

	T8 ACC X	T8 ACC Y	T8 ACC Z	T8 ACC
M13_1	[-24 g 37 g]	[-21 g 11 g]	[-8 g 24 g]	[0 g 38 g]
M13_2	[-33 g 42 g]	[-10 g 10 g]	[-35 g 58 g]	[0 g 62 g]
M78_1	[-21 g 44 g]	[-13 g 11 g]	[-22 g 26 g]	[0 g 48 g]
M78_2	[-16 g 27 g]	[-8 g 7 g]	[-16 g 27 g]	[0 g 32 g]
M128_1	[-20 g 29 g]	[-13 g 10 g]	[-17 g 44 g]	[0 g 48 g]

On contrast to the previous graph presented in the report where all distances are overlaid, the following graphs ease the reading in comparing only test at a given distance. Those graphs intend to help assessing the variability of two different PMHS in similar conditions.

**Table 21 Spine accelerations in membrane configuration : distance 13mm**

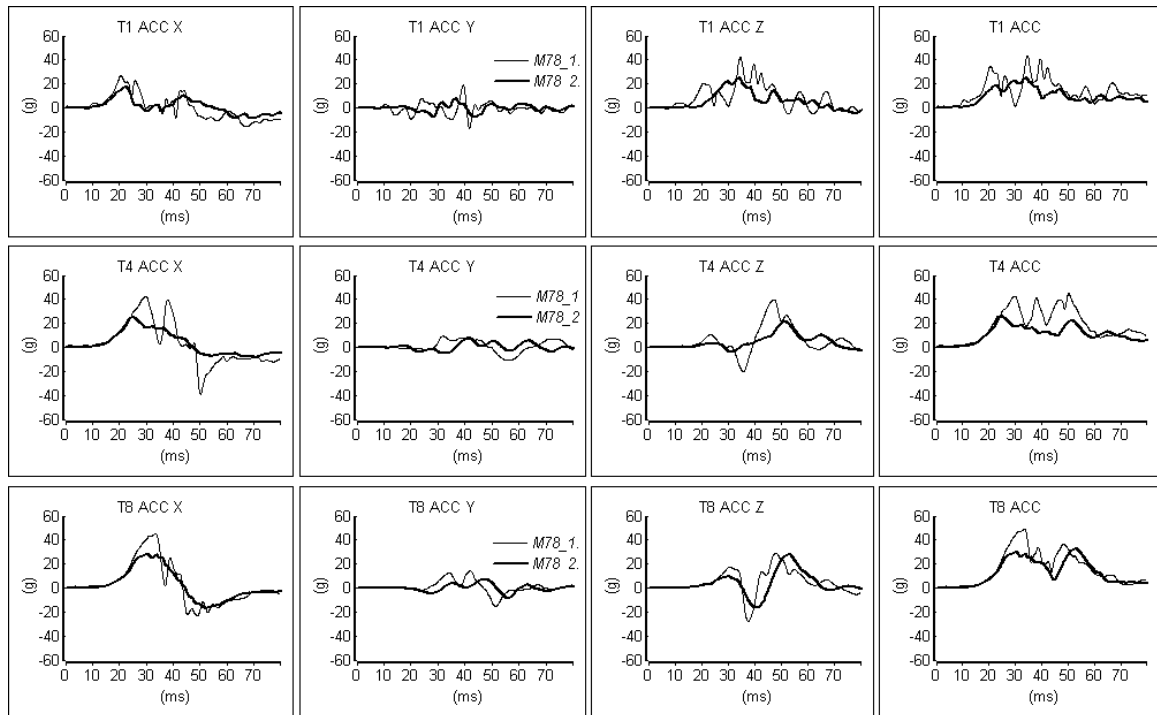


	<b>T1 ACC X</b>	<b>T1 ACC Y</b>	<b>T1 ACC Z</b>	<b>T1 ACC</b>
M13_1	[-34 g 28 g]	[-19 g 32 g]	[-32 g 44 g]	[0 g 54 g]
M13_2	[-30 g 43 g]	[-18 g 33 g]	[-23 g 49 g]	[0 g 53 g]
	<b>T4 ACC X</b>	<b>T4 ACC Y</b>	<b>T4 ACC Z</b>	<b>T4 ACC</b>
M13_1	[-21 g 37 g]	[-9 g 9 g]	[-6 g 28 g]	[0 g 39 g]
M13_2	[-22 g 42 g]	[-16 g 20 g]	[-6 g 49 g]	[0 g 51 g]
	<b>T8 ACC X</b>	<b>T8 ACC Y</b>	<b>T8 ACC Z</b>	<b>T8 ACC</b>
M13_1	[-25 g 39 g]	[-22 g 12 g]	[-10 g 25 g]	[0 g 39 g]
M13_2	[-36 g 43 g]	[-10 g 12 g]	[-37 g 62 g]	[0 g 65 g]

Spine accelerations are CFC 180 filtered and the initial offset is removed.

Peak values range from 54G at T1 for M13\_1 to 65G at T12 for M13\_2.

**Table 22 Spine accelerations in membrane configuration: distance 78mm**

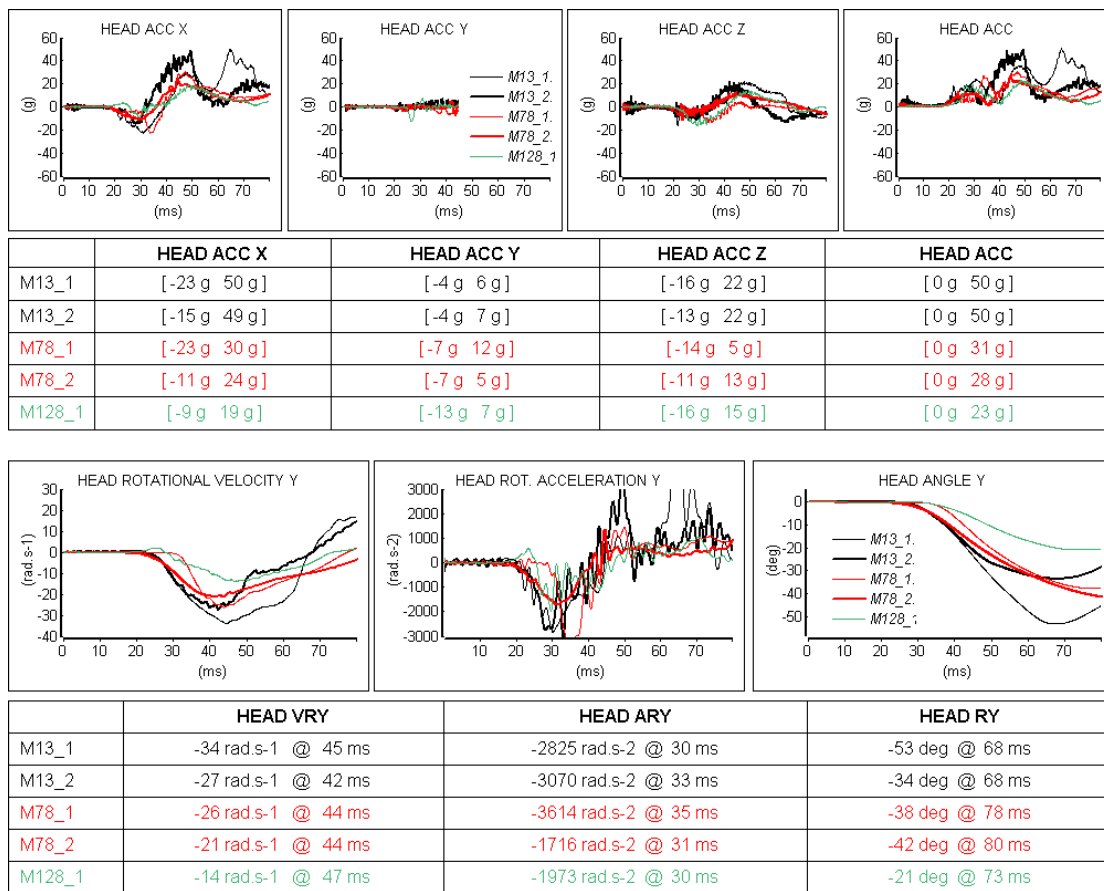


	<b>T1 ACC X</b>	<b>T1 ACC Y</b>	<b>T1 ACC Z</b>	<b>T1 ACC</b>
M78_1	[-15 g 26 g]	[-18 g 19 g]	[-5 g 42 g]	[0 g 43 g]
M78_2	[-9 g 17 g]	[-8 g 8 g]	[-5 g 25 g]	[0 g 25 g]
	<b>T4 ACC X</b>	<b>T4 ACC Y</b>	<b>T4 ACC Z</b>	<b>T4 ACC</b>
M78_1	[-39 g 42 g]	[-11 g 9 g]	[-21 g 40 g]	[0 g 45 g]
M78_2	[-8 g 25 g]	[-5 g 8 g]	[-4 g 21 g]	[0 g 26 g]
	<b>T8 ACC X</b>	<b>T8 ACC Y</b>	<b>T8 ACC Z</b>	<b>T8 ACC</b>
M78_1	[-23 g 45 g]	[-15 g 14 g]	[-28 g 29 g]	[0 g 49 g]
M78_2	[-17 g 28 g]	[-8 g 7 g]	[-17 g 28 g]	[0 g 33 g]

Spine accelerations are CFC 180 filtered and the initial offset is removed.

Peak values range from 33G at T12 for M78\_2 to 49G at T12 for M78\_1.

**Table 23 Head kinematics in membrane configuration: all distances CFC 1000**

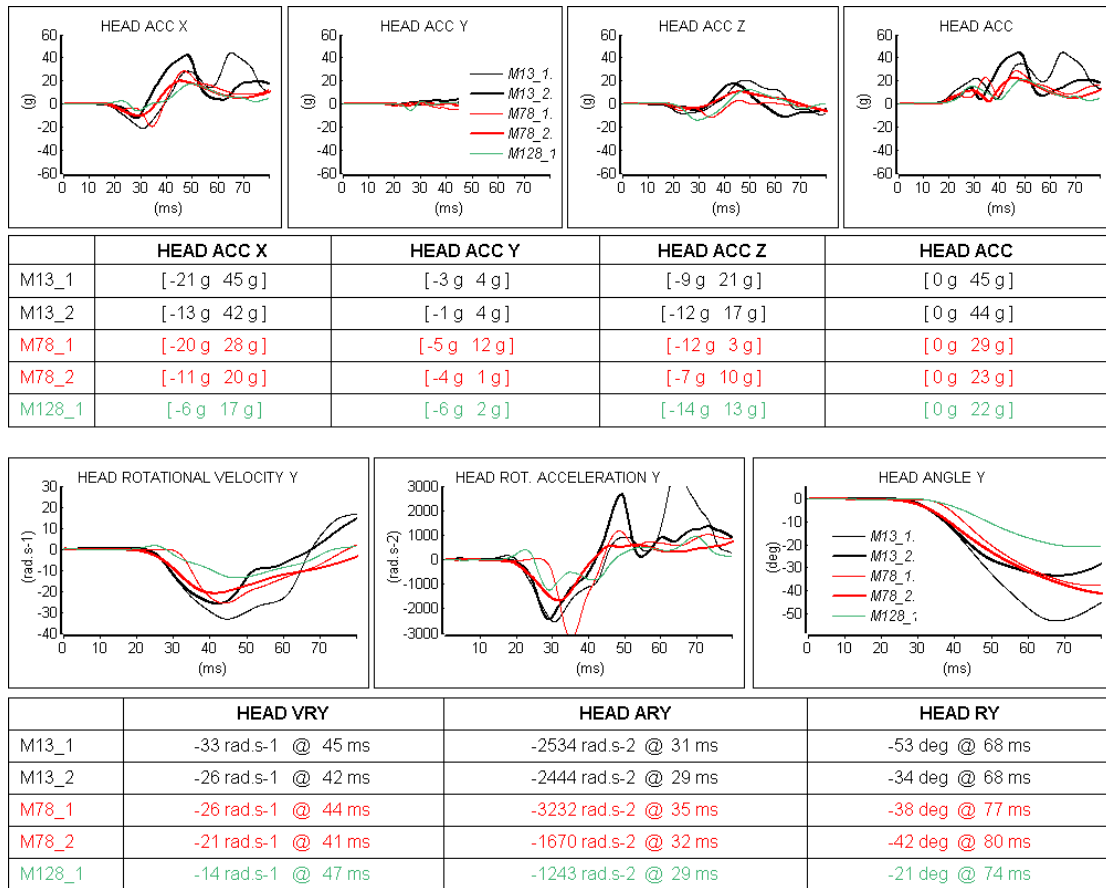


Head accelerations :

- CFC 1000 filtered and the initial offset was removed
- Expressed in local sensor frame
- Note that the sensor is not located at head CG

In order to ease the reading of the curves , the graph below show the same curves with a CFC 60. Note that in the provided iso files the computed accelerations are CFC 1000 filtered.

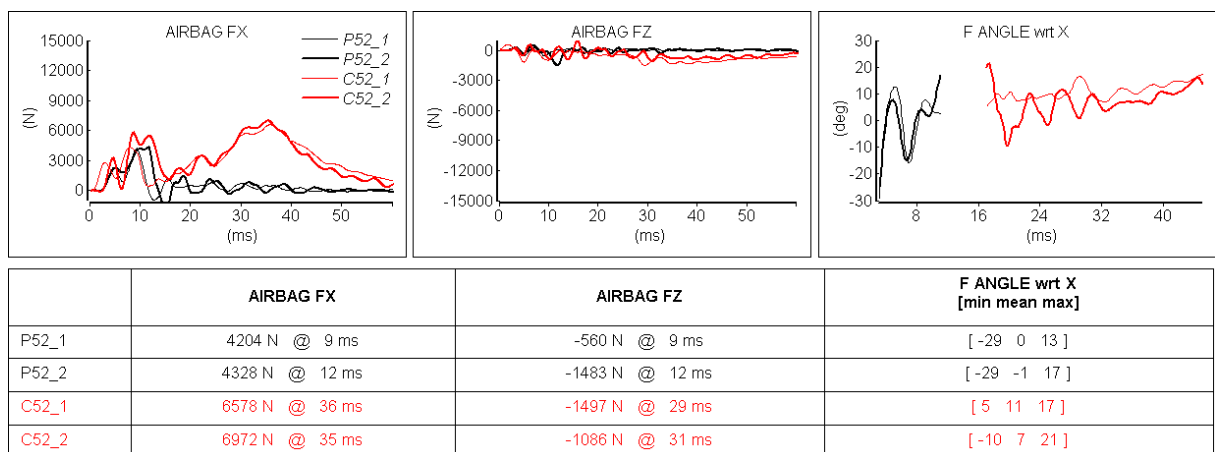
**Table 24 Head kinematics in membrane configuration: all distances CFC60**



#### 4.5.2 Punch out and combined configuration

The following graphs present results for punch out and complete configurations.

**Table 25 Airbag forces in punch-out and complete configurations.**

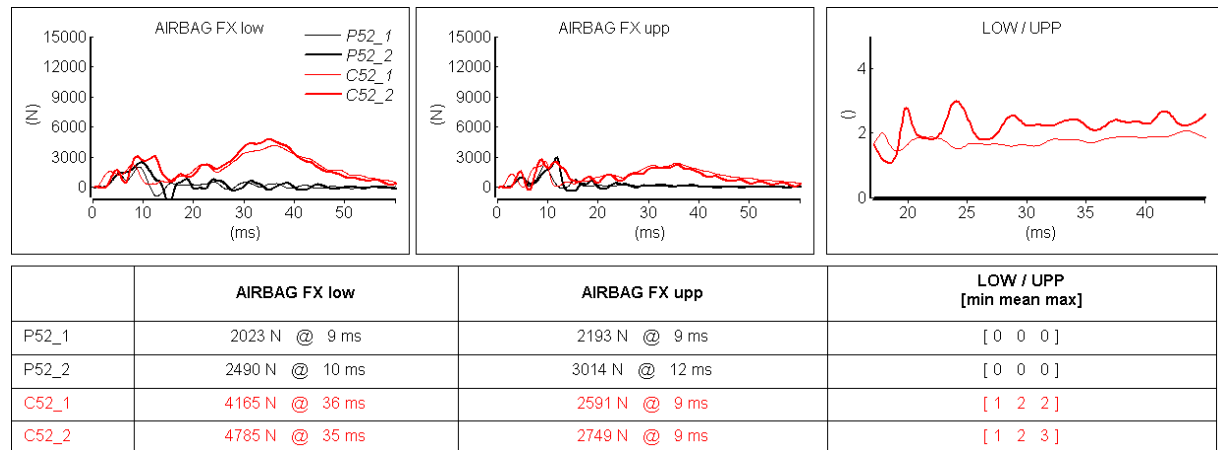


Airbag forces:

- CFC 180 filtered and the initial offset is removed
- Expressed in the airbag plate frame

As for the membrane configuration, the airbag mainly acts in the X-plate direction. As expected the two configurations are comparable up to 15ms which correspond to the punch-out phenomenon.

**Table 26 Airbag forces in punch-out and complete configurations: upp / low balance**

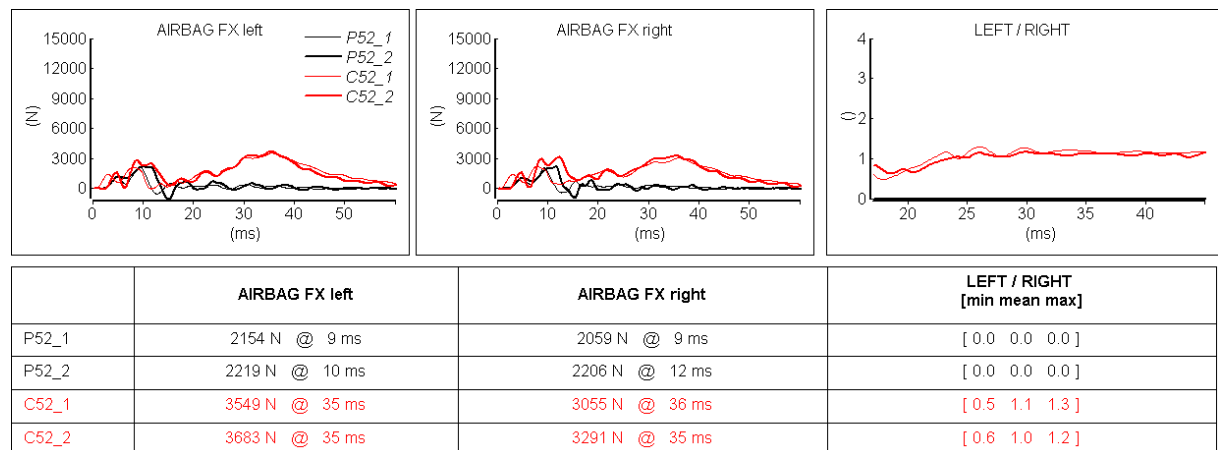


Fx airbag loading is mainly applied to the lower part of the plate.

The low / up balance is only assessed for the membrane phase of the complete configuration.

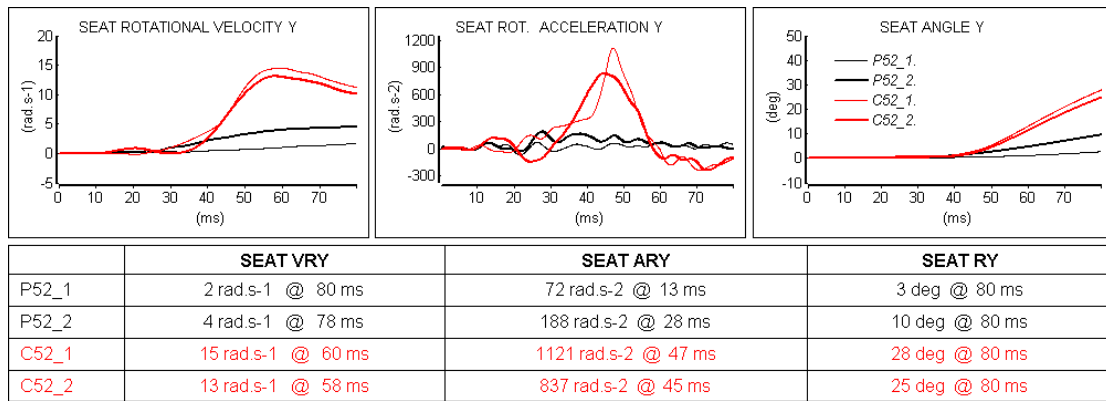
The low / up ratio is computed only for the membrane phase of the complete configuration. The average value is around 2 and doesn't increase as much as for membrane configuration.

**Table 27 Airbag forces in punch-out and complete configurations: left / right balance**



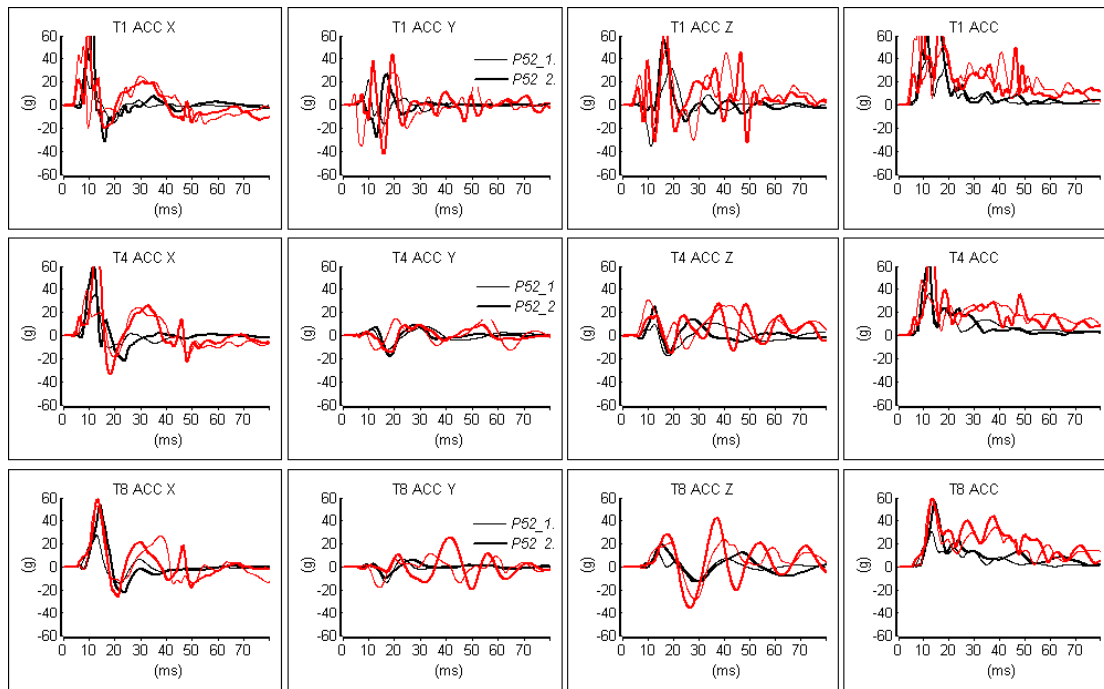
As for membrane configuration, the loading is symmetrical with regard to X Z plane for punch out and complete configurations (the left / right value is computed only for membrane phase of the complete configuration).

**Table 28 Airbag forces in punch-out and complete configurations: Seat kinematics**



Angular Y velocity is CFC 60 filtered and the initial offset is removed.

**Table 29 Spine accelerations for punch-out and complete configurations,CFC1000**



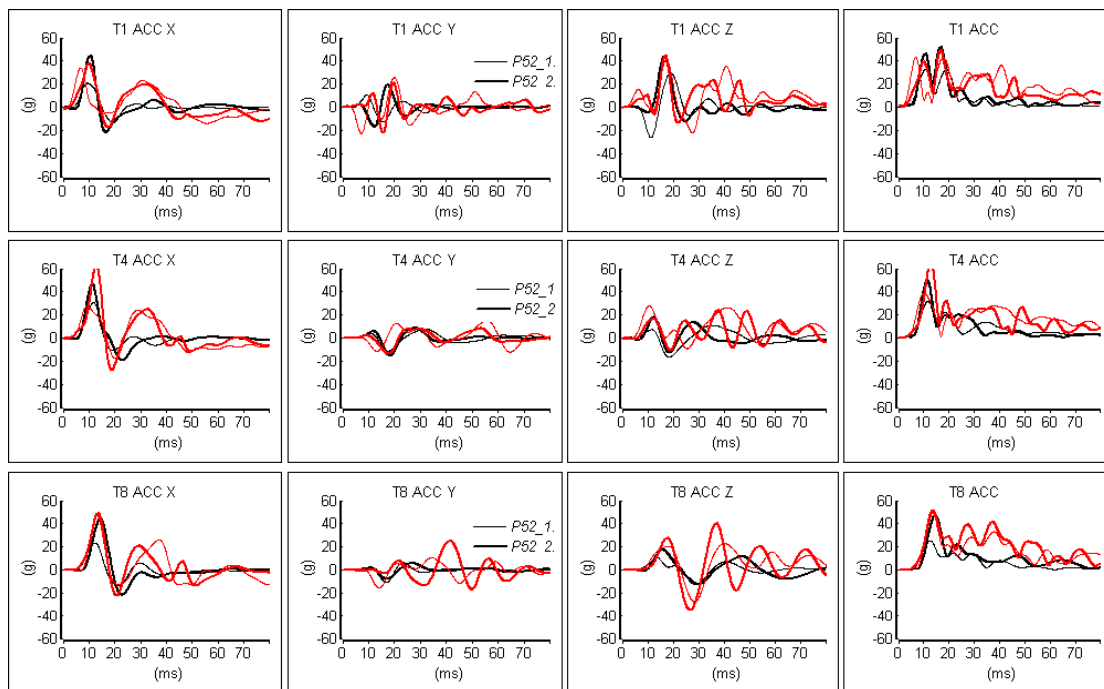
	T1 ACC X	T1 ACC Y	T1 ACC Z	T1 ACC
P52_1	[-15 g 27 g]	[-17 g 22 g]	[-36 g 32 g]	[0 g 42 g]
P52_2	[-31 g 71 g]	[-28 g 27 g]	[-15 g 56 g]	[0 g 72 g]
C52_1	[-20 g 51 g]	[-36 g 34 g]	[-31 g 48 g]	[0 g 63 g]
C52_2	[-20 g 68 g]	[-43 g 44 g]	[-33 g 68 g]	[0 g 79 g]
	T4 ACC X	T4 ACC Y	T4 ACC Z	T4 ACC
P52_1	[-11 g 35 g]	[-12 g 8 g]	[-17 g 11 g]	[0 g 37 g]
P52_2	[-22 g 62 g]	[-18 g 9 g]	[-15 g 25 g]	[0 g 66 g]
C52_1	[-19 g 39 g]	[-13 g 16 g]	[-12 g 31 g]	[0 g 48 g]
C52_2	[-34 g 82 g]	[-15 g 9 g]	[-16 g 28 g]	[0 g 84 g]
	T8 ACC X	T8 ACC Y	T8 ACC Z	T8 ACC
P52_1	[-14 g 28 g]	[-13 g 7 g]	[-13 g 15 g]	[0 g 31 g]
P52_2	[-23 g 53 g]	[-10 g 6 g]	[-13 g 19 g]	[0 g 56 g]
C52_1	[-15 g 53 g]	[-17 g 12 g]	[-28 g 24 g]	[0 g 58 g]
C52_2	[-26 g 59 g]	[-20 g 25 g]	[-36 g 43 g]	[0 g 59 g]

Spine accelerations are CFC 180 filtered and the initial offset is removed.

In order to ease the reading of the curves , the graph below show the same curves processed with a CFC 60 filter.

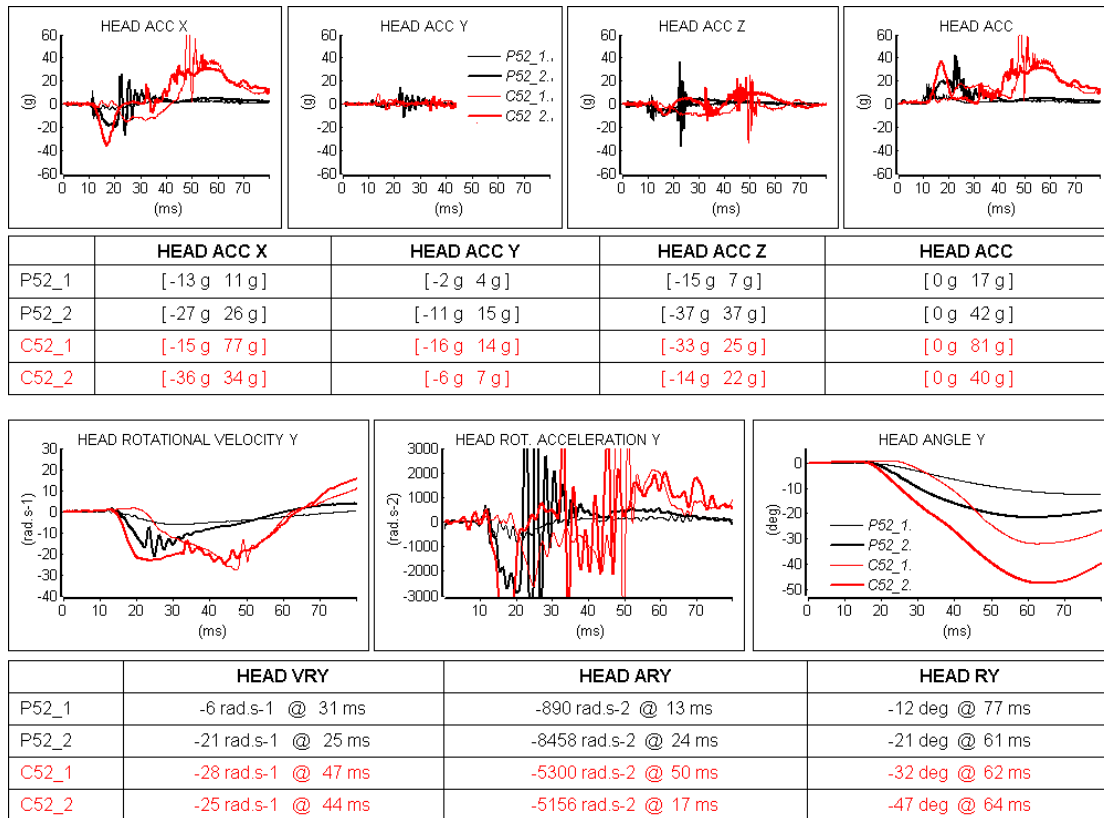
Note that in the provided iso files the computed accelerations are CFC 180 filtered.

**Table 30 Spine accelerations for punch-out and complete configurations,CFC60**



	<b>T1 ACC X</b>	<b>T1 ACC Y</b>	<b>T1 ACC Z</b>	<b>T1 ACC</b>
P52_1	[-13 g 21 g]	[-13 g 10 g]	[-26 g 29 g]	[0 g 33 g]
P52_2	[-22 g 44 g]	[-17 g 19 g]	[-12 g 44 g]	[0 g 52 g]
C52_1	[-14 g 34 g]	[-23 g 26 g]	[-22 g 41 g]	[2 g 43 g]
C52_2	[-17 g 38 g]	[-22 g 21 g]	[-14 g 45 g]	[0 g 50 g]
	<b>T4 ACC X</b>	<b>T4 ACC Y</b>	<b>T4 ACC Z</b>	<b>T4 ACC</b>
P52_1	[-11 g 31 g]	[-11 g 8 g]	[-17 g 11 g]	[0 g 32 g]
P52_2	[-19 g 47 g]	[-15 g 9 g]	[-13 g 18 g]	[0 g 50 g]
C52_1	[-18 g 28 g]	[-12 g 15 g]	[-9 g 28 g]	[1 g 39 g]
C52_2	[-28 g 63 g]	[-14 g 8 g]	[-11 g 24 g]	[0 g 65 g]
	<b>T8 ACC X</b>	<b>T8 ACC Y</b>	<b>T8 ACC Z</b>	<b>T8 ACC</b>
P52_1	[-13 g 23 g]	[-11 g 6 g]	[-13 g 11 g]	[0 g 25 g]
P52_2	[-22 g 44 g]	[-8 g 6 g]	[-12 g 18 g]	[0 g 47 g]
C52_1	[-13 g 47 g]	[-16 g 11 g]	[-27 g 23 g]	[0 g 51 g]
C52_2	[-22 g 49 g]	[-17 g 25 g]	[-35 g 40 g]	[0 g 51 g]

**Table 31 Head kinematics for punch-out and complete configurations: CFC1000**

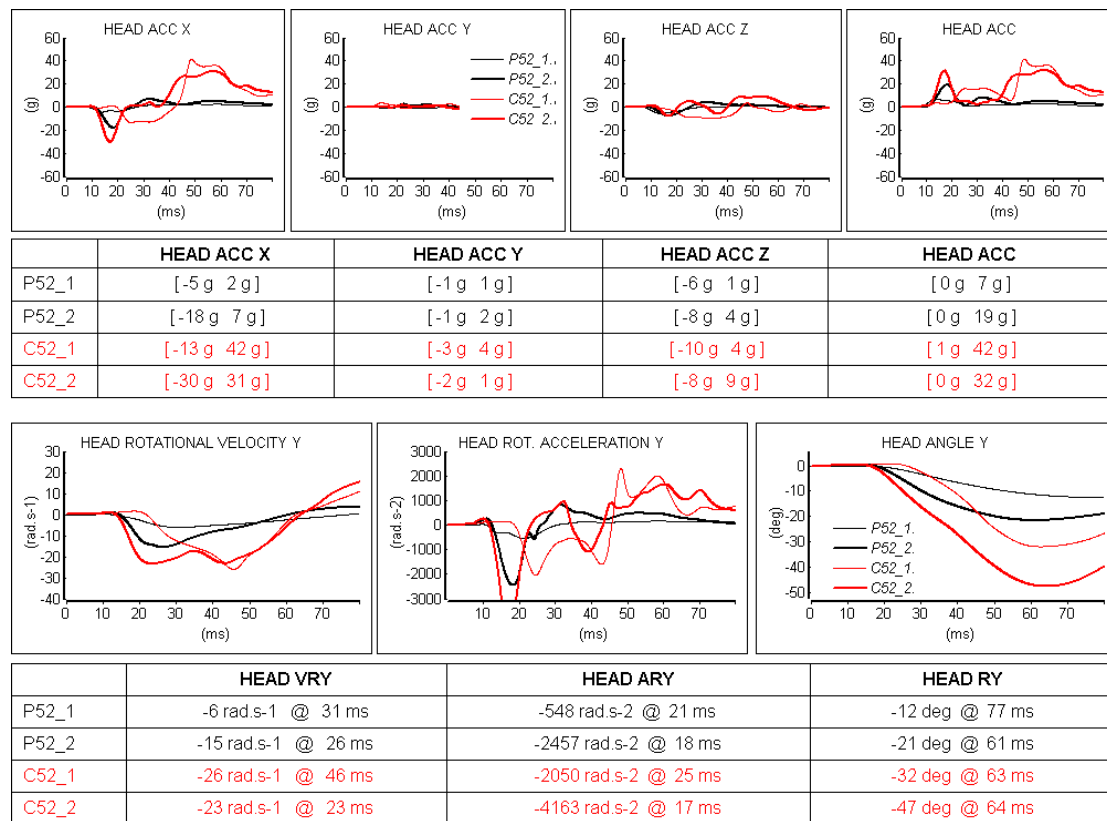


**Head accelerations:**

- CFC 1000 filtered and the initial offset was removed
- Expressed in local sensor frame
- Note that the sensor is not located at head CG

In order to ease the reading of the curves , the graph below show the same curves with a CFC 60. Note that in the provided iso files the computed accelerations are CFC 1000 filtered.

**Table 32 Head kinematics for punch-out and complete configurations: CFC60**



### 4.5.3 Injury details for LAB 2005 surrogates

#### Soft tissue injuries:

A slight liver laceration was found on C52\_1.

Subject C52\_2 sustained slight liver lacerations and severe heart injury resulting in AIS 6.

No other soft tissue injury were found on the other pmhs.

#### Rib fracture injuries:

##### Membrane configuration

Three of the five membrane-only tests caused thoracic injuries:

- Both tests at 13 mm of plate distance M13\_1 and M13\_2
- One of the two tests at 78 mm M78\_1

No injury was found for the other 78 mm test M78\_2 or for the 128-mm test M128\_1.

All rib fractures were located approximately midway between the sternum and the spinous process except for M13\_1, which exhibited many fractures at the costal cartilage junctions on the right side.

### Punch out configuration

Both punch-out-only tests resulted in thoracic injuries. P52\_1 sustained one sternum fracture and P52\_2 sustained ten rib fractures, all on the anterior area of the thorax.

The following table presents the rib fracture detail and AIS figures.

**Table 33 Rib fracture detail**

Test reference	M13_1	M13_2	M78_1	M78_2	M128_1	P52_1	P52_2	C52_1	C52_2
PMHS code	554	555	559	561	560	557	558	562	565
MAIS	3	2	2	0	0	0	2	3	6
Skeletal Thorax AIS	3	2	2	0	0	0	2	3	4
Total number of rib fractures	12	15	11	0	0	0	10	15	23
Nb of separated rib fractures	3	3	3	0	0	0	1	10	5
Total number of sternum fractures	2	1	1	0	0	1	2	0	0

The rib fractures localizations are shown below and a description of the symbols used is given in the following table.

Skeletal thoracic AIS (STAIS) and total rib fracture number are reminded for each test.

●	complete with displacement (D)
●	complete without displacement (ND)
▲	partial with rupture of the external cortical bone (PE)
▲	partial with rupture of the internal cortical bone (PI)
●	vertebral (V)

**Table 34 Rib fracture detail: membrane configuration (13 - 52 - 128 mm)**

<p><b># 554</b></p>	<p><b># 555</b></p>
<p><b>M13_1      STAIS: 3      rib fx nb: 12</b></p>	<p><b>M13_2      STAIS: 2      rib fx nb: 15</b></p>
<p><b># 559</b></p>	<p><b># 561</b></p>
<p><b>M78_1      STAIS: 2      rib fx nb: 11</b></p>	<p><b>M78_2      STAIS: 0      rib fx nb: 0</b></p>
<p><b># 560</b></p>	
<p><b>M128_1      STAIS: 0      rib fx nb: 0</b></p>	

**Table 35 Rib fracture detail: punch out configuration (52mm)**

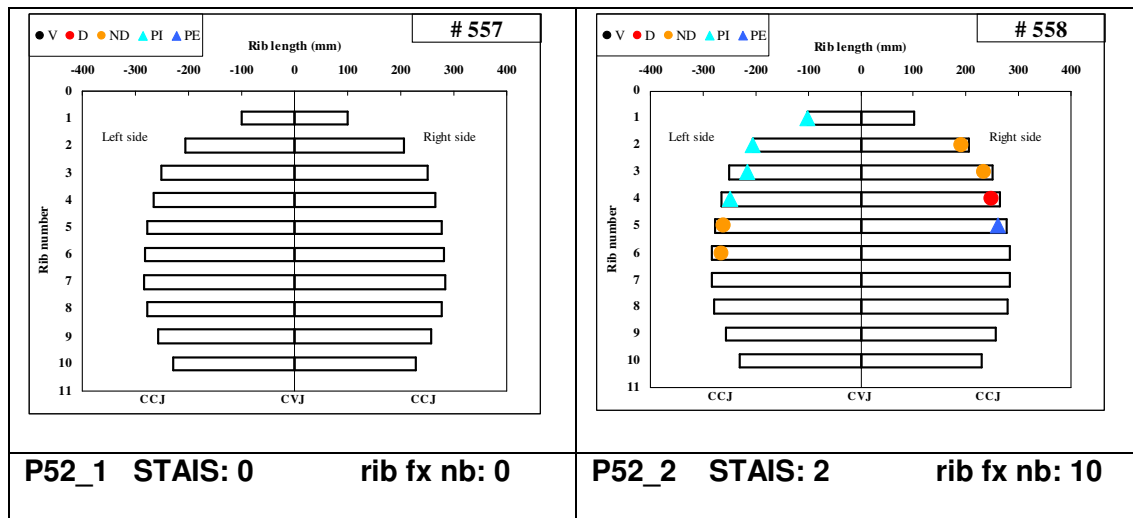
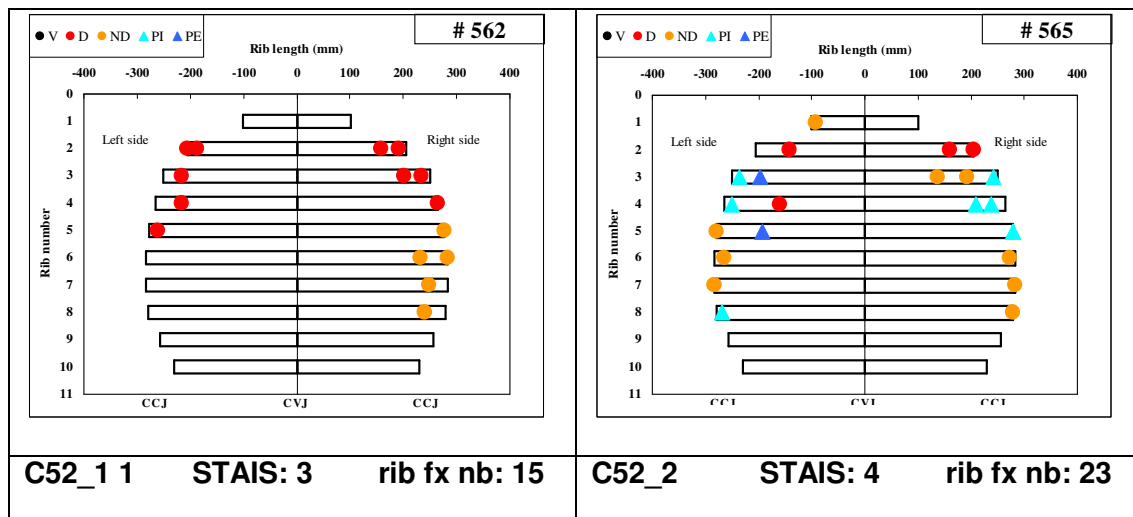


**Table 36 Rib fracture detail: complete configuration (52 mm)**



## 5 Thorax Test: LAB-2008

### 5.1 Context of the study

Thorax test LAB-2008 is based on the data of Trosseille et al 2008 where 8 subjects were submitted to different type of loading in order to study rib strain pattern. Among those tests, 4 configuration were regarding frontal impact and involved airbag, impactor as well as belt and harness.

Reference :Rib Cage Strain Pattern as a Function of Chest Loading Configuration – Stapp 2008 –Xavier Trosseille, Pascal Baudrit and Tiphaine Lepout

### 5.2 Test set-up

In those tests, PMHS ribs were heavily instrumented with strain gauges in order to study the rib deformation pattern when submitted to different loading cases.

The location of an event (gauge or fracture) is defined by the wrap-around distance (WAD) measured along the rib with a tape. It is given with respect to the costo-transverse joint (CTJ). In the paper, the curvilinear abscissa (s) is defined by the following formula:

$$s = \pm \frac{WAD(\text{strain\_gage})}{WAD(CCJ)} * 100$$

Four different loading cases have been studied. In the following, an overall description of the configurations is given. Main dimensions of the test set up are provided in appendix.

- **Airbag configuration: tests AB0\_1 and AB0\_2**

The test set up and airbag are similar to those used by Lebarbé in 2005.

The airbag is unfolded. The airbag module is centered on the sternum

The distances between the plate and the sternum are:

$$AB0\_1 = 73\text{mm}$$

$$AB0\_2 = 13\text{mm}$$

The subject pelvis is fixed to a rigid seat which allows rotation in y direction.

The subject is held in position by straps which are released at fire time

- **Impactor configuration: test IMP0\_1**

A 23.4kg impactor is used. It is similar in shaped to the one used by Viano (1989): a 152mm disc with flat contact surface.

The impactor is aligned with the center of the sternum body , propelled with an initial velocity of 4.3 m/s , and guided during the impact.

The subject is seated on a low friction surface and held in position by straps which are released at fire time.

- **Belt configuration: tests BLT\_1 and BLT\_2**

The belt is only composed of the shoulder belt. The two ends of the belt are retracted by the hydraulic machine.

The subject pelvis is fixed to a rigid seat which allows rotation in y direction.

Belt strap is dynamically retracted by a hydraulic machine which controls the applied tension to the two ends. Two different tension patterns are applied:

- BLT\_1 = tension load pattern 1
- BLT\_2 = tension load pattern 2

Thus BLT\_1 and BLT\_2 do not strictly correspond to the same conditions.

However, due to the low differences between the two loading patterns, those test are presented together

- **Harness configuration: test HRN\_1 and HRN\_2**

In the harness configuration a four ends belt is used. Only the two upper ends are retracted while the two lower ends are fixed.

The subject pelvis is fixed to a rigid seat which allows rotation in y direction.

The same loading pattern is applied to both subjects.

### 5.3 Test Matrix

The following table summarize the different frontal configuration of the campaign LAB\_2008

Test code	Loading type	Configuration	PMHS number
AB0_1	Airbag	78 mm	594
AB0_2	Airbag	13 mm	607
IMP0_1	Impactor	4.3 m/s	589
IMP0_2	Impactor	4.3 m/s	621
BLT_1	Belt	Load pattern 1	595
BLT_2	Belt	Load pattern 2	609
HRN_1	Harness	Load pattern 2	599
HRN_2	Harness	Load pattern 2	610

### 5.4 PMHS anthropometry

Test Ref.	PMHS Code	Sex	Age	Total weight (kg)	Height (m)	Thorax		
						depth (m)	width (m)	circumference (m)
AB0_1	594	M	78	65	1.70	0.23	0.30	0.95
AB0_2	607	M	84	56	1.75	0.19	0.28	0.84
IMP0_1	589	M	88	60	1.69	0.20	0.30	0.89
IMP0_2	621	M	82	78	1.71	0.23	0.36	1.03
BLT_1	595	M	74	69	1.74	0.22	0.30	0.94
BLT_2	609	M	69	71	1.70	0.25	0.34	1.02
HRN_1	599	M	73	72	1.82	0.23	0.32	0.97
HRN_2	610	M	70	60	1.70	0.23	0.31	0.99

## 5.5 Results

### 5.5.1 Data processing

The heavy instrumentation used in those LAB2008 tests gives access to two kinds of outputs:

First, conventional sensor time history signals are available. Those signals will be referred as “global responses” and includes:

- time history of the applied load such as impactor contact force, airbag contact force, belt tension
- global kinematics of the subject such as spine accelerations or test setup kinematics in case of movable parts

Secondly local responses are based on the strain gauges analysis presented in reference 3. Strain field analysis involves considering gage signals in two different perspectives:

- time history signals
- spatial strain profile

The strain profile (strain as a function of the curvilinear abscissa) can be drawn, as illustrated in Figure 8 in Trosseille et al 2008 for each costal ring. This profile is a deformation state as function of space, along the rib length, at a given time.

For a given loading force, measured strain values are influenced by rib cross section properties as well as bone material properties. In order to allow for the comparison of different subjects, the strains values were normalized. For that purpose, an effective strain,  $\epsilon_{RMS}$  (Root Mean Square) was calculated for each costal rib. Then, each strain of the costal ring was divided by the effective strain to obtain a normalized strain  $\epsilon_N(s, t)$ .

$$\epsilon_{RMS}(t) = \sqrt{\frac{1}{((s1 - sn)_{left} + (sn - s1)_{right}) \left( \left( \int_{sn}^{s1} (\epsilon(s, t))^2 ds \right)_{left} + \left( \int_{sn}^{s1} (\epsilon(s, t))^2 ds \right)_{right} \right)}}$$

Where  $\epsilon(s, t)$  is the strain measured at the curvilinear abscissa  $s$  as a function of time,  $s1$  the curvilinear abscissa of the first gauge and  $sn$  is the curvilinear abscissa of the  $n^{\text{th}}$  gauge

$$\epsilon_N(s, t) = \frac{\epsilon(s, t)}{\epsilon_{RMS}(t)}$$

It should be noted that the presented strain profile is related to a given time.

In order to access the whole available information, all the recorded profiles would have to be overlaid, resulting in non-readable figures. Another option would be to present strain signals as a color map with two axes dedicated to respectively time and space. Tough this approach doesn't allow for easy comparison.

In this analysis, as presented in reference 3, rib strain signals are then characterized by the mean of two curves instead of considering the whole set of gage signals. This approach relies on the assumption that the strain profile can be simplified at any time in such a way:

$$\varepsilon(s,t) = \varepsilon_N(s,t) \cdot \varepsilon_{RMS}(t) \approx f(s) \cdot g(t)$$

The previous relation means the strain profile over time  $\varepsilon(s,t)$  could be approximated as a single given profile  $f(s)$  whose evolution over time is only driven by a magnitude scaling with a scaling factor expressed in function of time  $g(t)$ .

In the current analysis,  $g(t)$  has been chosen to be the RMS strain. Other options could be considered, for instance  $g(t)$  could be set to be the maximum raw strain as a function of time. Though, this latter option would lead to be too much sensitive to the number of gages of the rib. Indeed, maximum peak strain is not necessarily located close to a gage, so that this value would be randomly picked up or missed by the sensors. The RMS strain, as a weighted average of the gages signals, is much less sensitive to that aspect, and is therefore a better candidate.

As a consequence, the  $f(s)$  function is naturally built from the normalized profiles  $\varepsilon_N(s,t)$ . A simple way to derive a single function from this set of profiles is to average the  $\varepsilon_N(s,t)$  over time.

To assess how valid this simplification is, one option is to assess how far the real  $\varepsilon(s,t)$  function differs from the simplified  $f(s) \cdot g(t)$  by the mean of standard error.

In the following plots, high standard error around gages values therefore indicates that, for this given gage, the simplification is less valid. This case is met for instance when inertia effects lead to bi-modal loading patterns or when non-periodical measurement noise is involved. Note that in reference 3 terminology, those signal with high standard errors, are referred as “unstable”.

In the current analysis, signals are considered within a time interval window defined by:

- $t_1$ = time when RMS strain reaches 10% of the maximum RMS, allowing to get rid of the noisy part of the signals at the beginning of the loading process
- $t_2$ = time of 99% when RMS strain reaches 99% of the maximum RMS value which allows to skip the part of lower interest such as unloading phase or events occurring after rib fractures.

Outputs of the strain analysis are summarized in a figure of 10 by 4 plots. Each one of the 10 lines is related to a rib level while columns are dedicated to various signal types such as:

- RMS strain time history
- normalized averaged strain profile
- normalized strain at time when RMS strain is maximum or rib fractured
- raw strain profile at time when RMS strain is maximum or rib fractured

Below is shown a sample figure illustrating that outputs for rib level 1 to 5. Each color is related to a different test. In that sample case, red lines are results coming from Humos2LAB model whose ribs are instrumented with more than 40 gages allowing for continuously defined profiles compared to PMHS results where interpolation has to be used in between gages locations.

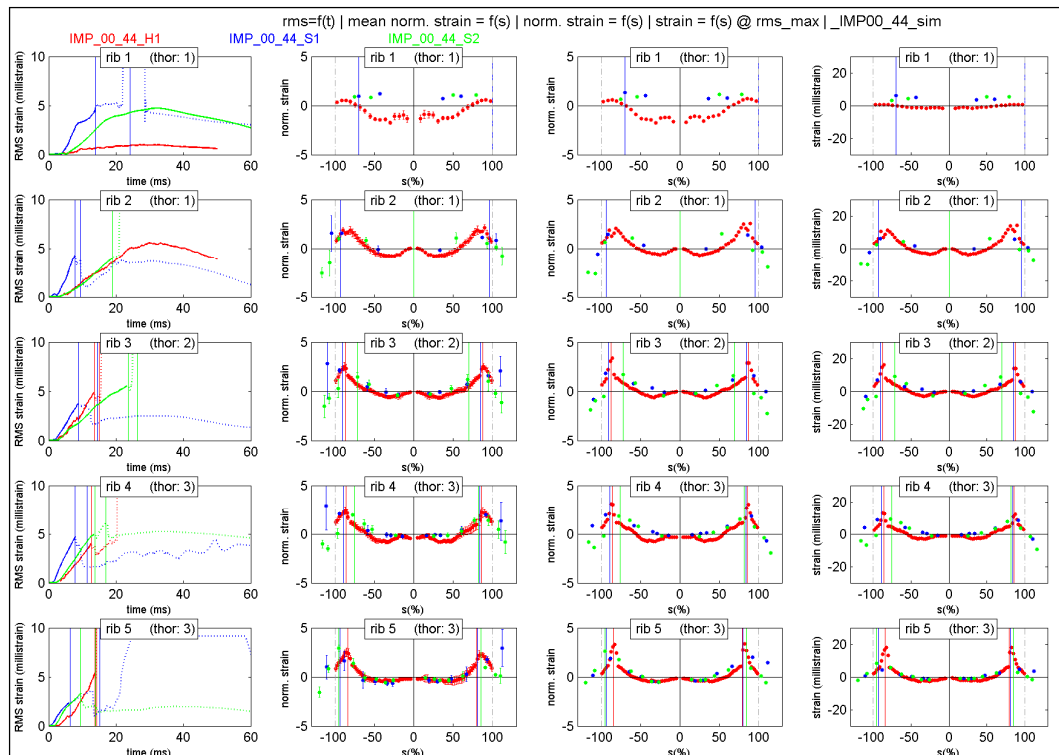


**Figure 2 Sample gage analysis plot**

In the following are described the four columns content:

Column 1: RMS strain as a function of time

Column 1 shows Root Mean Square of strain as a function of time. This metric indicates the global loading state of the rib. In case of pure bending, and for a given material law and cross section property, this metric can be shown to be proportional to the rib deformation energy.

It is a convenient way to take into account all the strain sensor signals of the rib and to derive a single time history curve from a set of curves. This signal is of help to assess phasing in between loading time history and rib fractures.

The RMS value should be seen as an energy equivalent strain where the loading pattern would be a constant moment along the rib length. Therefore maximum RMS strain values should be not compared to raw measured strain values. One can notice that, for a given strain profile, RMS strain value will always be lower than the profile peak strain value.

It should be noted that RMS value is influenced by rib cross section properties as well as material properties. Therefore using RMS strain value to normalize raw strain value is a way to limit effects of geometry and material variability in between surrogates.

Also note that for a given profile, RMS value is sensitive to the number of gages used to build the strain profile. Therefore, in the case of rib levels 1,2 and 10 which are instrumented with few gages, RMS values are raw approximations and should be considered with care.

On the column 1 plots, a vertical solid line indicates fractures when occurring. Note that in case of multiple fractures for a given rib, only the first one is displayed. In case both sides are fractured, two solid lines are shown though. Cartilages fractures are not considered in this analysis. After rib fractures, RMS strain signal is shown in dotted line.

The following figure illustrates RMS strain signal comparison in the case of rib level 3 for impactor loading . Blue and green lines are PMHS signal, compared to red line which is HUMOS2 LAB output.

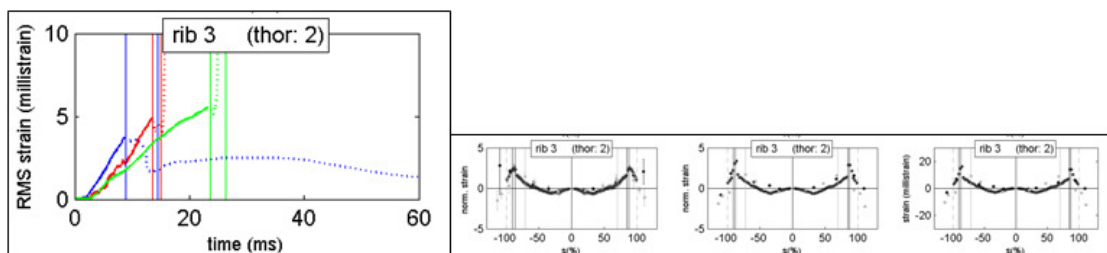


**Figure 3 Sample RMS strain as a function of time**

Column 2: averaged normalized strain profile

Column 2 shows the averaged normalized strain as a function of curvilinear abscissae.

This normalized strain profile is averaged in the time interval between 10% and 99% of the maximum RMS value and therefore account for the main time history content of the loading phase. Small standard error demonstrates that the strain profile only varies in magnitude over time, while exhibiting the same shape.

Being normalized, the strain profile magnitude doesn't include relevant information, only its shape has to be considered, in particular tension–compression spread over rib length is of interest. Among other, weakly loaded ribs are exhibiting normalized strain profile whose magnitude is comparable to the one of highly loaded ribs. This aspect has to be kept in mind when comparing strain distribution over rib levels.

This profile allows for comparison in between subjects. Among other it can be used to assess how comparable are strain profile for a given loading type, whatever the severity. Indeed, varying the loading severity shouldn't modify this profile, while altering the RMS strain time history.

Vertical solid lines indicate fractures locations.

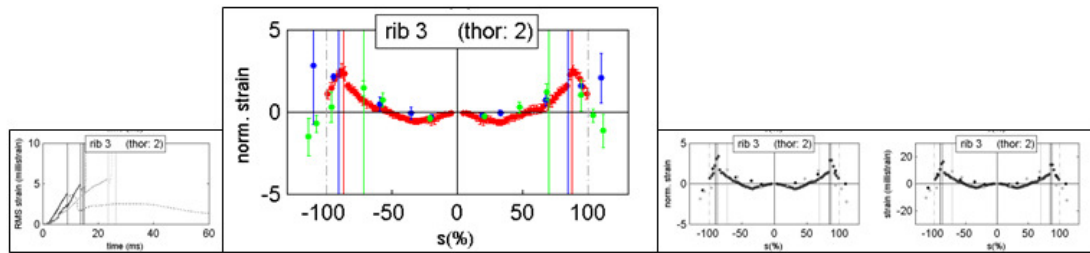


**Figure 4 Sample averaged normalized strain profile**

Column 3: Normalized strain profile at the time when RMS strain is maximum

Column 3 shows the normalized strain as a function of curvilinear abscissae at the time when RMS strain is maximum or at the time the first fracture occurs.

This strain profile is comparable to the previous one excepting that it relates to a single time event rather than the whole loading history. This is of great help in the case the averaged profiles exhibit high standard errors. Indeed, in that case, one cannot have a clear idea of the strain profile shape since this shape varies in time. It is then needed to select a given time to plot the profile. In that perspective, the time of rib fracture or of maximum loading state, is the time of higher interest.

In the case of small standard errors, this profile shape is very comparable to the previous one and doesn't provide additional information.

Vertical solid lines indicate fractures locations.

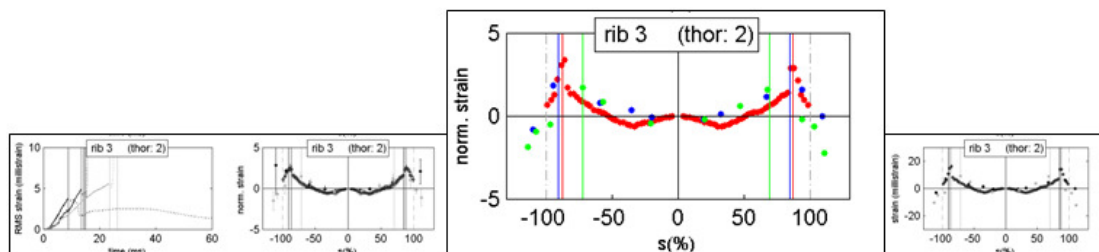


**Figure 5 Normalized strain profile at RMS max**

Column 4: Raw strain profile at the time when RMS strain is maximum

Column 4 shows the raw, or non-normalized, strain as a function of curvilinear abscissae at the time when RMS strain is maximum or at the time the first fracture occurs.

This profile, like the previous one, is useful in the case of high standard error.

Since it is non-normalized, the profile magnitude is of interest but should be interpreted with care. Indeed, for a given subject, increasing the loading severity should increase the profile magnitude. But comparison in between subjects can be spoiled by cross sectional properties differences. For a given loading pattern, a higher strain profile magnitude can be explained both by either an increased severity or a higher rib cross section height.

One should note that for a given subject, in the case of rib fracture, increasing severity will not increase the profile magnitude since this one is plotted at the time of rib fracture.

Vertical solid lines indicate fractures locations.

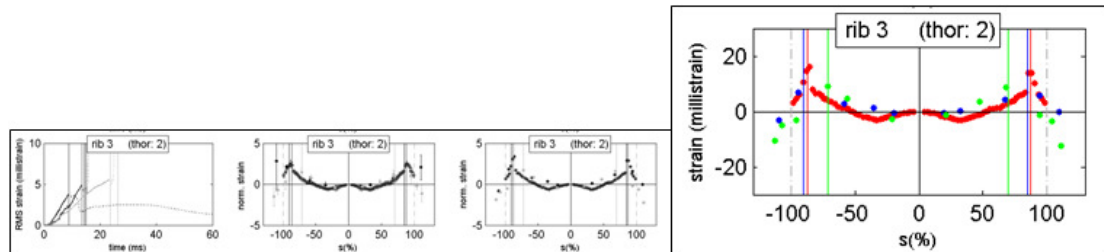


**Figure 6 Strain profile at RMS max**

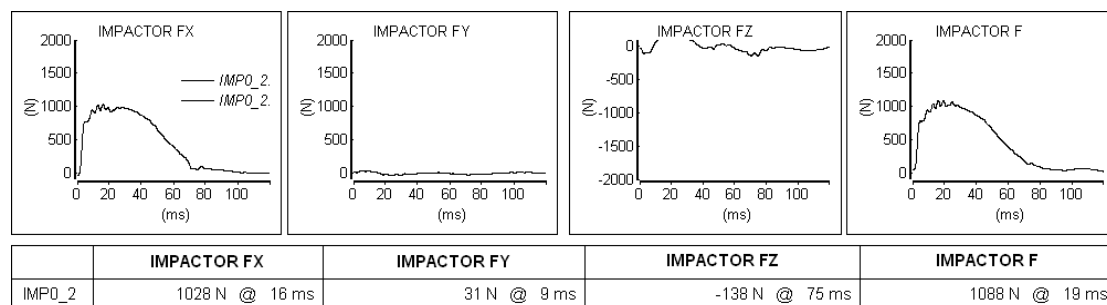
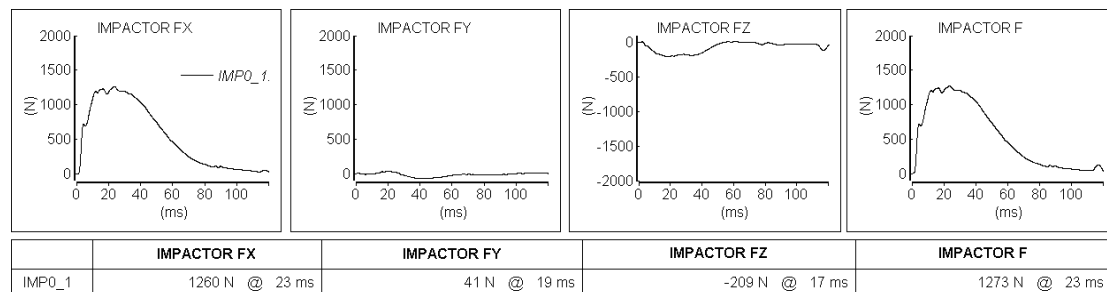
In the following sections are presented the test results for the four loading configurations: impactor , airbag , belt and harness.

For each configurations, two tests are available. Sensor time histories and peak values are presented first. Secondly are presented the injury details. Thirdly are shown gage analysis results. A last section gives conclusions regarding the configuration results.

### 5.5.2 Impactor test results

In LAB 2008 data set , the impactor configuration is comparable to the standard Kroell 4.3 m/s. Differences with Kroell are position of the arm and the hub guiding system .

**Table 37 IMP0\_1 and IMP0\_2 Impactor force**



Impactor force:

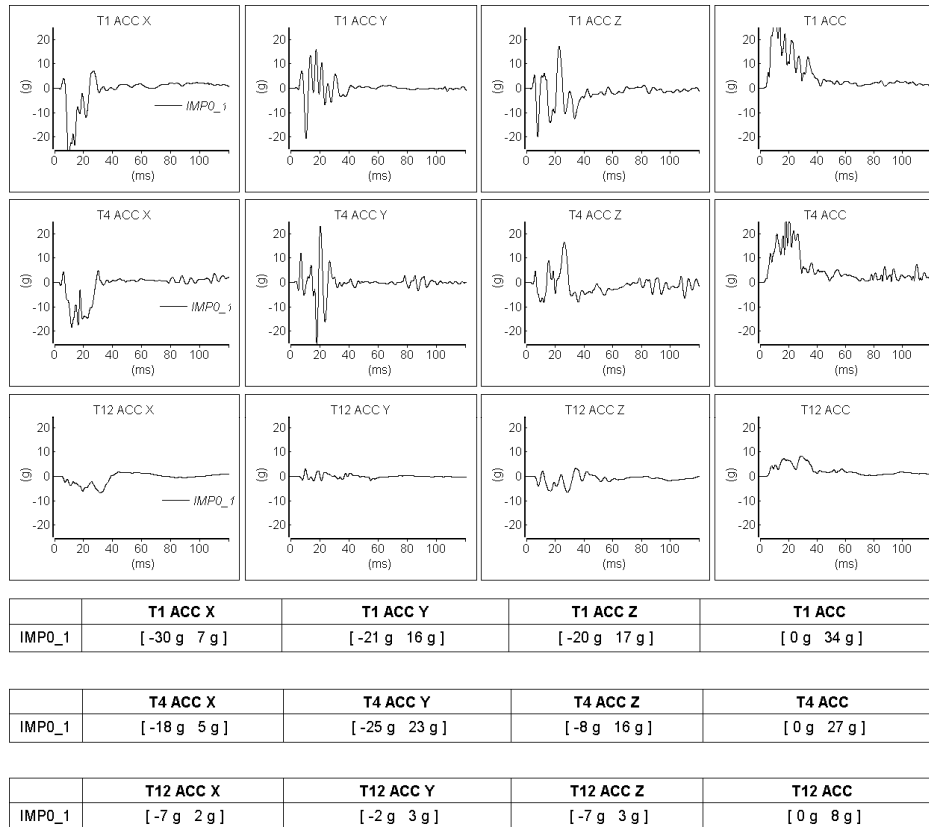
- CFC 180 filtered and the initial offset was removed

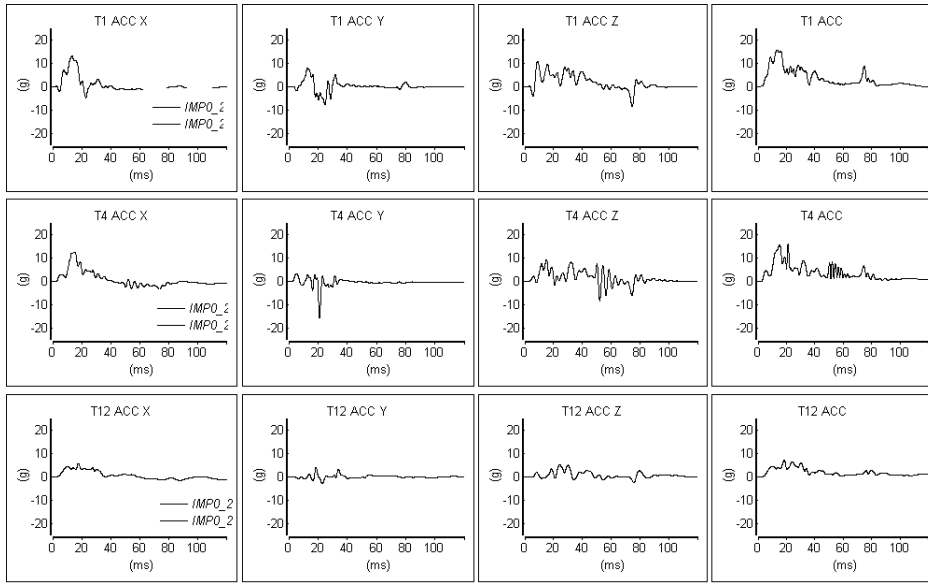
- inertially compensated with a mass of 2kg

Due to the guiding the impactor also slightly acts on the Z direction during the impact.

Peak impactor forces differs by 18% in between both subjects. One should note that IMP0\_1 subject is 18kg lighter than IMP0\_2

**Table 38 IMP0\_1 and IMP0\_2 Spine accelerations**





	T1 ACC X	T1 ACC Y	T1 ACC Z	T1 ACC
IMP0_2	[-5 g 13 g]	[-8 g 8 g]	[-8 g 11 g]	[0 g 16 g]

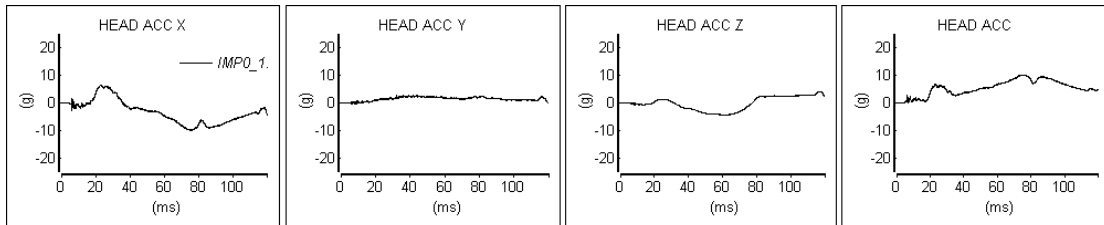
	T4 ACC X	T4 ACC Y	T4 ACC Z	T4 ACC
IMP0_2	[-4 g 13 g]	[-16 g 3 g]	[-8 g 9 g]	[0 g 16 g]

	T12 ACC X	T12 ACC Y	T12 ACC Z	T12 ACC
IMP0_2	[-1 g 6 g]	[-3 g 4 g]	[-2 g 5 g]	[0 g 7 g]

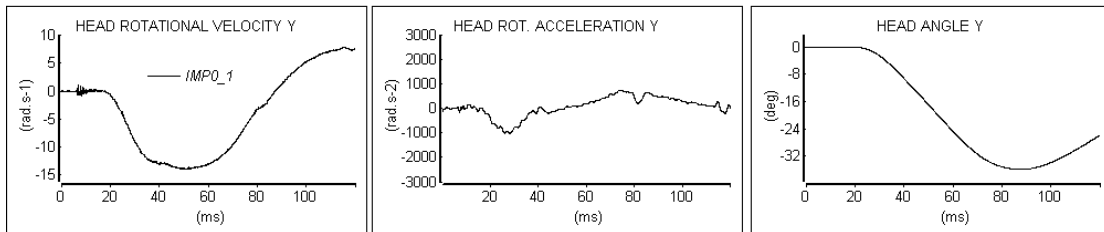
Spine accelerations:

- CFC 180 filtered and the initial offset was removed
- Expressed in local sensor coordinate

**Table 39 IMP0\_1 IMP0\_2 and Head kinematics**



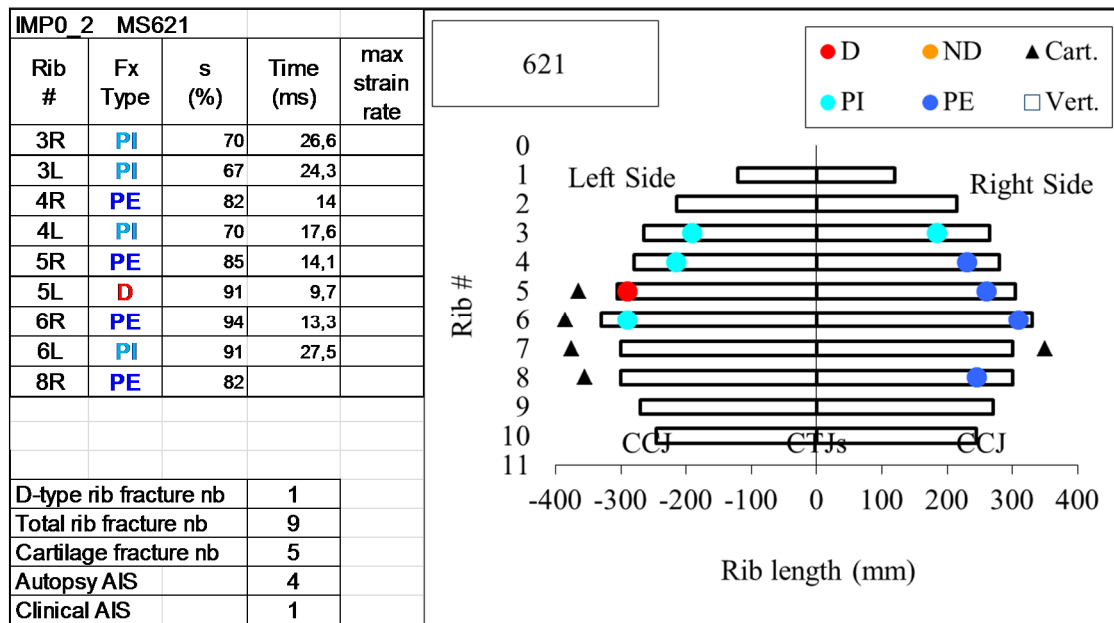
	HEAD ACC X	HEAD ACC Y	HEAD ACC Z	HEAD ACC
IMP0_1	[-10 g 6 g]	[-0 g 3 g]	[-4 g 4 g]	[0 g 10 g]



	HEAD VRY	HEAD ARY	HEAD RY
IMP0_1	8 rad.s-1 @ 115 ms	727 rad.s-2 @ 74 ms	0 deg @ 17 ms



**Table 41 IMP0\_2 Injury details**



In the presented plots, rib fractures were classified using four categories: (D) complete with displacement, (ND) complete without displacement, (PE) partial with rupture of the external cortical bone and (PI) partial with rupture of the internal cortical bone. Cart notation relates to cartilages fractures.

Both subjects sustained numerous rib and cartilage fractures: 15 and 14 fractures for IMP0\_1 and IMP0\_2 respectively. In both cases those fractures resulted in autopsy AIS 4.

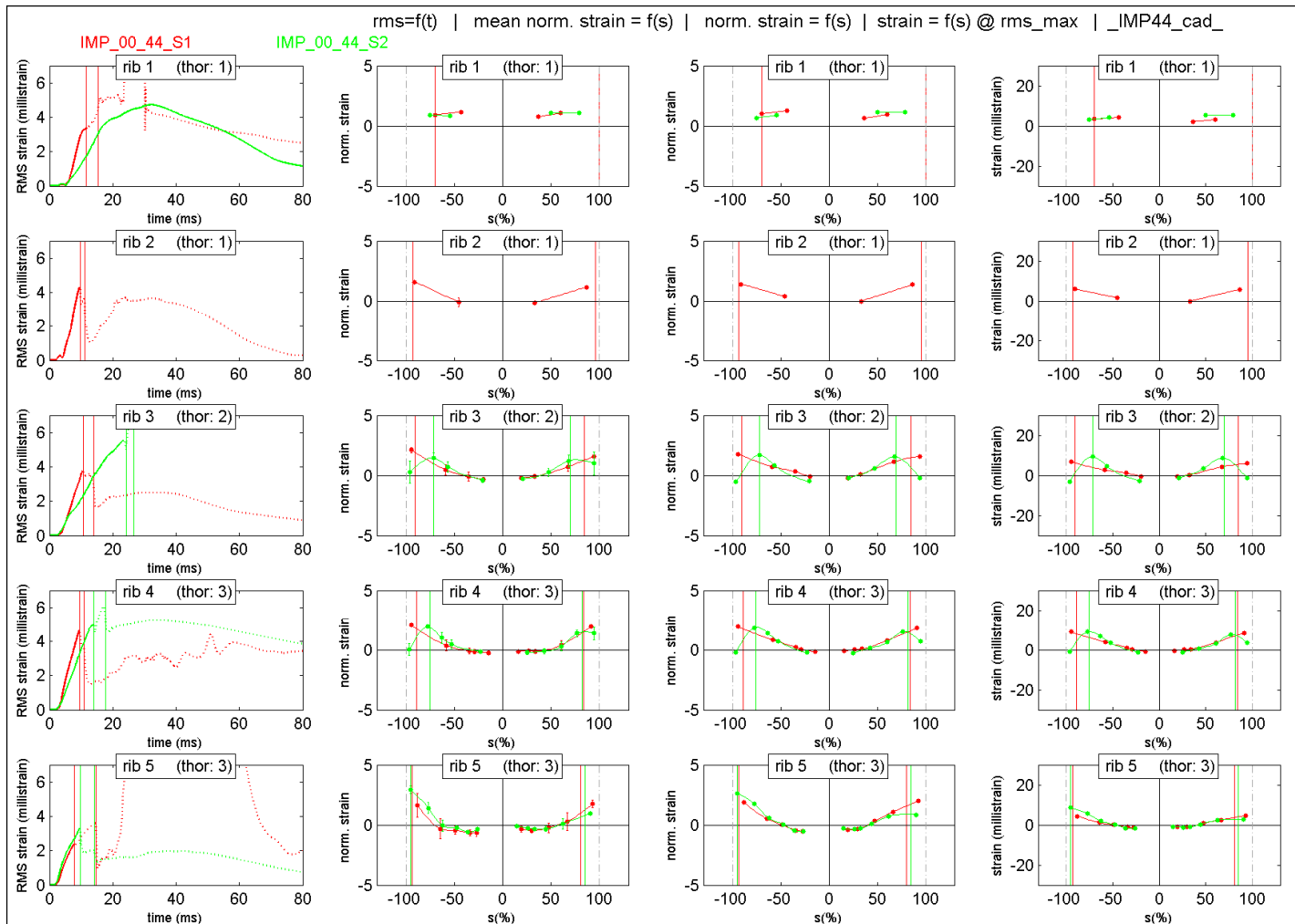


Figure 7 IMP0\_1 IMP0\_2 Strain pattern Rib 1-5

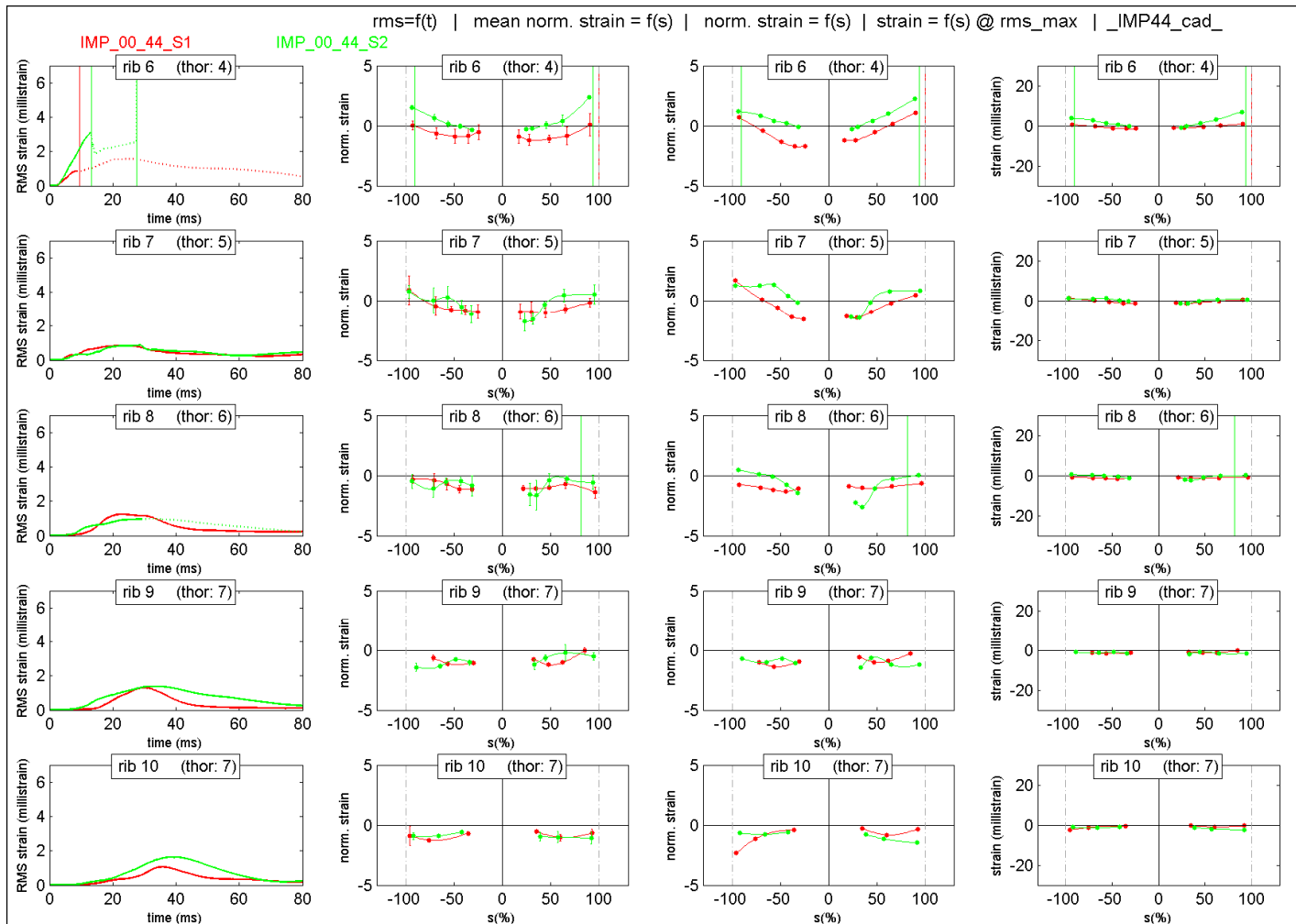


Figure 8 IMP0\_1 IMP0\_2 Strain pattern Rib 6-1

---

### 5.5.3 Conclusions on impactor loading

Both IMP0\_1 and IMP0\_2 tests have been run in conditions comparable to the standard Kroell 4.3m/s.

The impactor peak forces were 1260N (IMP0\_1) and 1028N (IMP0\_2).

Both surrogates sustained severe injury levels with 15 and 14 rib fractures.

One can observe that from rib level 1 up to rib level 6, strain profiles display the same pattern on the whole:

- negative strains (compression) at the rear part of the rib, with a minimum value close to the costo-vertebral joint.
- point of zero-strain for each left or right rib, whose location depends of the rib number.
- positive strains (tension) with maximum values at a location depending on the rib number.

Lower rib levels are exhibiting a different pattern and are mainly loaded in compression. Rib loading amplitude, as seen on peak values in column 1 and 4, are very low for lower rib levels (7,8,9,10) compared to the upper one.

In conclusion, both test are exhibiting comparable strain profiles where upper rib levels are mainly loaded in tension and lower one in compression. Transition from tension to compression occurs at rib level 6 or 7 depending on the subject.

### 5.5.4 Airbag test results

In LAB\_2005 LAB\_2008 and the same airbag is used and common distances have been tested.

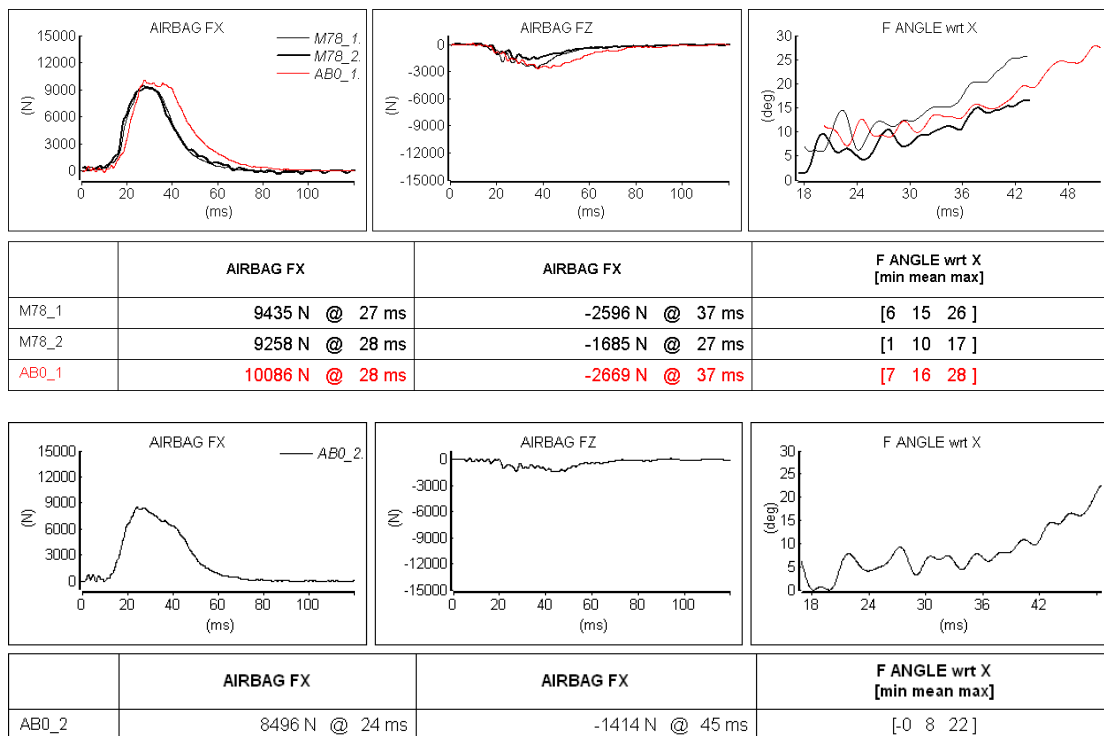
The major differences between the two test campaign are :

- LAB 2005 , plate force and surrogate were rotated 15° forward to ensure a stable position
- LAB 2008 , another subframe is used and the plate force and surrogate are positioned vertically

Therefore LAB 2008 airbag configuration is comparable to the LAB 2005 membrane configuration.

In the following the outcome of AB0\_1 (78mm) is overlaid to the response of M78\_1 and M78\_2.

**Table 42 AB0\_1 and AB0\_2 airbag force: FX / FZ balance**



Airbag forces:

- CFC 180 filtered and the initial offset was removed
- Expressed in the plate coordinate frame

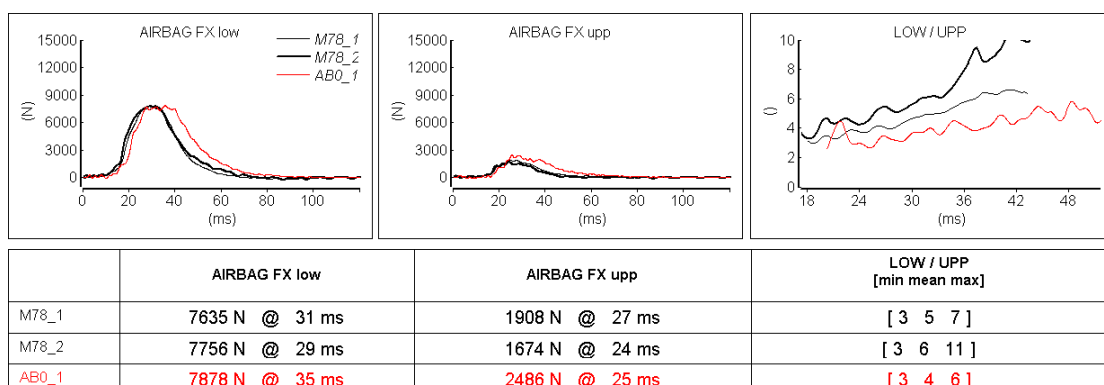
AB0\_1 presents airbag responses in accordance with M78\_1 M78\_2 in terms of magnitude, shape and balance. The airbag mainly acts in the X direction.

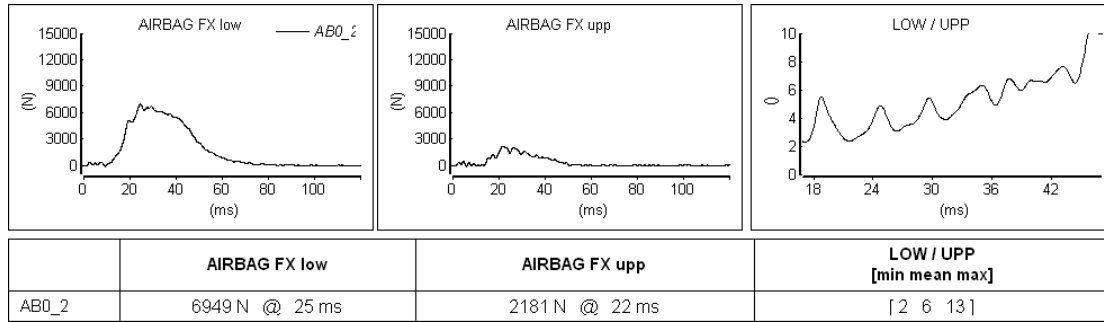
The lower airbag peak force obtained for AB0\_2 is an unexpected result since 13mm gap should have resulted in a higher force than the one measured at 78mm.

A post test airbag examination led to the conclusion that the pyro technic generator used in the case of AB0\_2 was out of nominal ranges. Thus this configuration can not be duplicated with a dummy since there is no mean to mimic this non standard airbag loading.

That's why AB0\_2 results are not compared to M13\_1 and M13\_2 tests from Lebarbe configurations and presented on their own.

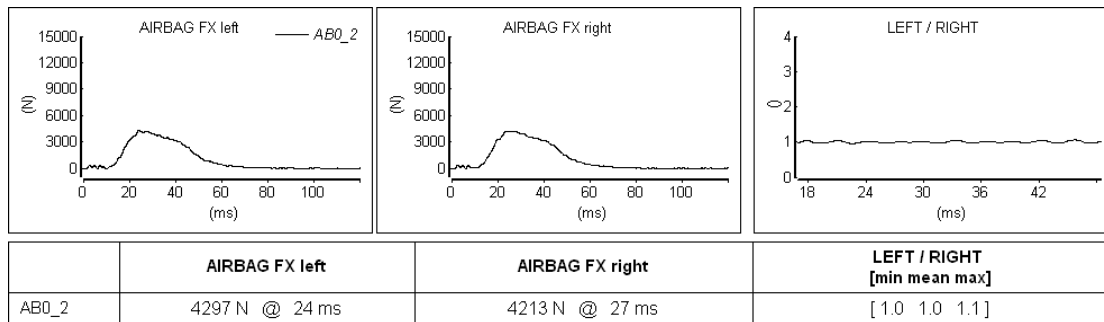
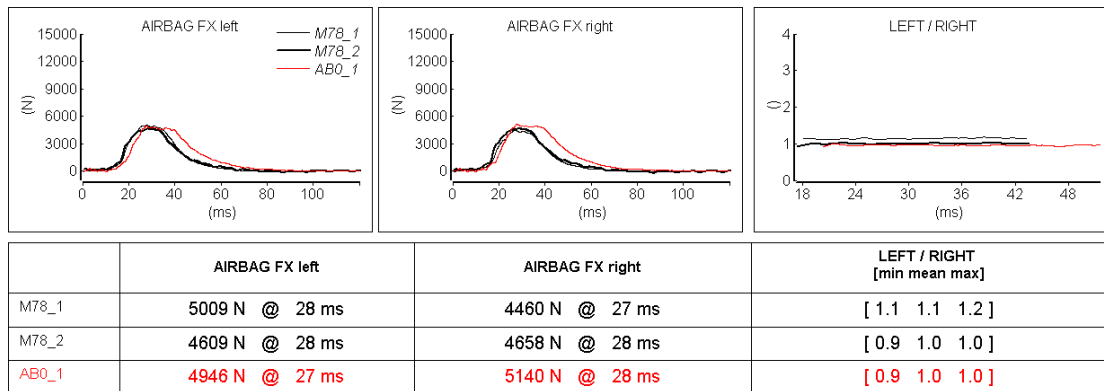
**Table 43 AB0\_1 and AB\_2 airbag force: low / upp balance**





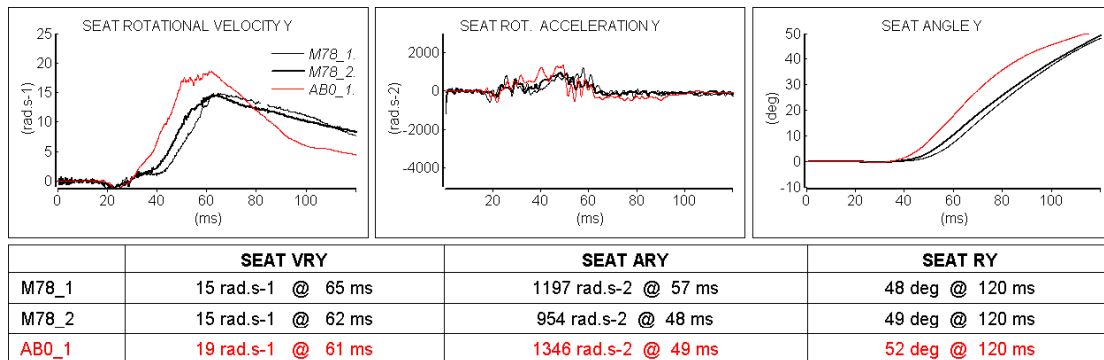
In accordance with M78\_1 and M78\_2, the airbag X force is mainly applied by the lower part of the plate. AB0\_2 presents the same trend in terms of low/upp ratio.

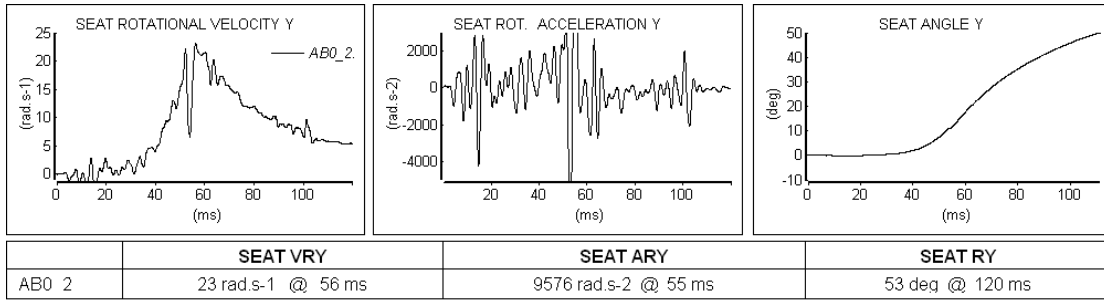
**Table 44 AB0\_1 and AB0\_2 airbag force: left / right balance**



In accordance with M78\_1 and M78\_2, the airbag X force is symmetric with regard to the X Z plane. AB0\_2 presents the same trend in terms of left/right ratio.

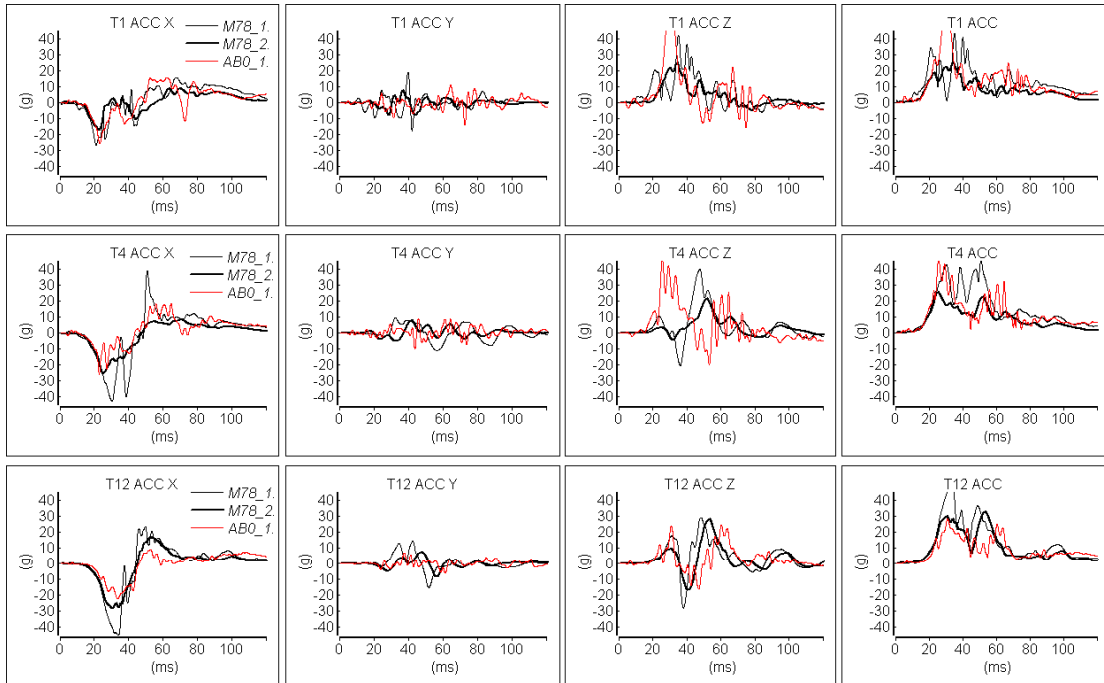
**Table 45 AB0\_1 and AB0\_2 sub frame seat kinematics**



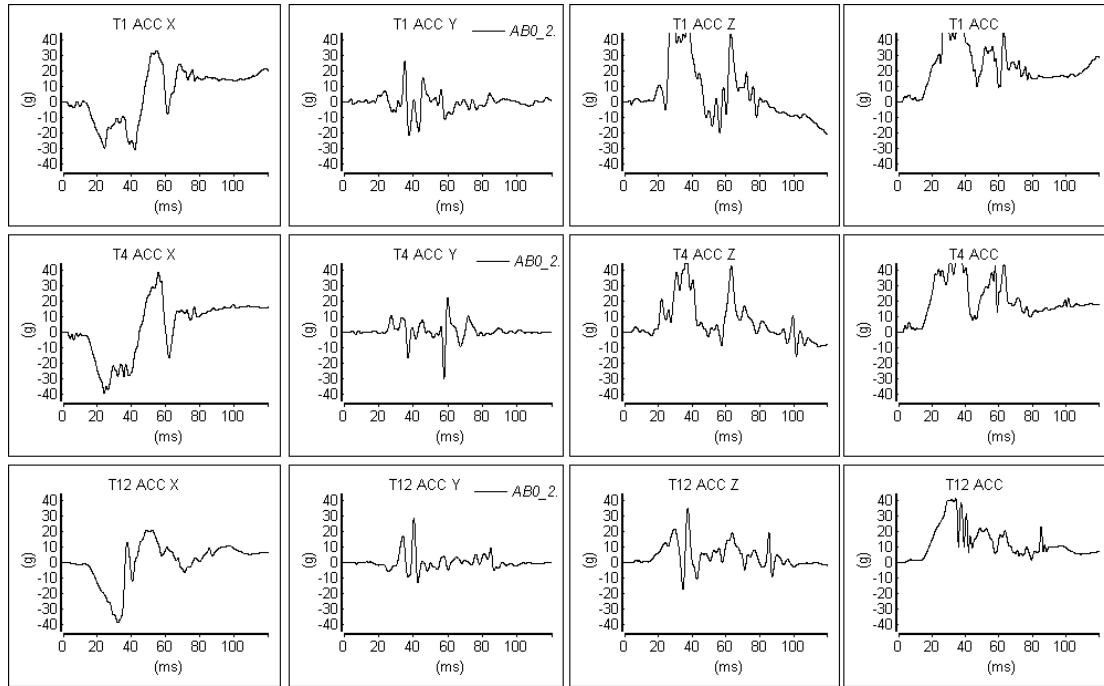


Angular Y velocity is CFC 60 filtered.

**Table 46 AB0\_1 and AB0\_2 Spine accelerations**



	T1 ACC X	T1 ACC Y	T1 ACC Z	T1 ACC
M78_1	[-26 g 15 g]	[-18 g 19 g]	[-6 g 42 g]	[0 g 43 g]
M78_2	[-17 g 9 g]	[-8 g 8 g]	[-5 g 25 g]	[0 g 25 g]
ABO_1	[-25 g 16 g]	[-14 g 11 g]	[-16 g 50 g]	[0 g 51 g]
	T4 ACC X	T4 ACC Y	T4 ACC Z	T4 ACC
M78_1	[-42 g 39 g]	[-11 g 9 g]	[-21 g 40 g]	[0 g 45 g]
M78_2	[-25 g 8 g]	[-5 g 8 g]	[-4 g 21 g]	[0 g 26 g]
ABO_1	[-26 g 18 g]	[-10 g 9 g]	[-20 g 46 g]	[0 g 46 g]
	T12 ACC X	T12 ACC Y	T12 ACC Z	T12 ACC
M78_1	[-45 g 23 g]	[-15 g 14 g]	[-28 g 29 g]	[0 g 49 g]
M78_2	[-28 g 17 g]	[-8 g 7 g]	[-17 g 28 g]	[0 g 33 g]
ABO_1	[-22 g 9 g]	[-6 g 7 g]	[-16 g 24 g]	[0 g 28 g]



	T1 ACC X	T1 ACC Y	T1 ACC Z	T1 ACC
AB0_2	[-31 g 33 g]	[-21 g 26 g]	[-21 g 71 g]	[0 g 73 g]

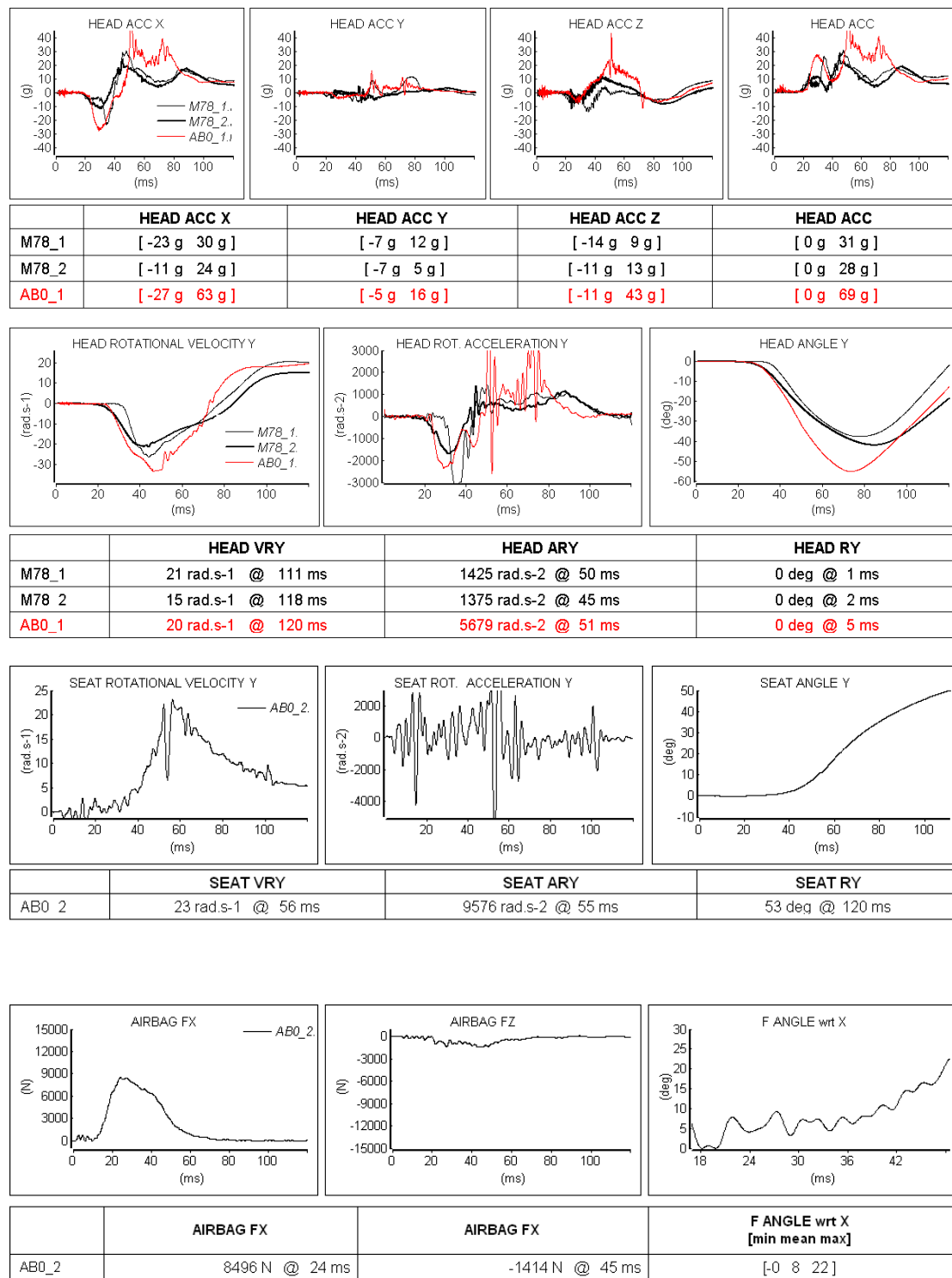
	T4 ACC X	T4 ACC Y	T4 ACC Z	T4 ACC
AB0_2	[-40 g 39 g]	[-31 g 22 g]	[-16 g 46 g]	[0 g 54 g]

	T12 ACC X	T12 ACC Y	T12 ACC Z	T12 ACC
AB0_2	[-39 g 21 g]	[-13 g 29 g]	[-17 g 35 g]	[0 g 42 g]

Spine accelerations:

- CFC 180 filtered and the initial offset was removed
- Expressed in local sensor coordinate
- **Remark:** for M78\_1 and M78\_2 the so called "T12" accelerometer was actually located on T8

**Table 47 AB0\_1 and AB0\_2 Head kinematics**



Head accelerations:

- CFC 1000 filtered and the initial offset was removed
- expressed in local sensor frame
- Note that the sensor is not located at head CG, see appendix



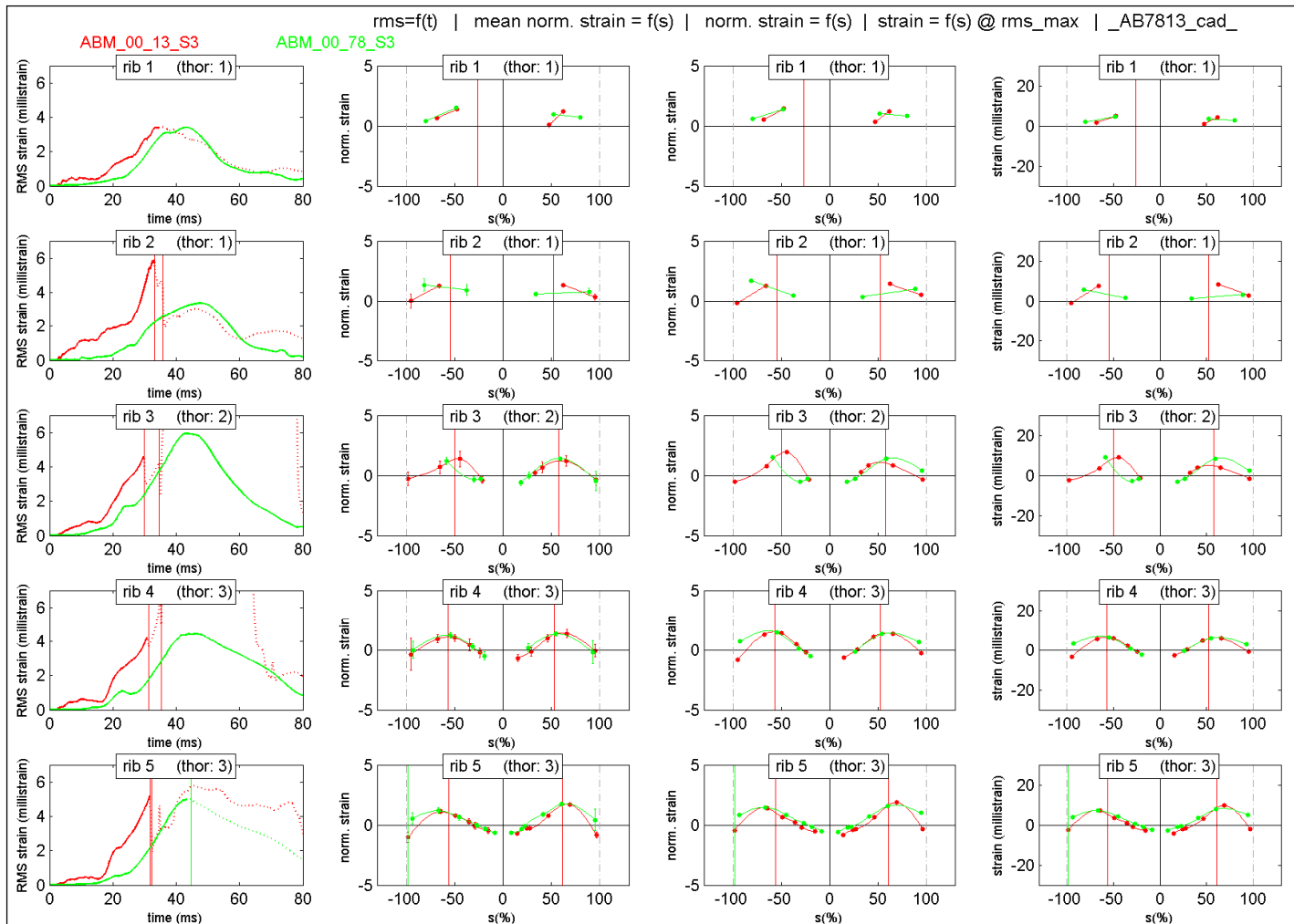


Figure 9 AB13 AB78 Strain pattern Rib 1-5

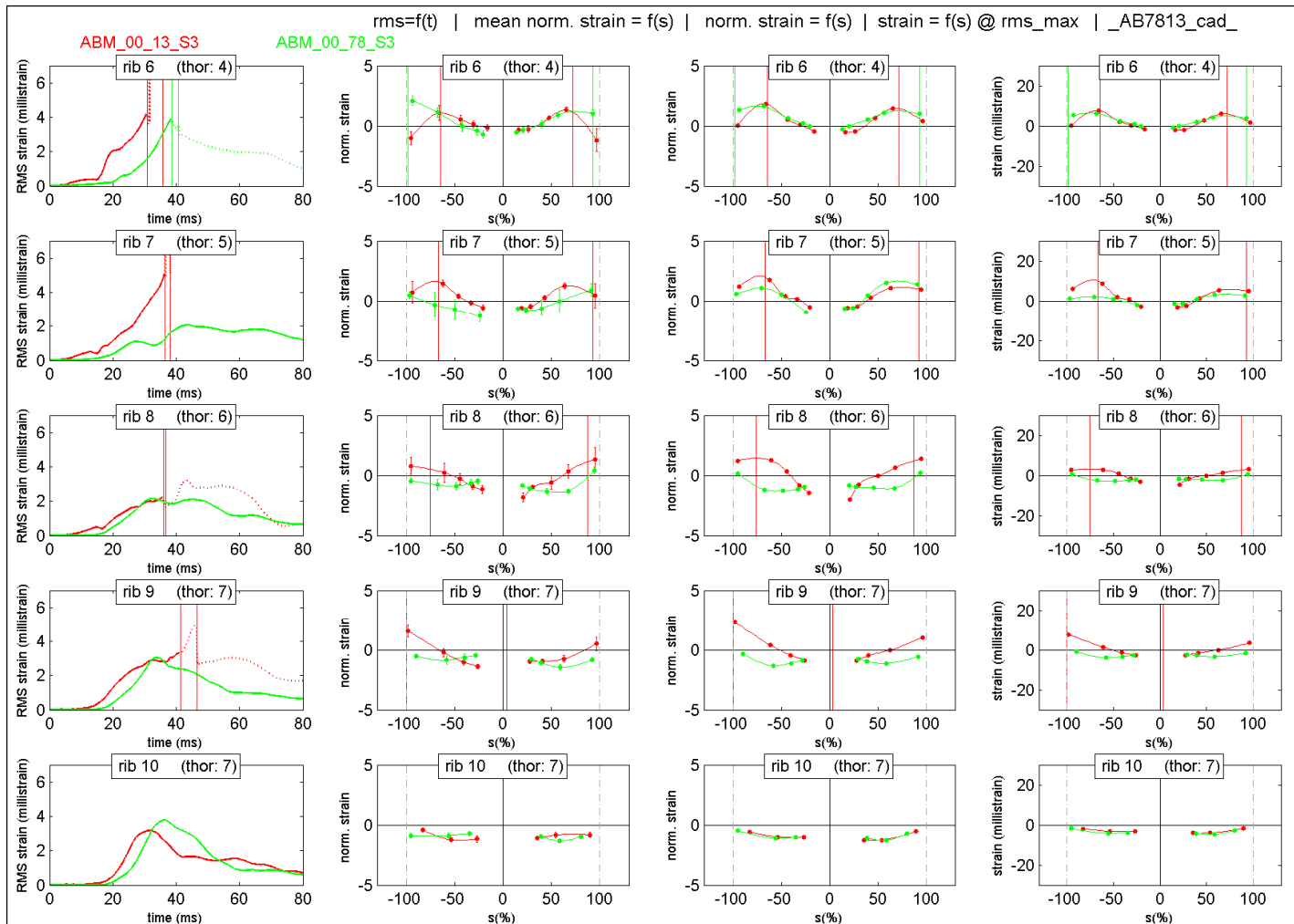


Figure 10 AB13 AB78 Strain pattern Rib 6-10

---

### 5.5.5 Conclusions on airbag loading

AB0\_1 and AB0\_2 tests have been run with different gap in between the airbag support and the PMHS sternum, resulting in different number of rib fracture.

The highest severity was obtained for:

- AB0\_2 with a 13mm gap and 24 rib and cartilages fractures compared to
- AB0\_1 where a larger gap of 78mm was used and led to 8 rib and cartilages fractures.

Since severity levels differ, strain profile comparison should be made by the mean of normalized data (column 2 and 3).

Despite of the difference in loading severity, on can observe that from rib level 1 up to rib level 6, strain profiles display the same pattern on the whole:

- negative strains (compression) at the rear part of the rib, with a minimum value close to the costo-vertebral joint.
- point of zero-strain for each left or right rib, whose location depends of the rib number.
- positive strains (tension) with maximum values at a location depending on the rib number.
- second zero-strain point close to the costo-chondral joint.

As far as the lower rib levels are concerned (rib 7-10), strain profiles seems at a first sight to differ from one test to another but differences are thought to be related to differences in gap between chest and airbag plate:

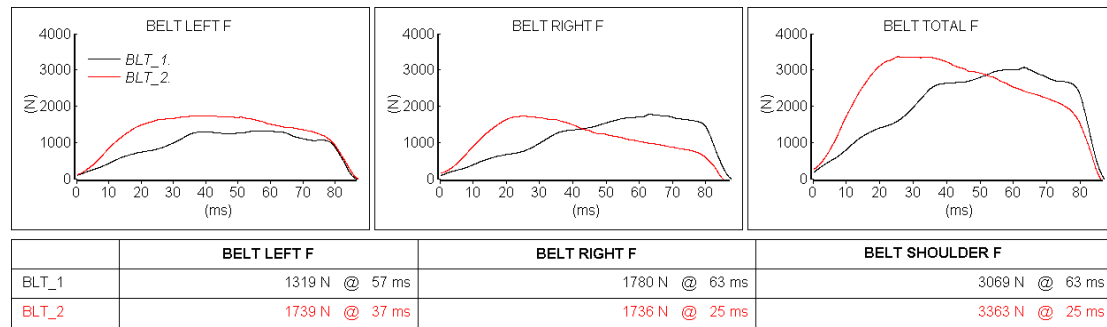
- In the case of AB0\_1 (78mm), the external surface of lower rib levels, in contrast to the upper ones, are mainly loaded in compression. This bulg-out deformation pattern, attributed to organ loading is observable from rib level 7 up to rib level 10.
- In the case of AB0\_2, the smaller gap between the subject and the airbag leads to an higher involvement of the lower rib levels which are loaded by the airbag rather than by the organs. As a consequence, the bulg-out deformation pattern is still observable with the lower rib level but is limited to levels 9 and 10 where the airbag loading is less significant.

At both distances, surrogates sustained injuries, with 22 fractures for the most severe distance and 3 for the softer one.

On conclusion, both tests are exhibiting comparable strain profiles where upper rib levels are mainly loaded in tension and lower one in compression. Transition from tension to compression occurs at rib level 7 for the largest gap and occurs at rib level 9 for the closest one.

## 5.5.6 Belt test results

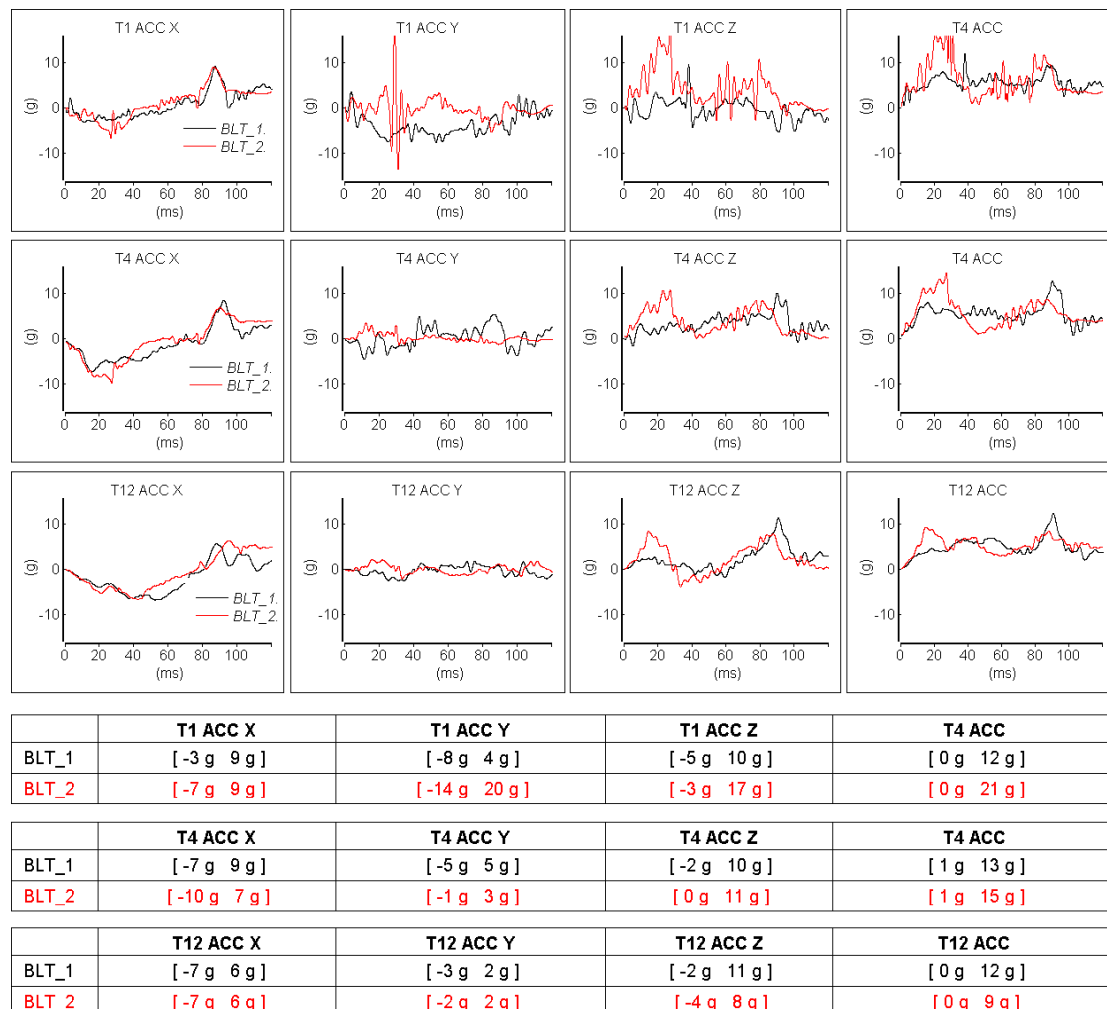
**Table 50 BLT\_1 and BLT\_2 Belt forces**



Belt forces were CFC 1000 filtered and the initial offset was removed.

As mentioned in the test description, the tension loading pattern applied by the hydraulic machine was not the same in the two test.

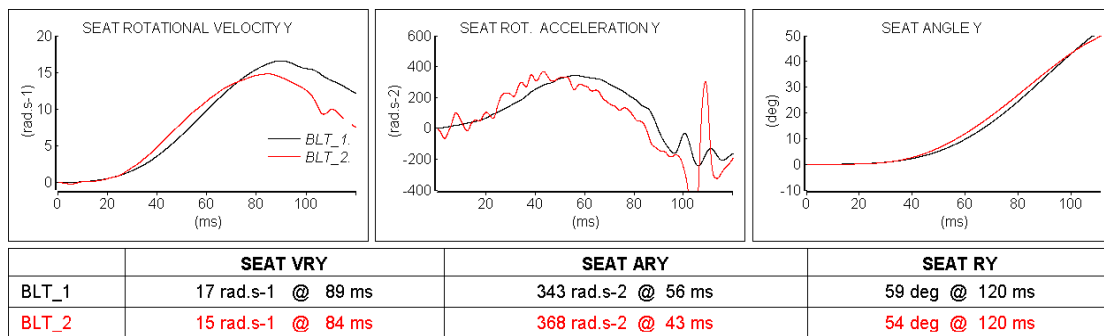
**Table 51 BLT\_1 and BLT\_2 Spine accelerations**



Spine accelerations:

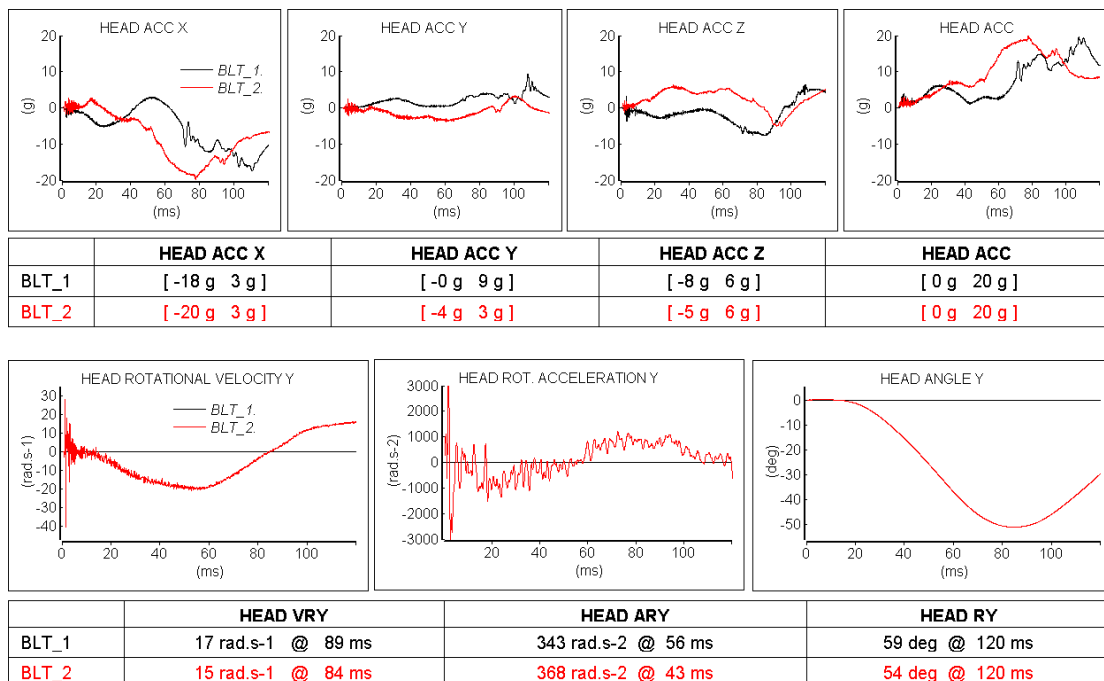
- CFC 180 filtered and the initial offset was removed
- Expressed in local sensor frame

**Table 52 BLT\_1 and BLT\_2 Seat kinematics**



Subframe Y angular velocity was CFC 60 filtered.

**Table 53 BLT\_1 and BLT\_2 Head kinematics**



Head accelerations:

- CFC 1000 filtered and the initial offset was removed
- Expressed in local sensor frame
- Note that the sensor is not located at head CG, see appendix.

Head angular velocity :

- CFC 1000 filtered and the initial offset was removed

The derived head angular acceleration has been CFC 180 filtered

For test BLT\_1 head rotational velocity didn't work properly and is not plotted.



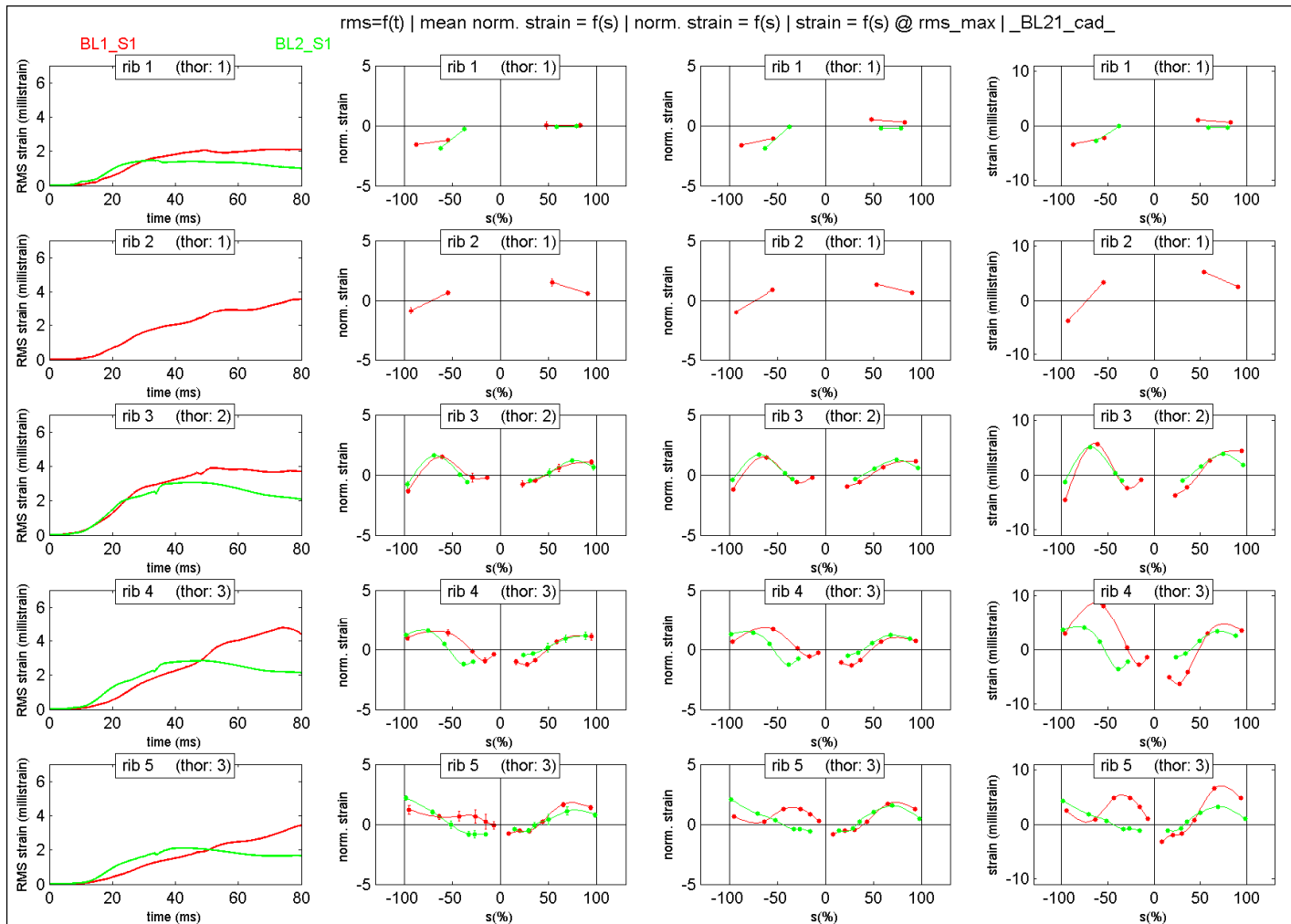


Figure 11 BLT\_1 BLT\_2 Strain pattern Rib 1-5

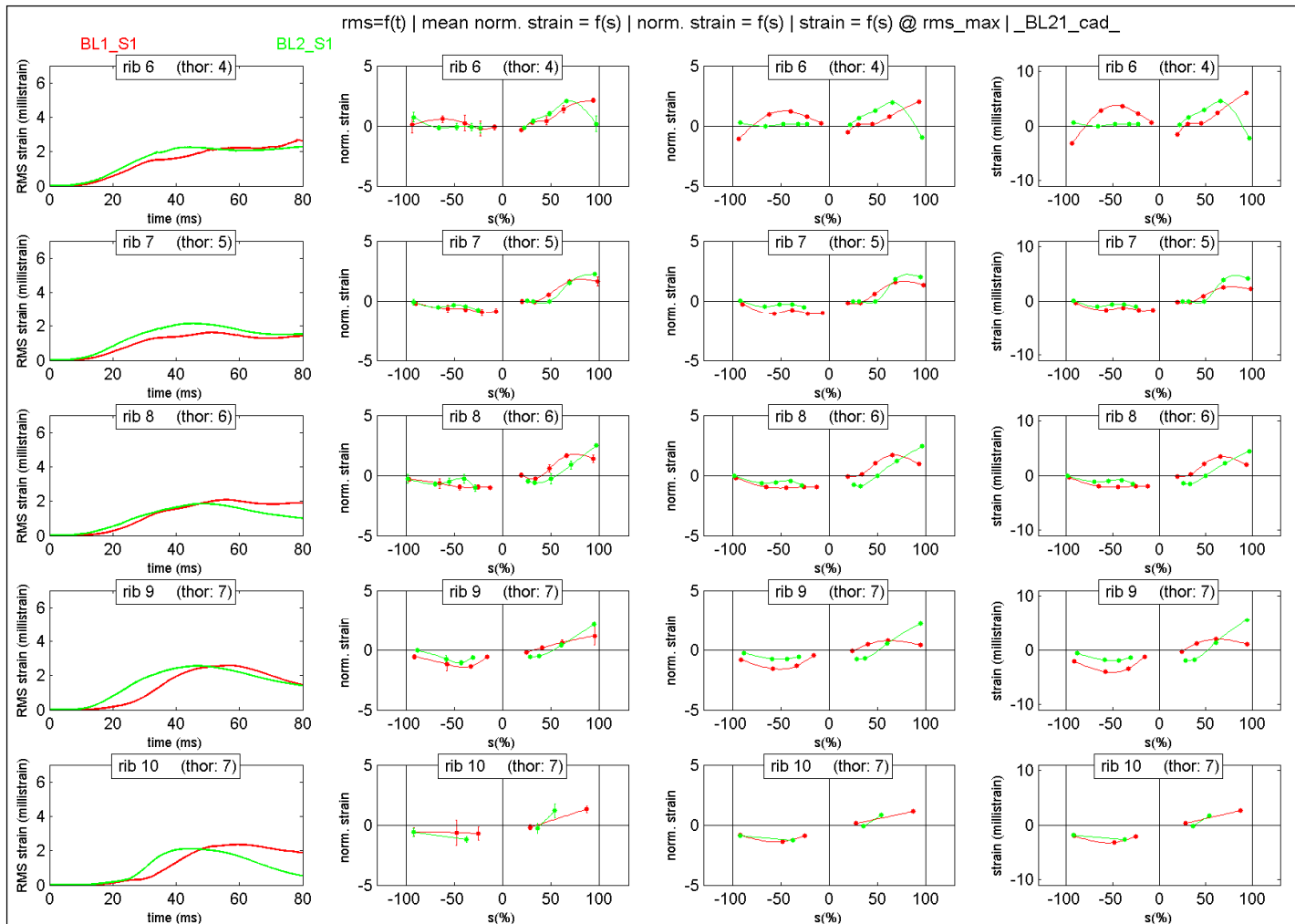


Figure 12 Table 56 BLT\_1 BLT\_2 Strain pattern Rib 6-10

---

### 5.5.7 Conclusions on belt loading

Due to the test set up as well as the way the load was applied to the subject's thorax, this testing configuration is very mild (compared with the other configurations described).

Indeed, in order to avoid interactions in between SHPM spine and a set up back plate, the belt load is applied on the thorax without any back support. The resulting belt tension is then related to the inertial loading of the thorax, which would have required a higher level of acceleration to reach classical belt tension levels such as 4000N. One should note that BLT\_2 was attempted to increase the belt loading tension with regard to BLT\_1.

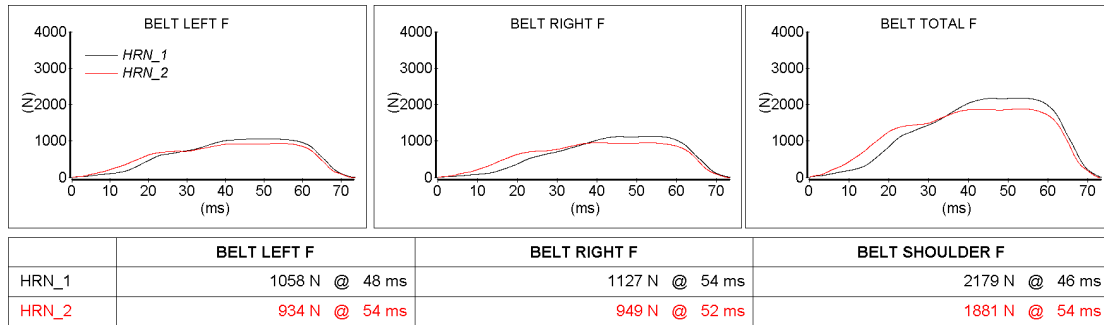
Due to that limitations, recorded belt loading were respectively of 3069N and 3363N for BLT\_1 and BLT\_2 respectively. This resulted in no rib fractures for neither of both surrogates. Only PMHS 595 sustained 3 cartilages fractures

Strain profiles are nevertheless of interest. One can observe that for rib levels 3-4-5 the strain profile exhibits a zero strain location close to 50% and a maximum strain location close to 75%. Below 50% the strain is negative and positive beyond. The right and left sides are exhibiting comparable patterns.

In the case of lower level ribs, a dissymmetric pattern occurs from rib level 6. Right side ribs are loaded mainly in tension while left side ribs are loaded in compression. Compression loading of the left side relates to bulging out of this area of the thorax.

## 5.5.8 Harness test results

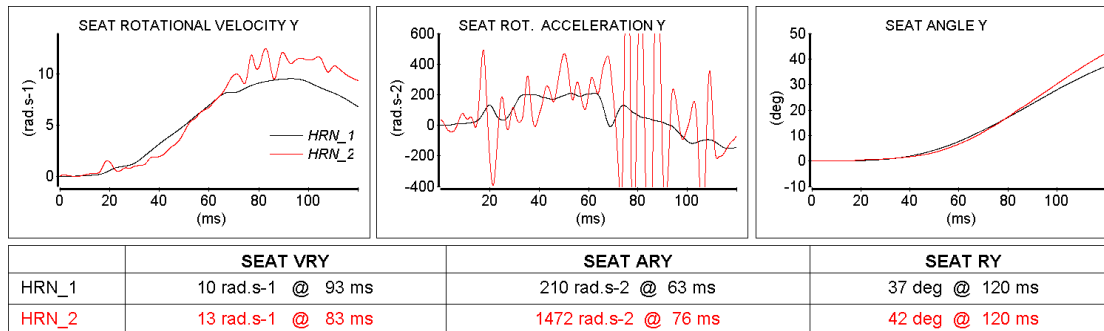
**Table 56 HRN\_1 and HRN\_2 Belt forces**



Belt forces were CFC 1000 filtered and the initial offset was removed.

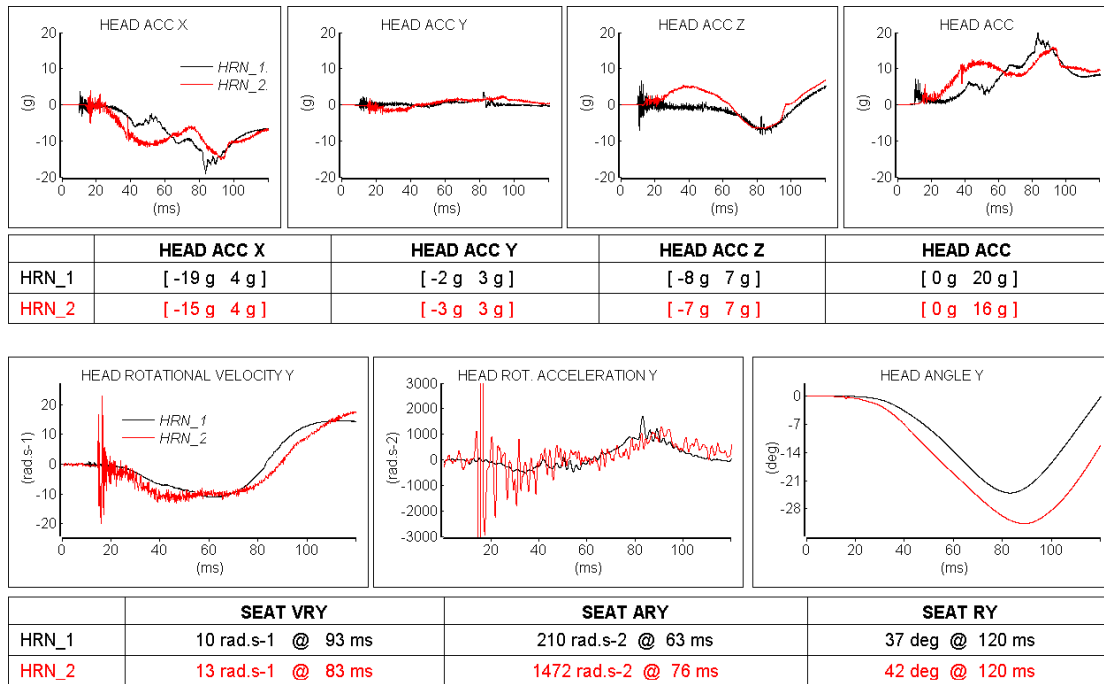
As mentioned in the test description, the tension loading pattern applied by the hydraulic machine was not the same in the two test.

**Table 57 HRN\_1 and HRN\_2 Sub frame kinematics**



Subframe Y angular velocity is CFC 60 filtered.

**Table 58 HRN\_1 and HRN\_2 Head kinematics**



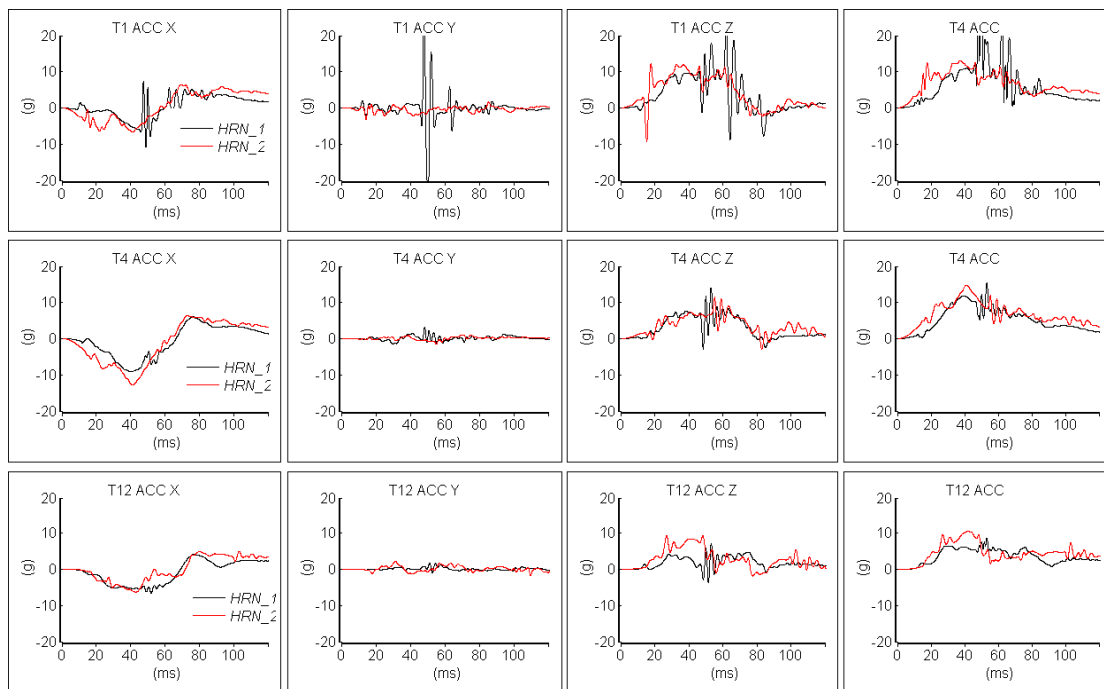
Head accelerations:

- CFC 1000 filtered and the initial offset was removed
- expressed in local sensor frame
- Note that the sensor is not located at head CG, see appendix

Head angular velocity:

- CFC 1000 filtered and the initial offset was removed
- The derived head angular acceleration has been CFC 180 filtered

**Table 59 HRN\_1 and HRN\_2 Spine accelerations**



	<b>T1 ACC X</b>	<b>T1 ACC Y</b>	<b>T1 ACC Z</b>	<b>T4 ACC</b>
<b>HRN_1</b>	[-11 g 7 g]	[-24 g 30 g]	[-9 g 26 g]	[0 g 30 g]
<b>HRN_2</b>	[-7 g 6 g]	[-3 g 2 g]	[-9 g 12 g]	[0 g 13 g]
	<b>T4 ACC X</b>	<b>T4 ACC Y</b>	<b>T4 ACC Z</b>	<b>T4 ACC</b>
<b>HRN_1</b>	[-9 g 6 g]	[-1 g 3 g]	[-3 g 14 g]	[0 g 15 g]
<b>HRN_2</b>	[-13 g 6 g]	[-2 g 1 g]	[-3 g 11 g]	[0 g 15 g]
	<b>T12 ACC X</b>	<b>T12 ACC Y</b>	<b>T12 ACC Z</b>	<b>T12 ACC</b>
<b>HRN_1</b>	[-7 g 4 g]	[-1 g 2 g]	[-4 g 7 g]	[0 g 9 g]
<b>HRN_2</b>	[-6 g 5 g]	[-2 g 2 g]	[-2 g 9 g]	[0 g 10 g]

Spine accelerations:

- CFC 180 filtered and the initial offset was removed
- Expressed in local sensor coordinate

The noisy part of the T1 signal around 50ms could be related to the rib fractures occurring at 50 (left) and 47 (right).

**Table 60 HRN\_1 Injury details**

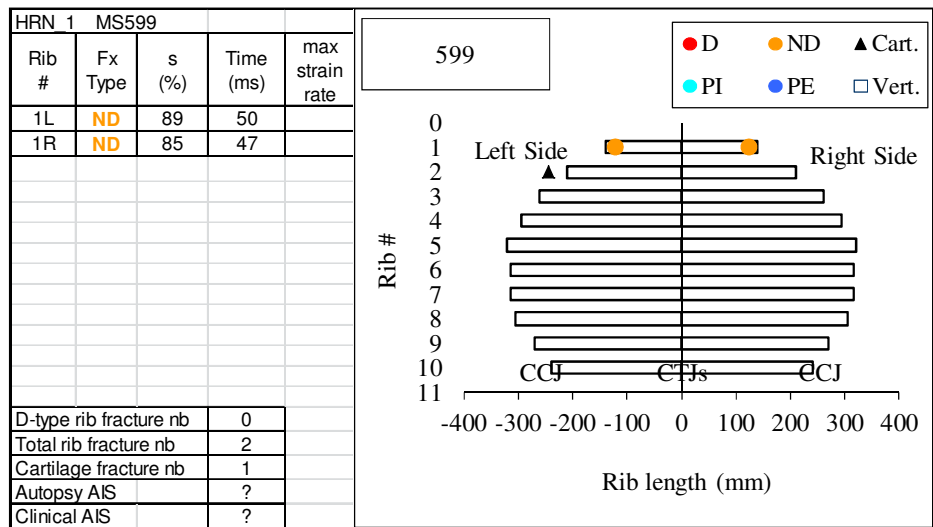
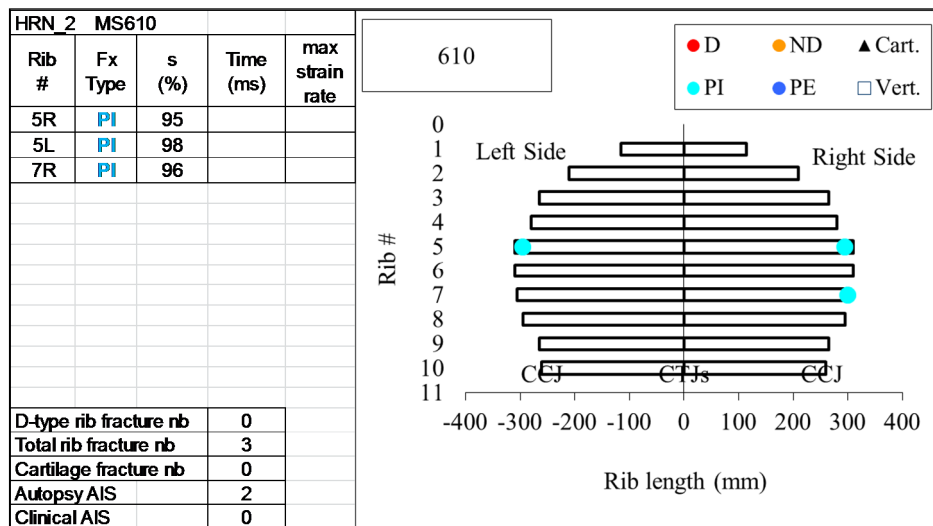


**Table 61 HRN\_2 Injury details**



Few injuries were observed in harness loading configuration.

For both subjects, no rib fracture with displacement was sustained.

Only 3 partial rib fractures were observed with subject 610 and 2 non disjoint fractures in the case of subject 599. In this latest case, no classical sharp drop of the strain signal was observed for ribs 5 and 6. Therefore, it could be that rib fractures didn't occur during the test.

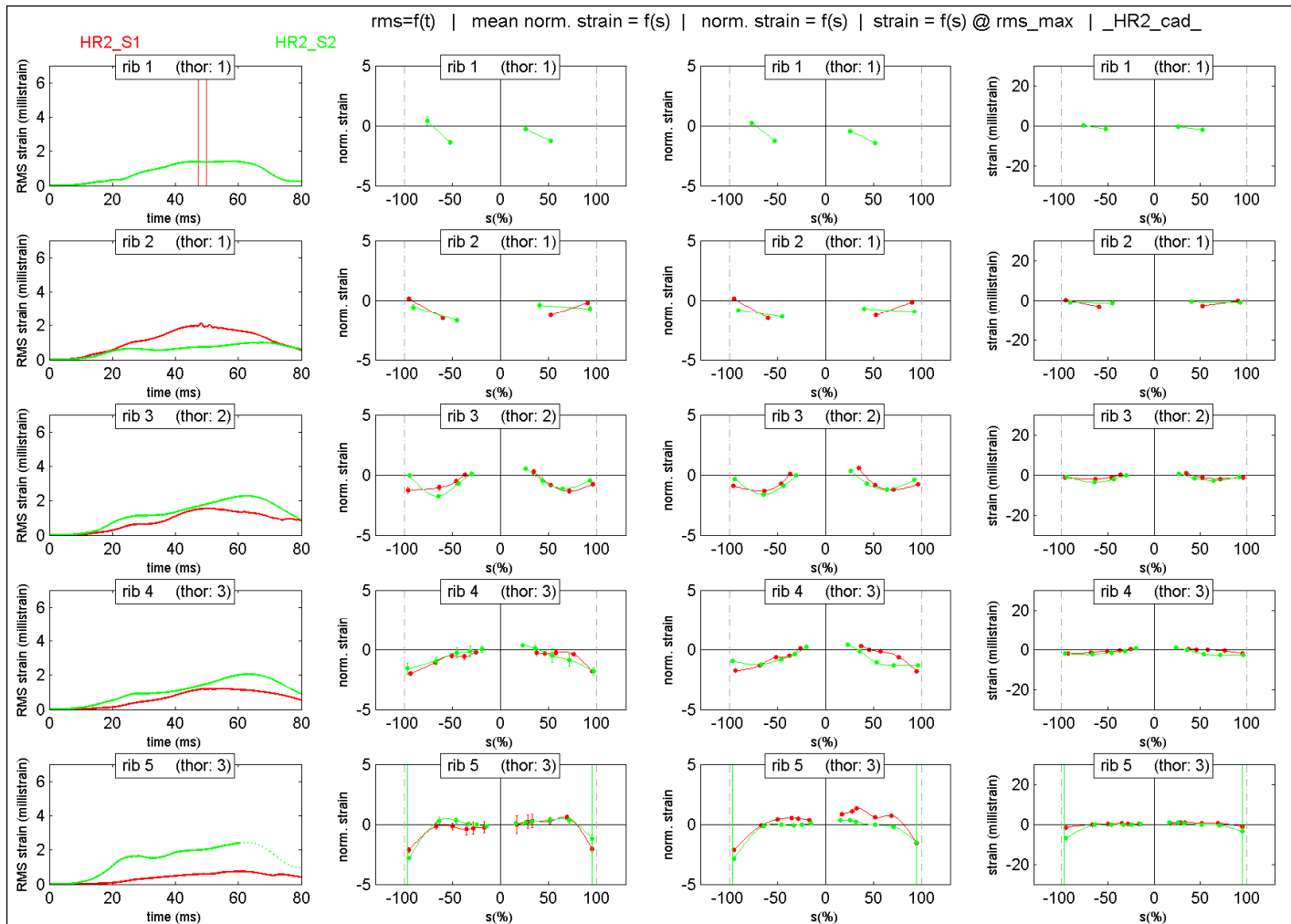


Figure 13 HRN\_1 HRN\_2 Strain pattern Rib 1-5

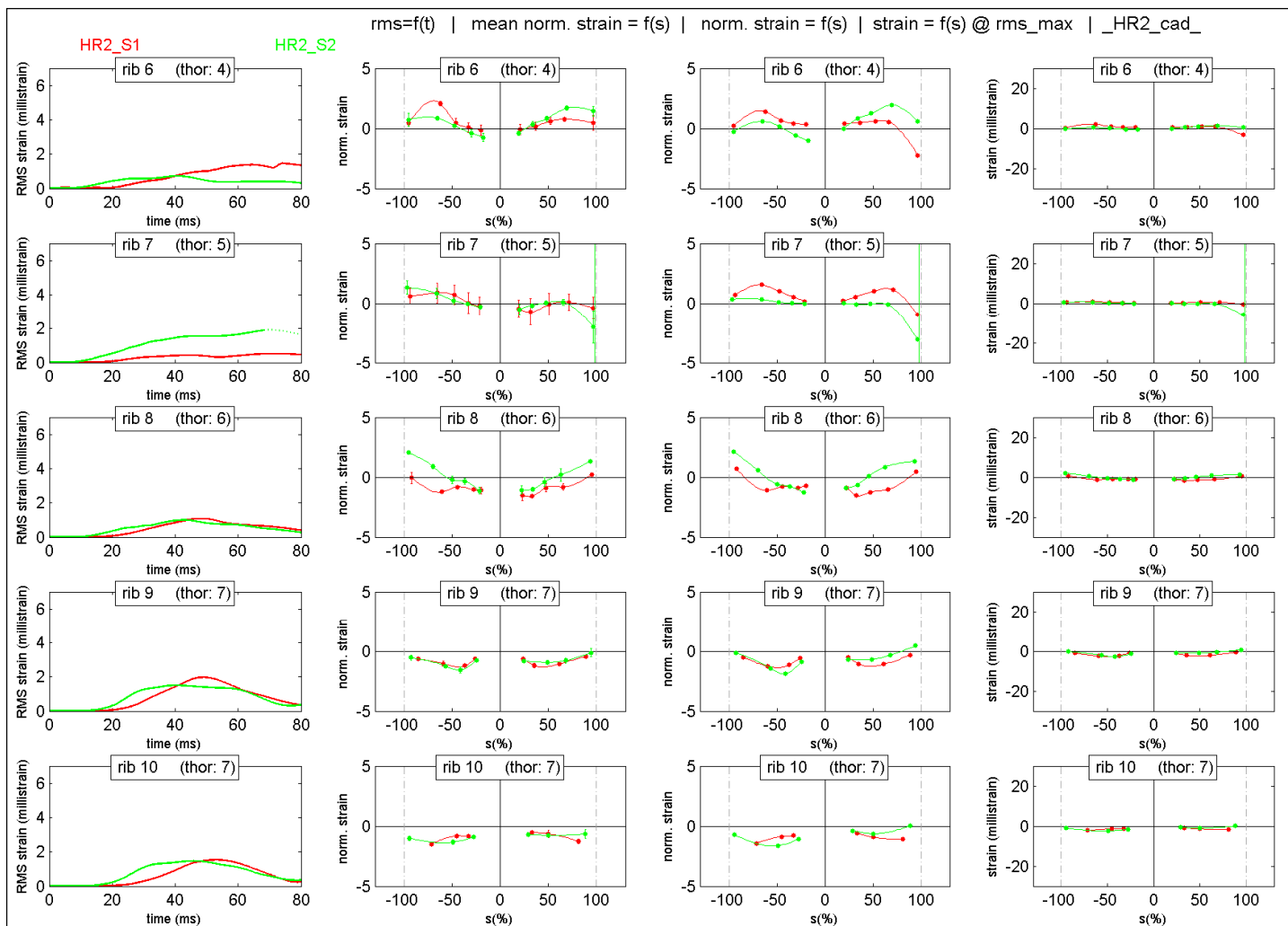


Figure 14 HRN\_1 HRN\_2 Strain pattern Rib 6-10



### **5.5.9 Conclusions on harness loading**

Similarly to belt loading configuration, inertial loading and set up capabilities led to very few injuries.

For both subjects, no rib fracture with displacement was sustained.

Only 3 partial rib fractures were observed with test HRN\_2 and 2 non disjoint fractures in the case of test HRN\_1.

Strain profiles are comparable in between left and right sides.

Upper rib levels are mainly loaded in compression, which relates to a rib arch opening outwards, while rib level from 5 to 8 are loaded in tension, meaning those rib arches are closing inwards. Finally, the last rib levels 9 and 10 are loaded in compression, in a comparable way than rib levels 1 to 4.

Compared to belt loading, strain patterns are symmetrical from left to right side. One can also observe that strain magnitudes are much lower in harness loading than in belt loading.

---

## 6 LAB references

LAB 2002 data set.

Laboratory Reconstructions of Real World Frontal Crash Configurations using the Hybrid III and THOR Dummies and PMHS — Stapp 2002 — Audrey Petitjean, Matthieu Lebarbe, Pascal Potier, Xavier Trosseille.

LAB 2005 data set.

Thoracic Injury Investigation using PMHS in Frontal Airbag Out-of-Position Situations – Stapp 2005 – Matthieu Lebarbé, Pascal Potier and Pascal Baudrit.

LAB 2008 data set.

Rib Cage Strain Pattern as a Function of Chest Loading Configuration – Stapp 2008 – Xavier Trosseille, Pascal Baudrit and Tiphaine Leport.

## 7 Appendices

### 7.1 Appendix: LAB data file organization

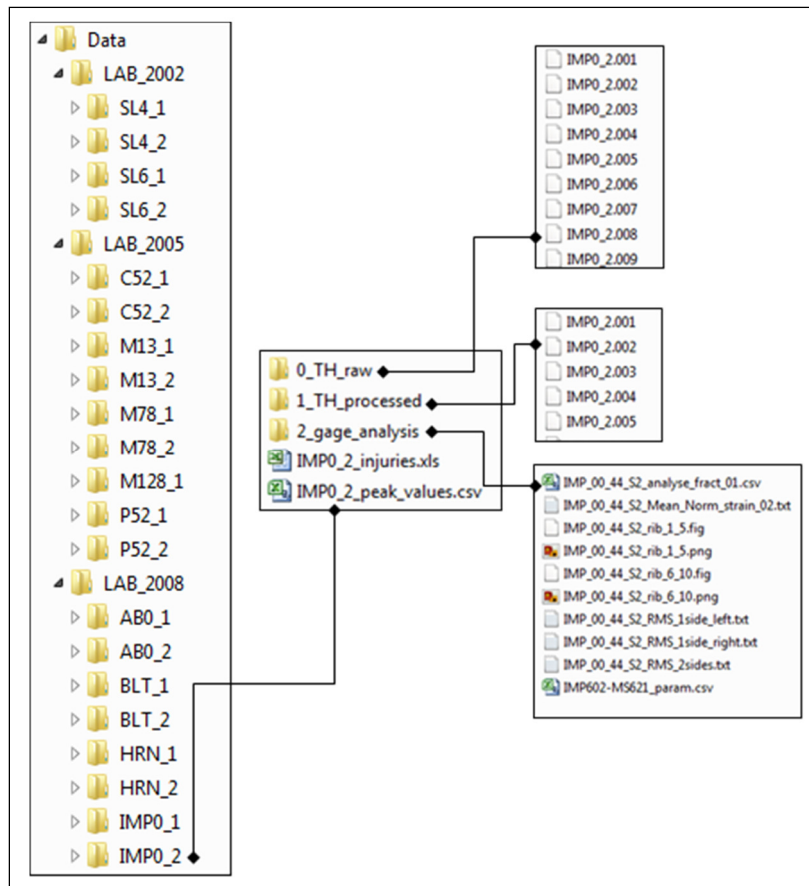
Raw and processed data presented in this document are provided in ascii formats. Each test data is placed in a folder which contains the following sub folder and files:

**Table 62 Result files description**

Name	Description
xxx_injuries.xls	injury details xls files
xxx_peack_values.csv	processed channels peak values
0_TH_raw folder	raw time history iso files
1_TH_processed	sensor processed time history iso files as described in the results section
xxx_Mean_Norm_strain_02.txt	Mean normalized strain profile as well as standard error, RMS and profile peak values
xxx_rib_x_x.png**	Gage analysis figure as shown in results section
xxx_RMS.txt	RMS time history for each rib level, computed on the whole rib level as well as for right and left side separately
xxx_param.csv	Gage and fracture location and type as well as time fracture

\* Where xxx refers to the test reference.

\*\* In case those analysis should be edited, .fig matlab files are also provided.



## 7.2 Appendix: LAB setup and sensor drawings

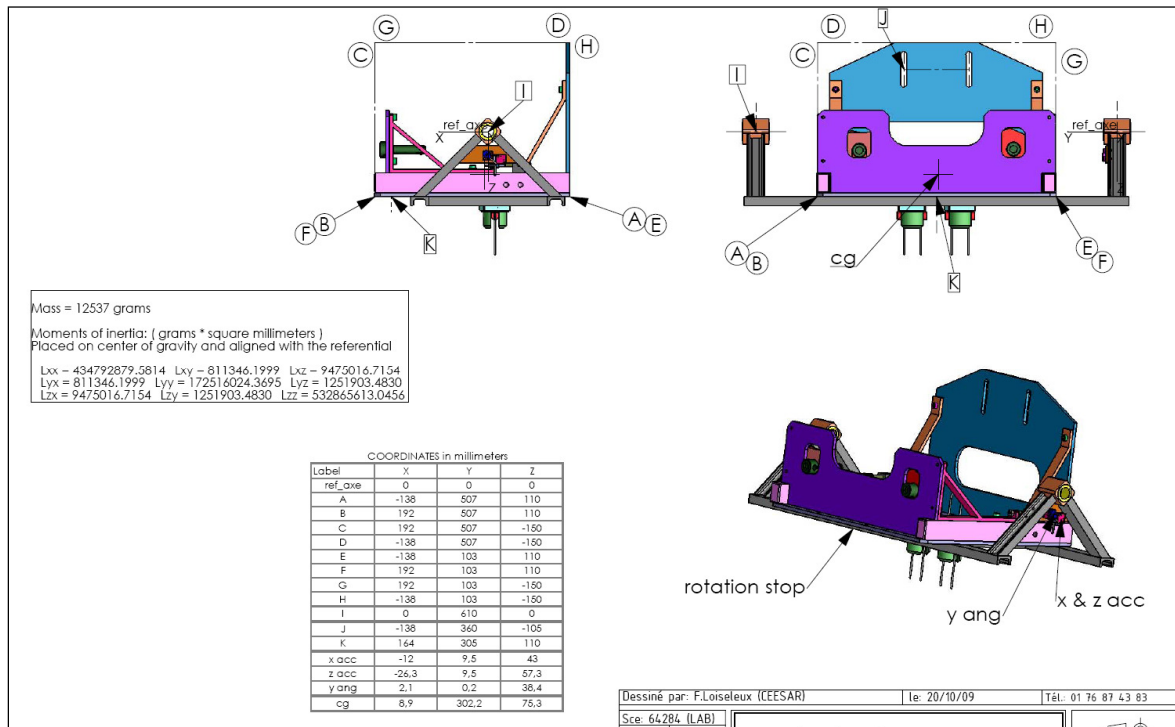


Figure 15 Rigid seat description (AB0\_1 AB0\_2 BLT\_1 BLT2 HRN\_1 HRN\_2)

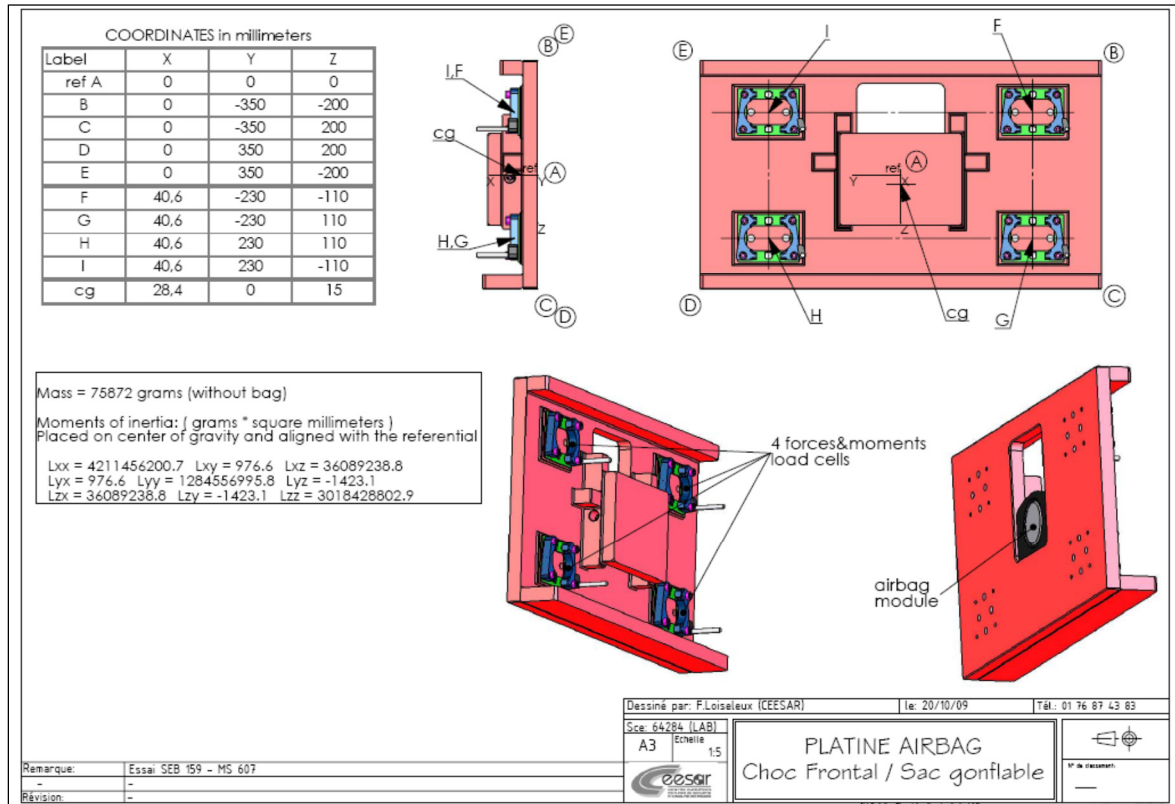


Figure 16 Airbag support plate (AB0\_1 AB02)

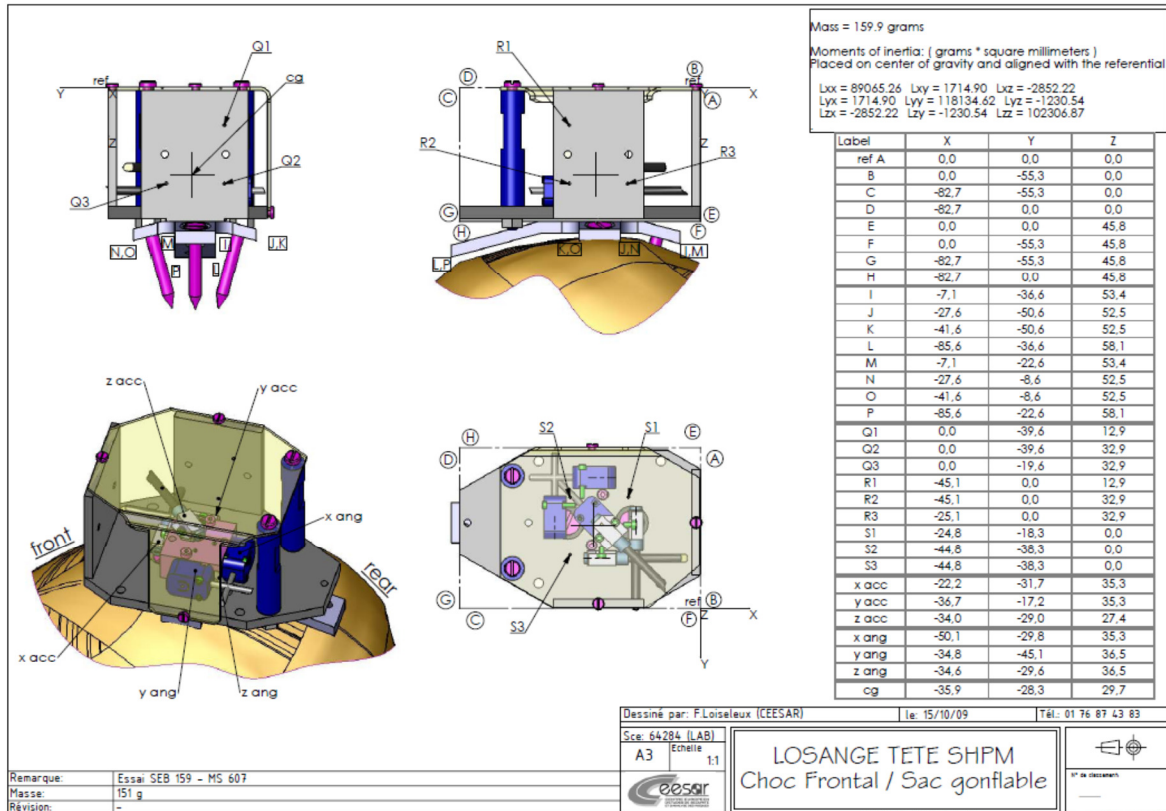


Figure 17 skullcap box and fixing plate

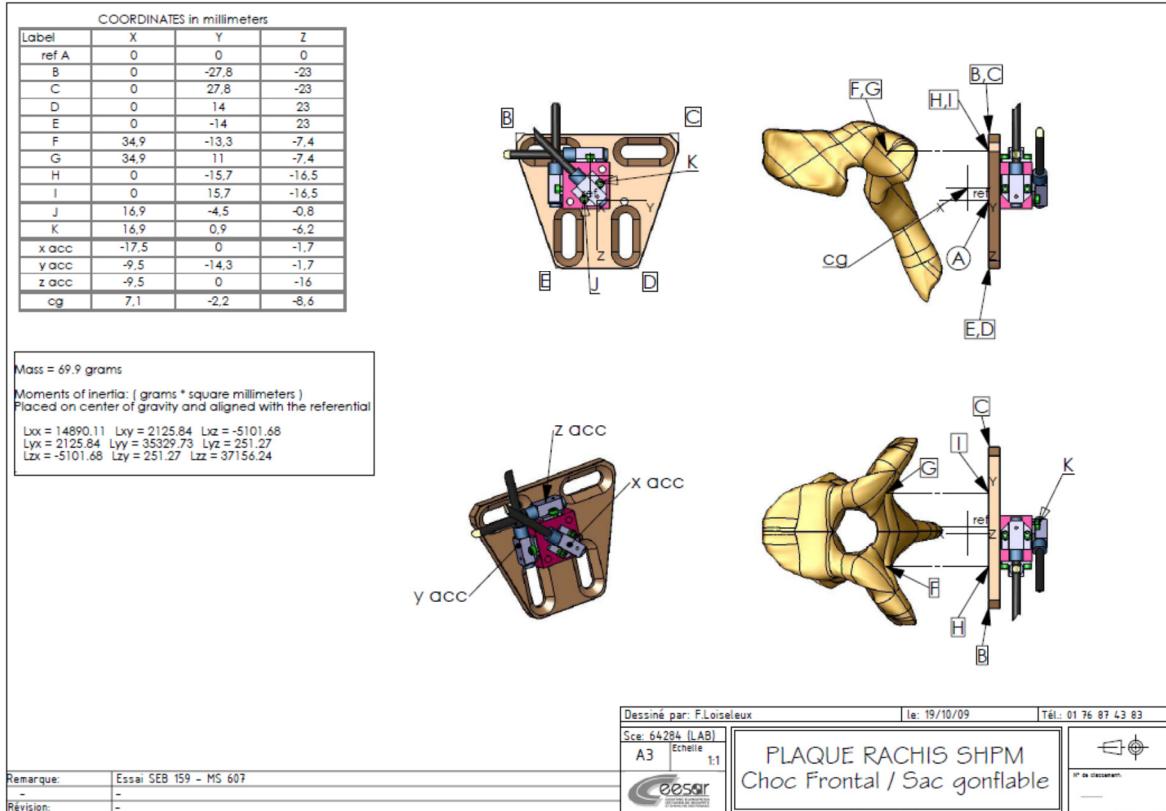


Figure 18 Vertebrae fixing plate

---

## Part B

### 1 Introduction

#### 1.1 Background

Around 42,500 people were killed and about 1.7 million injured in European road accidents in 2007 (CARE, 2009). Frontal collisions are one of the most frequent collision types that lead to injuries as well as fatalities. Thorax has become the most commonly injured (MAIS 2+) body region in frontal impacts. To reduce thorax injuries the performance of vehicle protective systems, for example seat belts and airbags, will have to be improved. Crash test dummies are intended to be used in the evaluation of restraints. The frontal crash test dummy has been evolving from its predecessors since the early 1950s (Andréasson and Bäckström, 2000). Currently the most common frontal dummy is the Hybrid III. The crash test dummy THOR is a more advanced frontal crash test dummy and is expected to replace the Hybrid III in the near future.

Until recently the shoulder complex, including the scapula and the clavicle bone, has received rather low priority in the development of frontal crash test dummies. Although the shoulders are rarely exposed to injuries in life-threatening frontal and oblique frontal collisions (Frampton et al. 1997), they influence the belt interaction with the torso (Adomeit et al. 1977), in particular when a three-point safety belt is used. A comparison of the thoracic response of belted dummies and cadavers suggested that well over half of the belt force is directed through the shoulder rather than through the sternum (Kent et al. 2003). Hence the shoulder response influences the chest deformation in frontal collisions and in oblique and small overlap collisions and may also, depending on belt-to-shoulder interaction, influence the head kinematics. Both the chest deformation and the head kinematics are important since these highly influence the risk of injuries to the chest and to the brain and face.

#### 1.1 Belt to shoulder interaction – Implications for dummy shoulder design

Shaw et al. (2004) reported that the shoulder belt on THOR Alpha dummy slipped laterally off the shoulder in frontal sled tests. A knob mounted on distal end of the clavicle under both bib and jacket was used in later tests and was found to be an effective method to prevent the belt from slipping laterally off the shoulder.

Törnvall et al. (2005a) compared frontal impact dummy kinematics with PMHS test data from sled tests with near-side and far-side belt geometries at 15°, 30°, and 45° angles in standard seats using 3-point belts. The authors found that a THOR Alpha dummy escaped from the shoulder belt in the 45° far side oblique impact, while the PMHSs did not. It was suggested that the dummy shoulder design, its motion and the soft lumbar spine contributed to this. In a static frontal impact loading test (Törnvall et al., 2005b) it was found that volunteers have much larger shoulder range-of-motion than the THOR Alpha dummy. Based on the sled tests and volunteer test data, a new dummy shoulder complex, upper arm, bib and jacket were designed to be mounted to the THOR-NT spine (Törnvall et al., 2007). This shoulder design, denoted SD-1, has a more human-like shaped clavicle, acromion and coracoid process; it had a greater shoulder range-of-motion in the forward-to-upward direction than the THOR-NT shoulder. New PMHS tests were carried out with the emphasis to study shoulder kinematics and belt interaction in laboratory settings by Törnvall et al. (2008). In this study three PMHS were exposed to 30° near-side, full frontal and 45° far-side tests. Also a Hybrid III, a THOR-NT and a THOR-NT with SD-1 were tested. The tests confirmed that the Hybrid III and the THOR-NT did not engage with the belt properly and indicated that the SD1-shoulder did engage properly with the belt in 45° far-side oblique impacts during the on-loading phase.

---

Shaw et al. (2004) suggested that the upper arm prevents excessive lateral belt slippage during a frontal collision by moving forward and upward with respect to the clavicle. Törnvall et al. (2008) hypothesised that the geometrical properties of the clavicle and coracoid process, as well as the shoulder rotations, posterior range-of-motion and stiffness may all affect the risk of belt slip.

### **1.2 Belt-to-clavicle interaction – Implications on dummy design**

In a study by Shaw et al. (2004) the clavicle in a THOR-NT was reversed. The study showed increased x-axis thorax deflection as indicated by the upper right CRUX measurements. This was considered as a more PMHS like response and suggested that the clavicle initial position is important when chest injury risk is to be predicted.

In the THOR-NT dummy evaluation report by Crandall et al. (2007), a “shoulder shielding” hypothesis was proposed as a condition in which the geometry of the shoulder and clavicle results in the belt producing high normal loads on these structures and relatively lower normal loads on the upper chest of the THOR-NT. In a continuation of this evaluation, using the THOR-NT with the SD-1 shoulder, the biofidelity was compared to PMHS tests, which commonly are referred to as the Gold Standard tests series. The initial position and forward displacement of the clavicle affected the upper chest deflection and as such confirmed the “shoulder shielding” hypothesis. In these gold standard tests, Crandall et al., (2008a, b) showed that the belted shoulder of PMHSs moved backward with respect to T8, while the THOR-NT shoulder moved forward.

### **1.3 Need for shoulder response data for evaluation of models of humans**

The shoulder of the THOR-NT may be shielding the upper chest from belt loads and can often invalidate injury risk predictions and prevent the development of advanced restraint systems. Based on this, and the observations presented in the introduction section, there is room for improvements to the shoulder-complex design of the THOR-NT dummy. In order for this future shoulder to be human-like, data that describe the shoulder in different types of frontal crashes are required.

In the field of biomedical research, shoulder kinematics during humeral elevation has been well documented since the 1990s (van der Helm et al. 1995, Meskers et al. 1998, Sahara et al. 2007, Ludewig et al. 2009) using photo markers glued on the skin, 3D electro-magnetic tracking systems, insertion pins into the bone of volunteers, and 3D MRI scanner techniques. Sahare et al. (2007) used the latter technique to study shoulder range-of-motion when seven male volunteers abducted their arm actively. The studied positions ranged from 0° to maximum at 30° interval. Clavicular and acromio-clavicular joint rotations were presented. In a study by Ludewig et al. (2009) transcortical pins, allowing for electromagnetic motion sensors to be rigidly fixed to the bones, were used in twelve subjects to study clavicle, scapula, and humerus motions while raising and lowering the arm in the sagittal plane, scapular plane, and the coronal plane. In the study, the scapular plane abduction was defined as a plane 40° anterior to the coronal plane of the trunk. The subjects were instructed to both raise and lower arm at low velocity (duration of 3s for each of the motions). Clavicular, scapular, and humeral motions were described relative to the thorax with use of the Cardan and Euler angles.

In the field of biomedical research, shoulder range-of-motion was studied by asking volunteers to move their shoulders in various directions while recording motions. Values presented were from non-loaded shoulders and under quasi-static conditions. However, in crashes the shoulder complexes are influenced by belt forces and by forces due to the deceleration of the arms. These loads will force the shoulder into more extreme positions as compared to the non-loaded volunteer tests.

---

In a study by Törnvall et al. (2005a) static forces to the shoulder complex of volunteers were introduced through the arms. The volunteers were seated in a Volvo S80 seat, restrained by a lap belt and a sternum support device, and both arms were pulled up to 400 N (200 N/shoulder) at 50 N intervals in three directions, namely 0°, 45° and 80° relative to the horizontal. A photo marker was applied to the volunteer at the posterior tip of the right acromion process. The movement during these tests was recorded by cameras that were positioned perpendicularly: one from above and the other from the right hand side. The resulting shoulder displacements were given according to a room fixed coordinate system (Törnvall et al. 2005a) and relative to T1 (Törnvall, 2008). However, in that study the loads were applied in the front-upward direction only and shoulder displacements were poorly isolated from torso and spine bending.

Other studies have exposed PMHSs to simulated car crashes and by some means assessed the shoulder complex interaction with restraints and their motions. As part of the Frontal Impact Dummy (FID) Project PMHS sled tests at 30 km/h and 50 km/h were undertaken to investigate shoulder kinematics. Resultant accelerations of the acromion and humerus were reported and proposed as dummy evaluation parameters (Veziin 2002a and 2002b and Veziin et al. 2002c). One limitation of these parameters is that these resultant accelerations are not sufficient to determine the level of biofidelity of a mechanical or mathematical model of a human. In addition, humerus angular displacement relative to the sled and shoulder relative to T1 displacements, or similar, are needed. Unfortunately, this data could not be derived since film/data have not been made public.

Törnvall et al. (2008) carried out 0° full frontal, 45° far-side and 30° near-side sled tests at 26 km/h with three PMHS restrained by a three point shoulder-lap belt and a foot rest using a rigid seat. Film analysis provided three dimensional displacements of photo markers that were rigidly attached to the right and left acromion, T1 and head. Belt loads and body accelerations were also recorded, but unfortunately chest deformation could not be provided.

The University of Virginia conducted a series of PMHS sled tests to study the response of average size males in frontal crashes restrained by a shoulder belt, a lap belt and knee block (Crandall, 2008, Ash 2012a). Instrumentation was comprehensive and enabled the extraction of acromion, spine, head and chest 6-D displacements using video analysis. In a number of publications chest compression and head, spine and acromion kinematics were provided (Shaw et al. 2009a and 2009 b, Ash et al. 2012b, Lessley et al. 2012 and Crandall et al. 2012). This data will be very useful for validation of future crash test dummies and human body models and will enable proper evaluation of shoulder complex kinematics, belt interaction and chest deformation of the complete model.

Unfortunately, evaluations of the shoulder complex kinematics require that crash tests are to be carried out, using an identical test setup as that used in the PMHS test. In addition, for proper evaluation of the shoulder response of a crash test dummy, or the human body model, the torso kinematics and belt slip along the shoulder should be very close to that of the tested PMHSs. Such tests are time consuming, introduce a number of uncertainties and may be difficult to perform in some laboratories. In addition, it is questionable if PMHS can be used to study the shoulder complex response since there is a lack of muscle tone and the scapula is attached to the chest and spine mainly through muscles. This suggests that additional shoulder complex response data that is easy to reproduce and that is generated using volunteers is made available.

During a frontal impact, the belted shoulder of an occupant is under the combined load which consists of seatbelt loads acting downward and rearward and forward and upward loads that arise from the inertia of the arm. Possibly these conditions can be mimicked in laboratory settings.

---

## 2 Aims

The purpose of this study is to establish volunteer shoulder complex response data in a test environment that can be reproduced easily using crash test dummies and human body models. The latter implies that the shoulder response should be isolated from the motion of the torso and spine.

---

### 3 Method

The test work described in this report was carried out at Chalmers University of Technology.

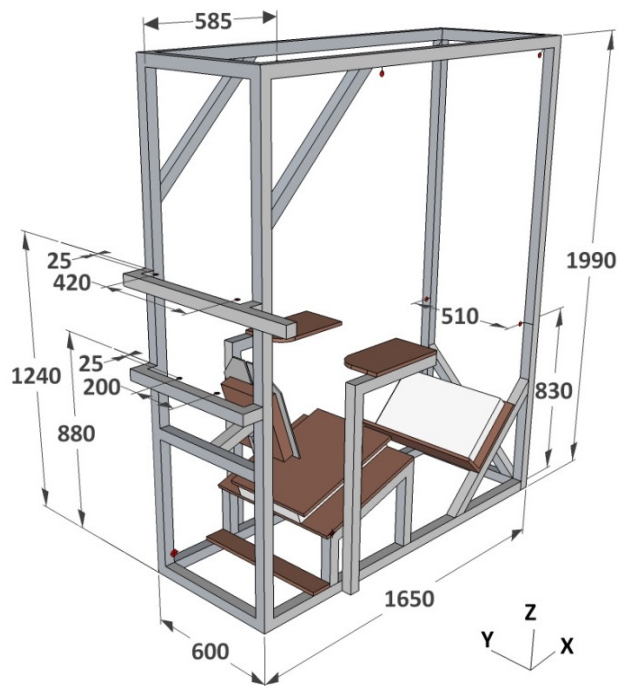
In brief, six male volunteers were seated in a rigid seat that simulated a driving posture in a specially designed test rig. Forward and upward pulling loads to the shoulders were applied through the arms by means of arm brackets fastened to the elbows. Rearward pulling loads were applied by means of straps that encircled the shoulder complex. Torso movements were prevented by restraining the volunteers with two X-shoulder belts guided close to the neck to avoid unwarranted interaction with the clavicle. Armrest supports held the arms in the direction of the applied loads. Both shoulders were statically loaded with increasing loads from 0 – 200 N/shoulder at 50 N/shoulder increments. The volunteer was subjected to four loading angles: shoulders pulled straight forward, angled forward-upward, upward, and rearward. Each volunteer was exposed to three tests per series. Three cameras were used to record shoulder, spine and head positions.

#### 3.1 Test rig

The basis of the range-of-motion study was a test device designed to fit average size male persons (Figure 3-1). It consists of a rectangular frame made from 45 × 45 mm aluminum profiles. To this frame a seat, a footrest, armrests, restraints, and loading systems were attached (Figure 3-1).

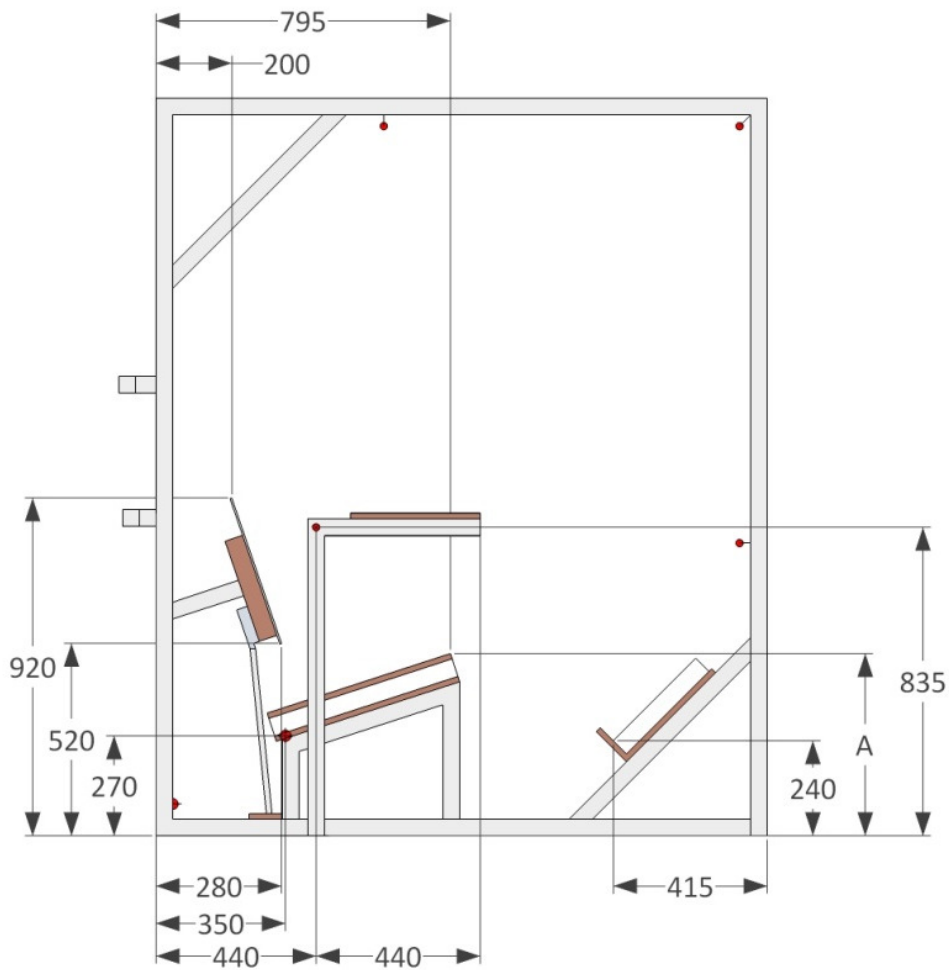


Figure 3-1: Test rig when used to evaluate shoulder range-of-motion of a THORAX dummy.



**Figure 3-2: Schematic of test rig; positions of the belt anchorage points and where the ropes, used to load the shoulders, were rerouted.**

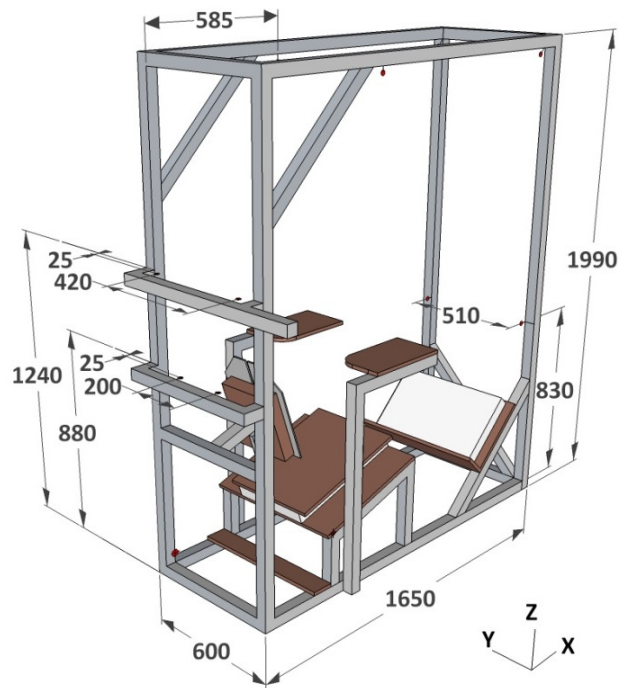
Seat dimensions were adopted from the R16 seat (United Nations, 1958) however the seat back covered 400 mm height of the back and was constructed from fibre reinforced polyester using a torso surface contour that resembles a seated 50 percentile male (Schneider et al., 1983). The seat back was attached to the base with a low friction linkage system and supported at the rear by a load cell (Figure 3-6). The resulting mid-sagittal plane seat back angle was approximately  $17^\circ$  for the segment between L1 and T8 vertebrae. In addition, the top left and right corners of the seatback were cut out to avoid scapula interaction (Figure 3-6); cut-outs in the mid-sagittal plane facilitated the installation of photo markers along the spine. The seat cushion and the footrest, angled  $18^\circ$  and  $45^\circ$ , respectively, were rigid. Comfort foam, 12 mm, covered the seat cushion surface. The seat cushion height was adjusted so that all volunteers had their clavicle bone at the same height. The arm rests were made of plywood; they were adjusted in height and angle to provide arm support (Figure 3-4).



**Figure 3-3: Schematic of test rig; Test rig dimensions, side view (mm). External dimensions were 1740 x 690 x 1990 mm (L x W x H)**

The restraint system consisted of a lap belt and two diagonal belts (crossed) with fixed anchorage points. The lap belt anchorage points were located at the base of the test rig frame (Figure 3-3). During the tests these were tightened until there was a minimum pelvis-to-belt play without being painful. The anchorage points for the diagonal belts were arranged

so that the belt applied loads to the chest and only slightly to the proximal end of the clavicle



bones (

Figure 3-2 and Figure 3-6). Each diagonal belt was attached to a load cell which was attached to a rope system that allowed for application of diagonal belt loads.

The test rig was designed so that shoulder loads could be applied in virtually any direction in the sagittal plane. In this study the shoulders were pulled straight forward, forward-upwards, upwards, and rearward. These directions are referred to as 0°, 45°, 80° and 180° series for which the angle is relative the horizontal plane (Figure 3-4). For the first three directions, loads were applied via arm brackets attached to the arms (Figure 3-5). For the 180°, loads were applied via straps encircling the shoulder complexes (Figure 3-5). Thin ropes were connected to the brackets/straps and guided through four low-friction roller-bearing fitted pulleys to the rear of the test rig where weights were applied.



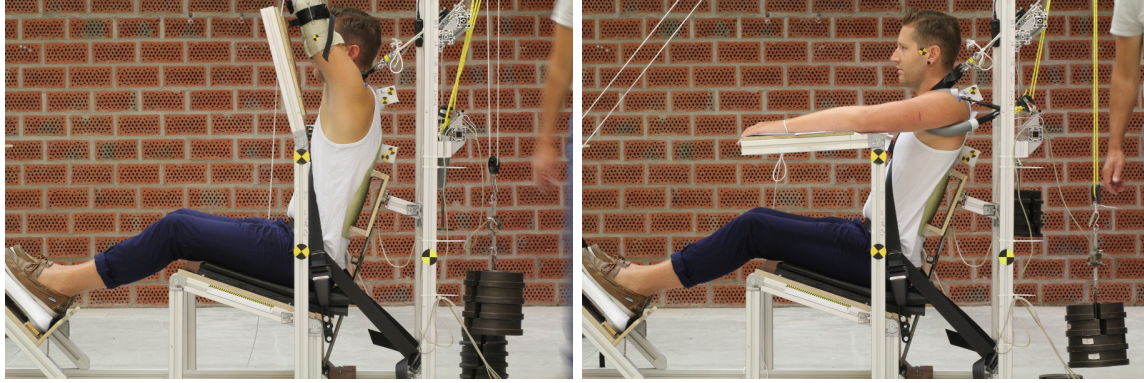


**Figure 3-4: Direction of load applied in the study and armrest positions. Top left: 0° series; top right: 45° series; bottom left: 80° series; bottom right: 180° series.**

The arm brackets, made of Plexiglas, were fitted two straps each to secure to the arm (Figure 3-5). The arm bracket fixed the elbow at a 45° angle to allow for rope attachments without inducing bending of the brackets and to ensure minimum bicep and tricep muscle activity. This angle also allows the loading point to be in line with the humerus. The shoulder straps, a 20 mm wide band covered by ethylene tubing, had a diameter of 35 mm. Arm rest friction was reduced by application of a thin layer of dry Teflon spray to the surfaces and to papers that were introduced between the arms and the surfaces.

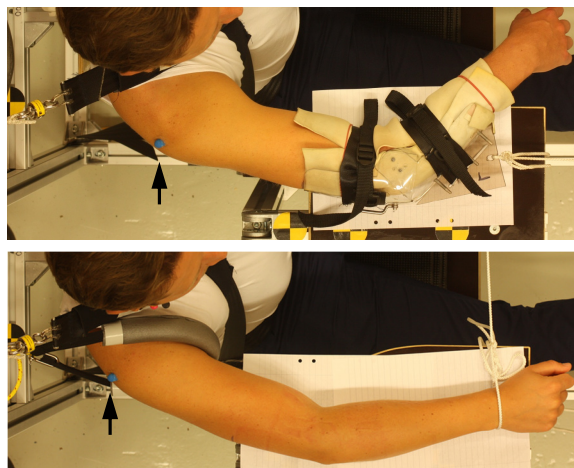


**Figure 3-5: Load application system e.g. arm bracket (top) and shoulder strap (bottom). Position of shoulder photo marker (marked with an arrow).**

### 3.2 Instrumentation

Photo markers were mounted to the volunteers' skin; multiple markers on the head, clavicle, chest, hands, T1 and T4 (Figure 3-6). On the posterior tip of acromion process a marker was mounted after the bone was located via palpation. This was done when the volunteer was seated and had his arms on top of the armrest. In addition, photo markers were mounted to the sides of the test rig at a distance of 0,345 m from the test rig centre line.

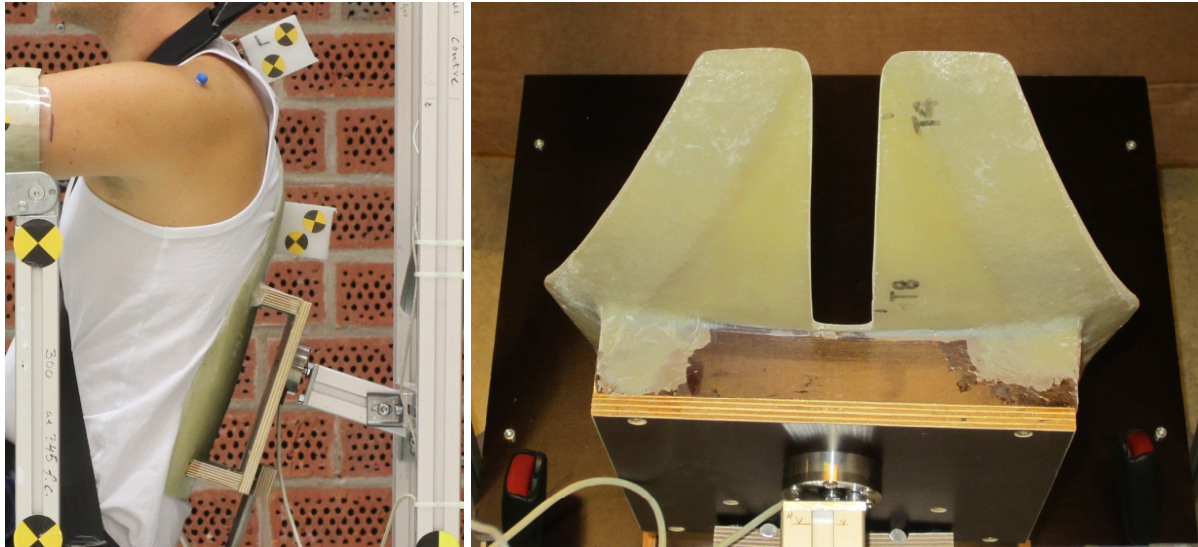


**Figure 3-6: Photo of photo marker mounts and seat back.**

The position of the shoulder complex was recorded by digital cameras using long lenses to reduce distortion of the captured images. The cameras were positioned perpendicularly: one from above (Canon EOS 450D with a 50 mm lens, film plane to reference distance 2,53 m, Figure 3-7) and the other from the right (Canon Power Shot S70 with lens adjusted to 100 mm, film plane to reference distance 3,87 m) and left hand side (Canon EOS 550D with 85 mm lens, film plane to reference distance 6,94 m).

Belt, seat back and applied loads were recorded in these tests to enable a comparison between dummy position and reactions as compared to those of volunteers. Two load cells that measure tension loads (Futek, LCM300) were connected to the upper end of the diagonal belts. A third tension/compression load cell (Burster 8424-6010) measured the forces normal to the seat back pane. A fourth load cell measured the load applied to the ropes that were attached to either the arm brackets or the shoulder straps.

A measurement system (Brick, GMBH Engineering, Inc.) was used to measure the loads. Sampling frequency was 200 Hz using an anti-alias filter cut-off frequency of 50 Hz. All load signals were adjusted to zero offset before storage.



**Figure 3-7: Top camera view.**

---

### 3.3 Volunteers

The Regional Ethical Review Board in Gothenburg granted the ethical permission, application number 322-10, for this study. The volunteers were insured by Chartis Europé AS, insurance number 0004440719.

Male volunteers with an average stature of  $1.81 \pm 0.07$  m, weight of  $79 \pm 5$  kg and age of  $42 \pm 13$  years with no record of shoulder injury were selected for the study (Table 3-1). The volunteers were fit; on average the volunteers did some type of fitness activity about 3 times a week.

**Table 3-1: Volunteer age, stature, weight, fitness, sitting height, and biacromial shoulder width.**

Volunteer	Age [yrs]	Stature [m]	Weight [kg]	Fitness level [times exercises per week]	Sitting height [m]	Biacromial shoulder width [m]	Dimension A in Figure 3-3 [m]
1	59	1.78	83	2-3	0.93	0.41	0.469
2	50	1.73	70	1	0.89	0.38	0.507
3	29	1.92	82	> 3	0.97	0.39	0.442
4	33	1.86	82	2-3	0.96	0.43	0.442
5	50	1.82	82	> 3	0.94	0.38	0.457
6	29	1.77	77	1	0.93	0.38	0.472

### 3.4 Test procedure

The volunteer was dressed in a cotton sleeveless shirt. The seat cushion height and armrest positions were adjusted to allow the proximal end of the clavicle to be at a given height. Then the photo markers were mounted. Finally, the volunteer was belted, arm brackets mounted and attached to the loading ropes.

The measurement system was started to record loads. A total of 20 kg was added to the system of ropes that were connected to the two diagonal belts. Then these ropes were clamped and the weights removed. Thereafter the shoulders were loaded to by 200 N/shoulder with increments of 50 N/shoulder. Photos of the event were taken after seatbelt loads were applied and after each shoulder load increment. This measurement and the load applications were repeated three times for each series.

To assess the effect of the initial upper arm position, the acromion was palpated and positions were recorded when the upper arm was forward and resting in the lap.

### 3.5 Data processing

A single coordinate system was defined and used in this study (Figure 3-1). Film analysis was carried out using TEMA version 3.5-012 (Image systems AB). The right and left acromion processes relative to T1 displacements were used to calculate the shoulder range-of-motion in three directions.

Range-of-motion is a function of initial position. Inconsistency in initial position was compensated when the total forward-rearward acromion range of motion did not match the sum of those obtained in tests  $0^\circ$  and  $180^\circ$ . Preferred initial positions for all six tests, in  $0^\circ$  and

180° series, were compared and the acromion relative to T1 displacements were compensated to account for inconsistency in initial position.

Six volunteers were tested three times each under identical conditions. For each condition the acromion process relative to T1 displacement response corridors was established using average  $\pm$  one standard deviation (S.D.) of all tests for a given condition. Here S.D.s were calculated for all volunteers for each test condition (n=18).

An analysis of variance was used to calculate separate coefficients of variation (C.V.) for repeatability and inter-subject variability. The C.V.<sub>Repeatability</sub> and C.V.<sub>Inter-subject</sub> for a parameter,  $y$ , which are measures of pooled estimates of standard deviation ( $S_p$ ) and standard deviation between volunteers ( $\tau$ ), respectively, expressed as a percentage of the average peak value ( $\bar{X}_g$ ), are defined below;  $S_g$  is the standard deviation for the averages of the results for each volunteer.

$$C.V._{\text{Repeatability}} = \left[ \frac{S_p}{\bar{X}_g} \right] * 100\%$$

$$s_g^2 = \sum_{t=1}^k \frac{(\bar{y}_t - \bar{y})^2}{k-1}$$

$$C.V._{\text{Intersubject}} = \left[ \frac{\tau}{\bar{X}_g} \right] * 100\%$$

$$\tau^2 = s_g^2 - \frac{S_p^2}{k}$$

$$\bar{X}_g = \sum_{t=1}^k \sum_{i=1}^{n_t} \frac{y_{ti}}{N}$$

where  $t$  is the  $t^{\text{th}}$  to  $k^{\text{th}}$  test subject

$i$  is the  $i^{\text{th}}$  to the  $n^{\text{th}}$  test with the  $t^{\text{th}}$  subject

$$s_p^2 = \sum_{t=1}^k \sum_{i=1}^{n_t} \frac{(y_{ti} - \bar{y}_t)^2}{N-k}$$

$N$  is the total number of tests.

## 4 Results

### 4.1 Belt and seat back loads and directions of the applied shoulder loads

The applied shoulder load directions varied slightly between the subjects due to anatomical differences and preferred shoulder trajectory (Table 4-1). For the 0° series, the rope pulled the elbows slightly downward. However, the armrest restricted the downward motions. For the 45° series, the angle was slightly smaller but also here the armrest restricted the arm forward motion; the resulting arm trajectory was approximately 45°. For the 80° series, the armrest did not sufficiently support the arms. Here the arms were pulled in an angle of approximately 72°. For the 180° series, the shoulder straps and ropes were such that the shoulders on average were pulled upward by 3° relative horizontal (Table 4-1).

**Table 4-1: Loading angles for each volunteer and for the studied test series.**

Volunteer	Direction of applied load relative horizontal [°]				Direction of applied load in the horizontal plane relative forward [°]	
	0° series	45° series	80° series	180° series	0° series (pulling outward)	180° series (pulling inward)
1	-2	43	75	179	2	9
2	-3	41	71	174	3	13
3	-3	44	69	178	2	12
4	-3	41	73	179	3	14
5	-2	40	72	175	2	14
6	-2	41	71	177	4	13

The average belt load for each volunteer when no shoulder loads were applied and when the shoulder load was increased varied in-between volunteers (Figure 4-1). The average belt loads were rather consistent for zero shoulder loads. When shoulder loads were applied the changes in belt loads appear to be a function of the loading conditions (Table 4-3). Higher initial belt load commonly resulted in elevated belt loads at maximum shoulder loads (Figure 4-1). However, the variation in belt loads between volunteers (Table 4-3) and within each volunteer (Table 4-2) were considerable. Similar can be concluded for the seat back loads (Table 4-4).

**Table 4-2: Average and S.D. one side belt loads for each volunteer at maximum shoulder load (three test for each volunteer for the 0°, 45°, 180° series and one test for each volunteer for the 80° series).**

Volunteer	0° series		45° series		80° series	180° series	
	Average [N]	S.D. [N]	Average [N]	S.D. [N]	Average [N]	Average [N]	S.D. [N]
1	132	14	131	8	75	15	1
2	162	20	170	3	128	28	9
3	142	7	134	10	89	8	2
4	191	12	162	8	86	9	1
5	147	18	156	7	84	11	4
6	161	1	158	3	123	33	32

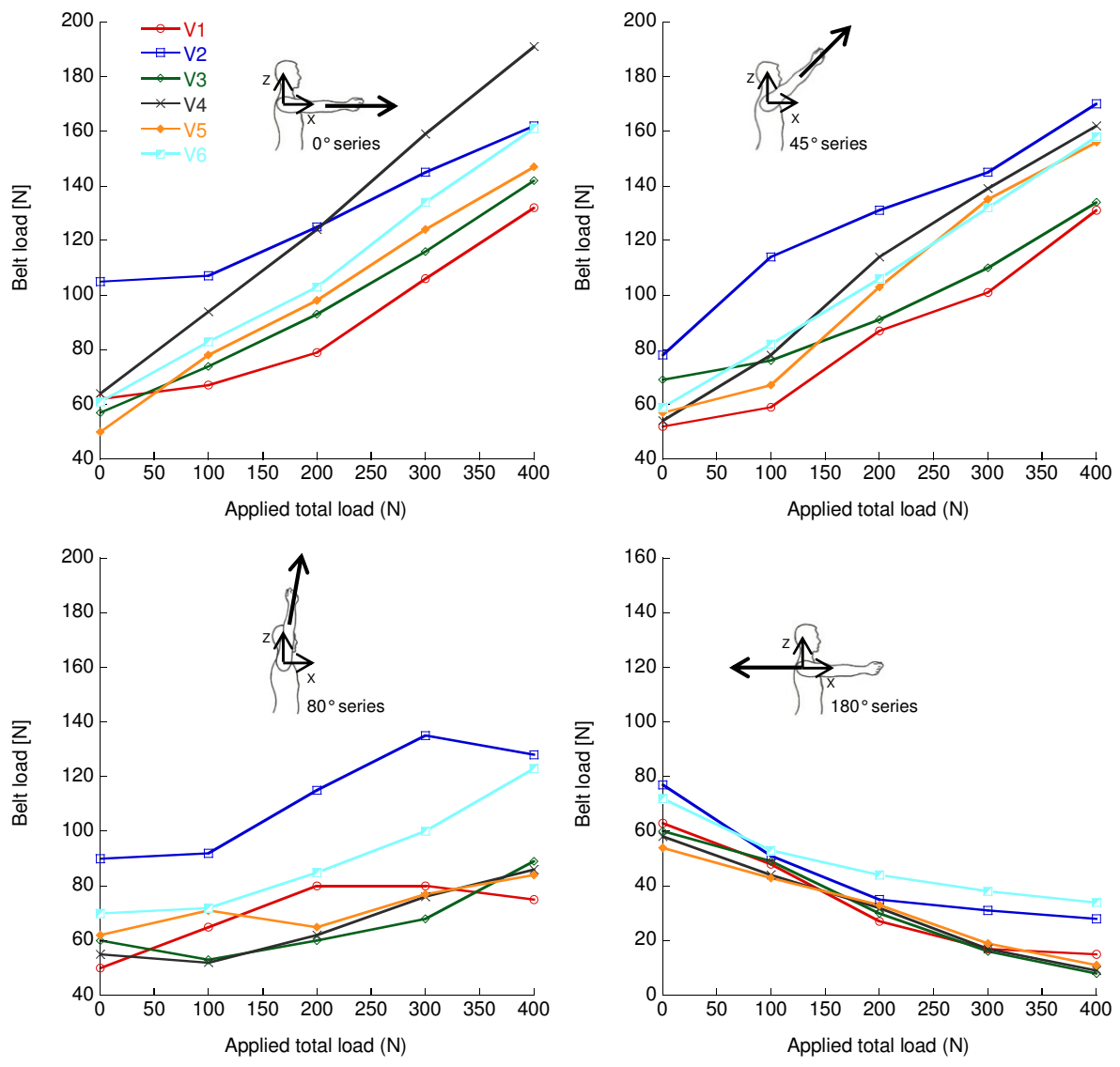


**Figure 4-1: Average right belt loads for each volunteer in the 0°, 45°, 80° series and 180° (three tests for each volunteer).**

**Table 4-3: Average and S.D. of right belt loads for each load increment (six volunteers, three tests each for the 0°, 45° and 180° series and one test each for the 80° series).**

Shoulder load [N]	0° series		45° series		80° series		180° series	
	Average [N]	S.D. [N]						
0	66	22	61	10	65	14	64	10
50	84	17	79	19	68	15	48	11
100	104	20	105	15	78	21	33	14
150	131	21	127	17	89	25	23	15
200	156	22	152	16	98	22	17	15

**Table 4-4: Average and S.D. seat back loads for each load increment (six volunteers, three tests each for the 0°, 45° and 180° series and one test each for the 80° series).**

Shoulder load [N]	0° series		45° series		80° series		180° series	
	Average [N]	S.D. [N]	Average [N]	S.D. [N]	Average [N]	S.D. [N]	Average [N]	S.D. [N]
0	377	34	451	30	496	53	395	28
50	338	51	383	44	407	50	458	46
100	284	55	327	60	366	42	540	67
150	239	64	279	63	332	54	624	83
200	202	72	232	71	309	62	706	106

## 4.2 Shift of torso angle

When loads were applied to the shoulders, either through the arm brackets or the shoulder straps, the seat flexed slightly and the volunteers curved or straightened their backs somewhat. Average torso angle change at maximum load, as compared to torso angle at zero loads and as measured between the T1 and T8 skin photo markers, was 3° for the 0° series. For the 45°, 80° and 180° series corresponding rotations were 2° forward rotation, 2° rearward rotation and 5° rearward rotation, respectively. Individual variation was present; the corresponding rotations varied from 0° to 7° in the 18 tests included in the 0° series.

For the 0° series, the T1 skin photo marker rotated forward on average 2° for a total shoulder load increase of 400 N. For the same load increase the T1 skin photo marker rotated rearward by 2° in the 45° and 180° series and rearward by 7° in the 80° series. Individual differences were rather large for the T1 skin photo marker.

## 4.3 Shift in position of the acromion at zero shoulder load

When the volunteers moved their arms from resting in the lap to resting on top of the armrest the preferred acromion position relative to T1 was shifted. When the armrest was set for the 0° and 180° series the following shifts were measured:

- Volunteer 1: Acromion moved 7 mm rearward and 25 mm upward (unrestrained)
- Volunteer 2: Acromion moved 10 mm rearward and 10 mm upward (unrestrained)
- Volunteer 3: No information
- Volunteer 4: Acromion moved 13 mm rearward and 49 mm upward (restrained)
- Volunteer 5: Acromion moved 7 mm rearward and 40 mm upward (restrained)
- Volunteer 6: Acromion moved 0 mm rearward and 25 mm upward (unrestrained)

When the armrest was set for the 45° series these acromion relative to T1 shifts were on average 26 mm rearward and 1 mm downward from the position preferred in the 0° series. Note that these shifts were recorded for restrained volunteers. Adjusting for the 80° series, these shifts were on average 24 mm rearward and 7 mm downward from the 45° series.

Tensing the belts made the volunteers move slightly into the seat. It also resulted in an acromion relative to T1 rearward motion that was rather small; less than 7 mm for all volunteers.

These changes in acromion relative to T1 positions may be used when assessing models of the human. Depending on the model to be assessed a compensation of the range-of-motions, as provided in this study, may have to be carried out. The results presented below have been compensated neither for the change in acromion relative to T1 distances due to elevation of the arm prior to application of shoulder loads, nor for acromion relative to T1 motion due to belt tensioning.

The preferred initial acromion relative to T1 positions were expected to be identical in the 0° and 180° series. However, for the restrained subjects and when the pulling ropes were attached, the acromion was in relation to T1 on average 16 mm further forward and 4 mm further above the initial position in the 0° series than the 180° series. The individual differences in preferred initial acromion relative to T1 positions were in general small but varied considerably between volunteers (Table 4-5). These differences appear, from an analysis of photos of seated volunteers without attached arm brackets and shoulder straps, to have arisen from posture shifts in either of the series or in both (Table 4-5). These differences in preferred initial positions may be caused by the order in which the tests were carried out; the 0° series was the first series whereas the 180° series was the final series to be performed. The differences observed could also be due to anticipation of the tests, to the influence of the arm brackets for the 0° series or the straps that encircle the shoulder complexes for the 180° series. Regardless of the reasons for these variations, the measured differences in preferred initial positions in the 0° and 180° series were used to compensate the ranges-of-motion. A single starting position in the x – z plane was used for each volunteer in all six tests; three repeated 0° series tests and three 180° series tests. For the 45° and 80° series no such compensations were carried out.

**Table 4-5: Initial average (n=3) acromion relative to T1 position differences between the 0° or 180° series (for positive values the preferred position was forward and above in the 0° series compared with the 180° series) and how these differences arose.**

Volunteer	x-direction (mm)	z-direction (mm)	Observations
1	15	10	Moved forward prior to the 0° series
2	40	6	Moved forward 20 mm prior to the 0° series, moved rearward 20 mm prior to the 180° series
3	-9	2	Moved rearward prior to the 0° series
4	6	6	Moved forward 6 mm prior to the 0° series
5	31	3	Moved forward 20 mm prior to the 0° series, moved rearward 11 mm prior to the 180° series
6	10	-1	Moved rearward prior to the 180° series

#### 4.4 Range-of-motion

When loading the volunteers' shoulders, in any of the four directions, 0°, 45°, 80° and 180°, the range-of-motions were a combination of anterior/posterior, medial and superior acromion relative to T1 displacements. The anterior/posterior and superior range-of-motions were dominant for all loading directions. For this reason these motions are presented prior to the medial motions.

The test 0° and 45° series show the greatest volunteer ranges-of-motion in the anterior/posterior direction followed by 180° series (Figure 4-2 and Figure 4-3). Both the 0° and 180° series showed small medial (Table 4-6) and superior range-of-motions. The 45° series also showed large ranges-of-motion in the superior direction; almost as large as in the anterior direction. The 80° series shows the largest superior range-of-motion and, despite the guidance by arm supports, large variability in the anterior direction. The range-of-motion increased slightly when initial acromion rel. T1 positions were compensated for (Figure 4-2 and Figure 4-3). The most apparent changes that the initial position compensation introduced were the spread in initial position at zero shoulder load and that the final range-of-motion at maximum shoulder load appeared to be more consistent for each volunteer.

Figure 4-2 and Figure 4-3 show that there were individual differences in the resistance to shoulder relative to T1 motions. Volunteer V3 appear to produce smaller such motions than the average volunteer did for all four loading conditions; although differences were small. Volunteer V2 produced smaller shoulder motions when loads were applied in the forward direction and the shoulder trajectory was more upward-rearward oriented for the other loading direction. The opposite appear to be the case for volunteer V4. This volunteer produced large forward shoulder motions for the 0° and 45° series, more forward motions but less upward motions than any of the other volunteers in the 80° series, and only average shoulder motions for the 180° series.

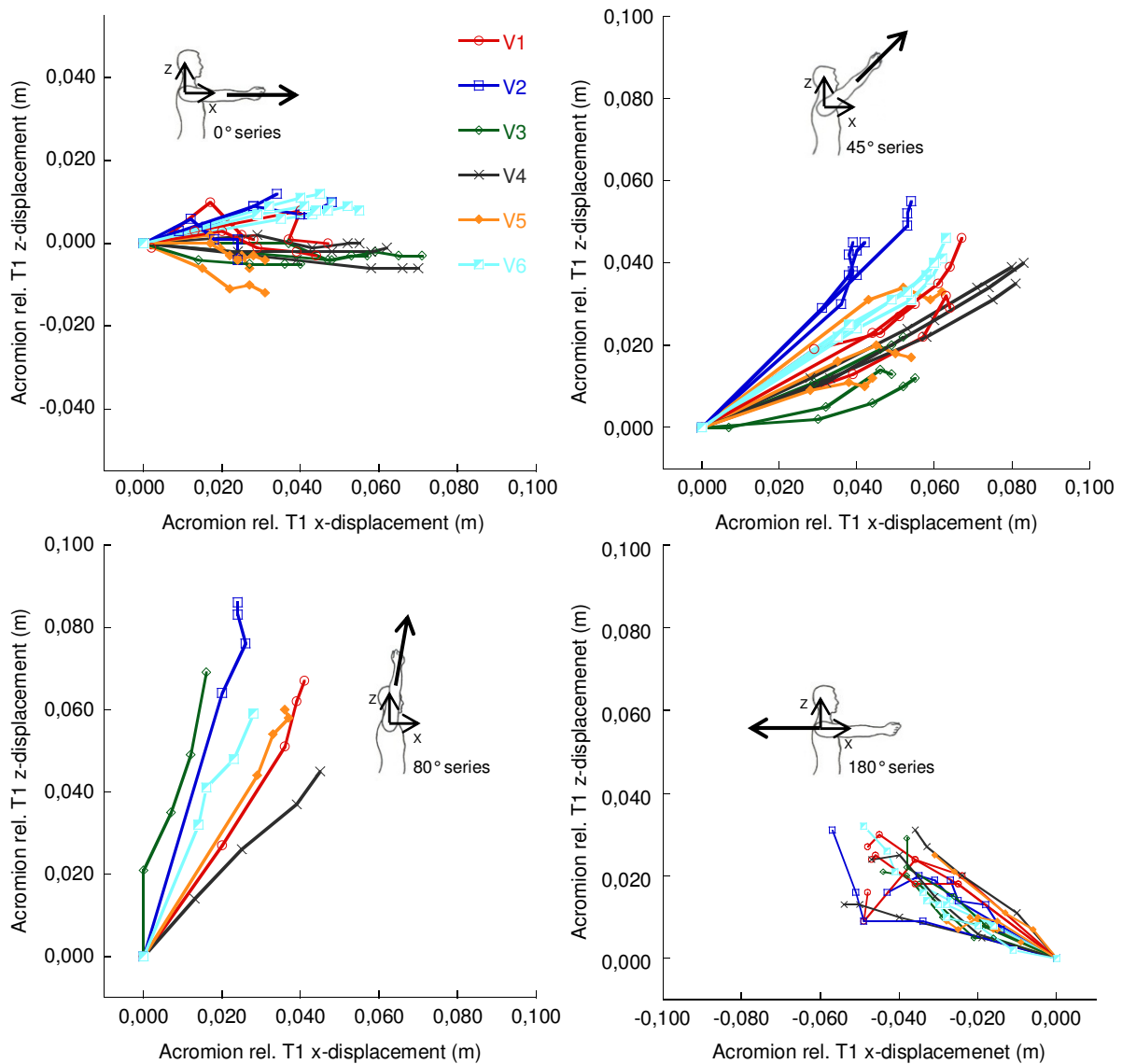


**Figure 4-2: Individual volunteer acromion relative to T1 x- and z-displacements for the included series. Data were not compensated for shift in initial acromion rel. T1 position. Values in origin correspond to zero shoulder loads. Successive points correspond to shoulder load increments of 50 N/shoulder.**

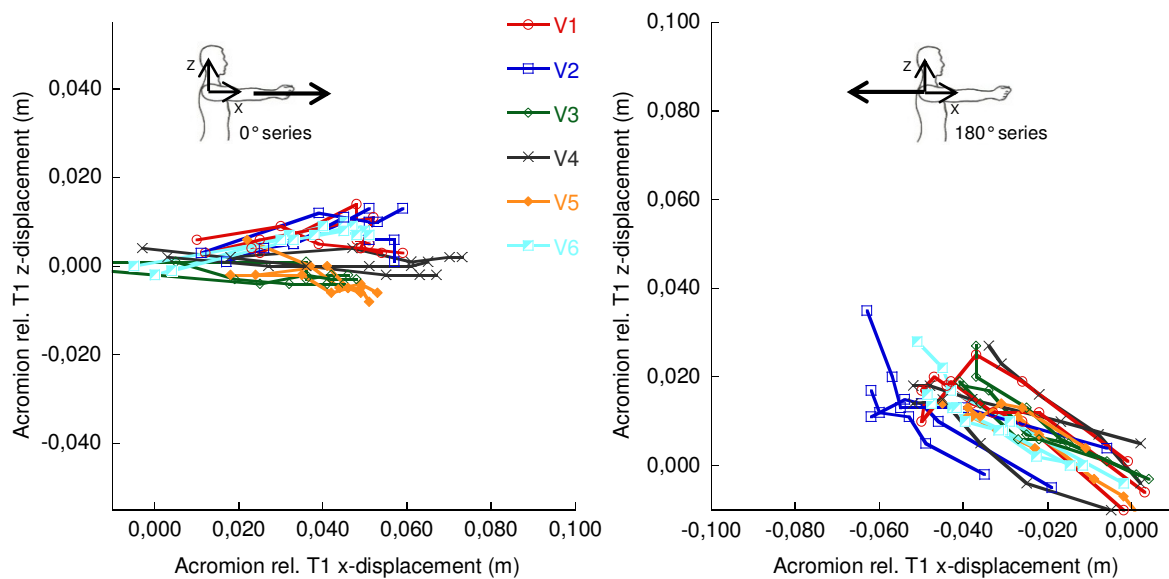


**Figure 4-3: Individual volunteer acromion relative to T1 x- and z-displacements for the 0° and 180° series. Data were compensated for shift in initial acromion rel. T1 position.**

Average and S.D. compensated acromion relative to T1 x-displacement was  $54 \pm 8$  mm for the 0° series,  $59 \pm 13$  mm for the 45° series,  $32 \pm 11$  mm for the 80° series and  $-47 \pm 10$  mm for the 180° series at maximum shoulder load (200 N/shoulder, Table 4-6). The associated z-displacements were  $2 \pm 6$  mm for 0° series,  $33 \pm 13$  mm for the 45° series,  $64 \pm 13$  mm for the 80° series and  $18 \pm 6$  mm for the 180° series.

**Table 4-6: Average and S.D. compensated acromion relative to T1 displacements [mm] as a function of applied total shoulder load.**

Force [N]	0° series						45° series						80° series						180° series					
	x		y*		z		x		y*		z		x		y*		z		x		y*		z	
	Ave.	S.D.	Ave.	S.D.	Ave.	S.D.	Ave.	S.D.	Ave.	S.D.	Ave.	S.D.	Ave.	S.D.	Ave.	S.D.	Ave.	S.D.	Ave.	S.D.	Ave.	S.D.	Ave.	S.D.
100	33	8	2	2	3	5	33	8	-1	4	18	10	16	10	2	2	34	18	-25	12	-1	4	7	6
200	44	8	1	2	3	6	49	8	-2	6	26	11	24	11	1	2	47	17	-35	11	-2	6	12	6
300	50	8	0	3	3	6	56	11	-4	5	31	12	29	11	0	3	56	16	-43	10	-4	5	15	5
400	54	8	-1	3	2	6	59	13	-6	5	33	13	32	11	-1	3	64	14	-47	10	-6	5	18	6
n	6 volunteers, 3 tests each						6 volunteers, 3 tests each						6 volunteers, 1 tests each						6 volunteers, 3 tests each					

\* Negative displacements were in the medial direction.

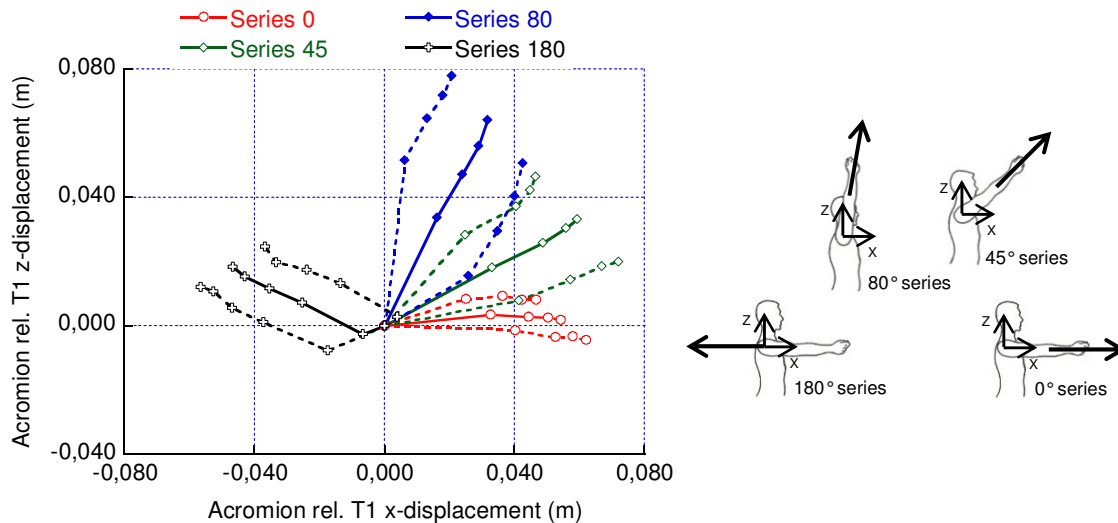


**Figure 4-4: Average ± S.D. volunteer acromion relative to T1 x- and z-displacements. Data were compensated for shift in initial acromion rel. T1 position.**

#### 4.5 Stiffness

The stiffness was calculated as the load build up per resultant displacement acromion relative to T1 displacement. The average stiffness was slightly higher in the rear direction than in the forward direction (Table 4-7). There was less resistance to upward motion than to horizontal motion of the shoulder.

**Table 4-7: Average and S.D. volunteer shoulder stiffness.**

Load [N]	0° series		45° series		80° series		180° series	
	Average [N/mm]	S.D. [N/mm]						
50	1,5	0,4	1,3	1,4	1,3	1,5	1,8	1,4
100	2,2	0,4	1,8	0,4	1,9	2,0	2,7	2,0
150	3,0	0,4	2,3	0,5	2,3	1,0	3,3	0,9
200	3,7	0,5	2,9	0,6	2,7	1,1	4,0	0,9

#### 4.6 Repeatability

The tests with volunteers provided measurements with reasonable repeatability; repeatability C.V. for resultant acromion relative to T1 ranged from 6 to 13%. The C.V. for inter-subject variability was slightly higher than the repeatability (Table 3-1)

---

Table 4-8).

---

**Table 4-8: C.V.<sub>Repeatability</sub> and C.V.<sub>Intersubject</sub> for acromion relative to T1 resultant displacement at maximum load.**

	<b>0° series</b>	<b>45° series</b>	<b>80° series</b>	<b>180° series</b>
C.V. <sub>Repeatability</sub> [%]	6	11	13	12
C.V. <sub>Intersubject</sub> [%]	14	18	n.a.	17
No. of repeated tests for each volunteer	3	3	1	3
No. of volunteers	6	6	6	6

---

## 5 Discussion

### 5.1 Range-of-motion

The range-of-motion of the shoulder, assessed as acromion relative to T1 displacement, has been studied for non-injurious loads applied to the shoulder via arm brackets or straps encircling the shoulder complex. The largest absolute range-of-motion was for loading applied upward for a seated volunteer: on average 70 mm for a load of 200 N/shoulder.

This study differs from many others on shoulder range-of-motion because loads were applied to joint complexes. It provided larger ranges-of-motion than if voluntary posture changes had been recorded.

Törnvall et al. [2] also applied loads to the arms in their study of shoulder complex range-of-motion. For the same arm load they reported larger acromion relative to T1 displacements. One reason for the differences could be attributed to the age of the volunteers. In this study the volunteers were on average 10 years older than in their study. Another more important differences lies in the boundary conditions.

One subject exhibited larger range-of-motions compared to the other five volunteers. This could be observed for all loading directions.

### 5.2 Isolation of volunteer shoulder complex responses

In this study, the volunteers did not curve their spines excessively forward or rearward when loads were applied to the shoulder complex. This was in contrast to other studies [2] that also loaded the shoulder complex for the study of forced shoulder range-of-motion. Hence, shoulder complex motion was successfully isolated and the results reflect almost pure shoulder motion relative to the spine. As such the data is suitable for dummy and HBM evaluations.

### 5.3 Usefulness of the data provided

The loads applied to the shoulder complex in this study of shoulder complex range-of-motion were quasi static and lower than those commonly seen in frontal crashes. However, the shoulder is highly mobile and its response to loads are largely dependent on muscle characteristics. As such studies using volunteers may be more suitable as compared to tests with PMHSs despite the fact that low loads must be used for volunteers.

Joints used in crash test dummies are not usually rate dependent; their responses are non-linear. For human body models rate dependency is commonly included in the model of joints, however joints are frequently modelled linear. For these reasons some additional analysis may be required when the data presented in this report are to be used for crash test dummy and human body model evaluations.

### 5.4 Stiffness

The average stiffness of the shoulder complex was estimated as the load divided by the resultant displacement of the acromion relative to T1. The stiffness increased when higher loads were applied. For 50 N/shoulder the shoulder complex produced a stiffness of approximately 1.5 N/mm whereas for 200 N/shoulder the stiffness ranged from 3 to 4 N/mm. The higher stiffness was measured in the 0° and 180° series. This finding may be due the design of the shoulder complex; the shoulder move rather freely in the plane tangential to the exterior surface of the upper right and left region of the ribcage. However, in the 0° and 180° series the loads applied to the shoulders are somewhat normal to this plane. This could partly explain the difference in stiffness between the 0° and 180° series on one hand and the 45° and 80° series in which the applied load was more vertical.

---

## 5.5 Repeatability

The repeatability and inter-subject variability was fair; CV at maximum shoulder load ranged from 6% to 13% for an average volunteer. The reason for this probably originates from variation in the initial position of the shoulder relative to the T1. However, the preferred initial starting position of the acromion process varied only slightly between the four load conditions.

Inter-subject variability was, as expected larger than variation for each volunteer; it ranged from 14% to 18%. A reason for this variation between subjects may be the difference in past physical activities. One of the volunteers had, for a prolonged period on a regular basis, trained front-crawl which loosened his shoulder complex. This volunteer had on average a range-of-motion on average 125% of the average for all volunteers in the 0° and 45° series. Differences were smaller for the other two series. Another volunteer exhibited only 60% of the average range-of-motion in the 180° series.

## 5.6 Sources of error

The main source of error in this study arose from differences in preferred shoulder posture. An attempt to compensate for this was developed and used for the 0° and 180° series. Shifts in preferred initial position of the acromion relative to T1 have been determined; they can be used for the 45 and 80° series to assess human body models or crash test dummy performance.

The belts applied some load to the proximal end of the clavicle bone, which may have influenced the forward displacements of the acromion relative to the T1. This effect was judged to be minor because the belt did not change its curvature near the clavicle bone.

The data presented here are not normalised. Possibly the inter-subject variation could be reduced by normalisation methods, based on acromion-to-acromion distance.

Ranges-of-motion were assessed by using photo markers on the skin of the volunteers. This induces some uncertainty since the markers can move relative to the bony landmarks of interest. This uncertainty is considered small because all of the volunteers were fit, and no loads were introduced to the skin near the photo marker. Previous studies have shown that skin markers are accurate enough for this type of study [13].

---

## **6 Conclusions**

### **6.1 Range-of-motion**

The range-of-motion of the shoulder, assessed as the acromion relative to the T1, was studied for non-injurious loads that were applied to the shoulder via arm brackets or straps that encircled the shoulder complex. The largest absolute range-of-motion was observed when the loading was applied upward for a seated volunteer; on average 70 mm for a load of 200 N/shoulder.

### **6.2 Repeatability**

The repeatability and inter-subject variability, assessed by using a coefficient of variation, was satisfactory. The reason for the limited repeatability is likely to have originated from variation in the initial position of the shoulder relative to the T1.

### **6.3 Stiffness**

The average stiffness of the shoulder complex, when subjected to loads of 150-200 N/shoulder was approximately the same in all directions tested. The shoulder complex was slightly more flexible, when exposed to upward loads for a seated volunteer, than for forward, forward-upward and rearward loads. These stiffness values can be used in developing mathematical models of the human that take rate dependency and nonlinearity into account.

---

## 7 References

- Adomeit, D., Goegler, H. and Vu Han, V., Expected belt-specific injury patterns dependent on the angle of impact, 3rd International Conference on Impact Trauma, Berlin, Germany, International Research Council on Biokinetics of Impacts, Bron, France, 1977.
- Andréasson, R. and Bäckström, C.-G. (2000) Bilbältet – Svenskt utvecklingsarbete för global bilsäkerhet, ISBN: 91-630-9388-X, Kulturvårdskommittén, Vattenfall, Stockholm, Sweden
- Ash J. H., Shaw C. G., Lessley D. J., Crandall J. R. (2012a) PMHS restraint and support surface forces in simulated frontal crashes, Japanese Society of Automotive Engineering Annual Congress, Yokohama, Japan, 2012, 64-2012522.
- Ash J. H., Lessley D. J., Forman J. L., Zhang Q., Shaw C. G., Crandall J. R. (2012b) Whole-Body Kinematics: Response Corridors for Restrained PMHS in Frontal Impacts, International IRCOBI Conference on the Biomechanics of Impacts, Dublin, Ireland, IRC-12-21, pp. 142-154.
- Crandall J, Lessley D, Shaw G, Ash J, Displacement response of the spine in restrained PMHS during frontal impacts, Japanese Society of Automotive Engineering Annual Congress, Yokohama, Japan, 2012.
- CARE (2009)
- Carroll J., Adolph T., Chauvel C., Labrousse M., Trosseille X., Pastor C., Eggers A., Smith, S. and Hynd D. (2010) Overview of Serious Thorax Injuries in European Frontal Car Crash Accidents and Implications for Crash Test Dummy Development, International IRCOBI Conference on the Biomechanics of Impacts, Hannover, Germany, pp. 217-234.
- Crandall et al. 2007, Anterior Chest Deflection Evaluation THOR NT Advanced Frontal Crash Test Dummy, UVA 1028-1044, NHTSA Biomechanics Test Database, 2007
- Crandall et al. 2008b, ATD Thoracic Response Test Development, UVA1286, 1287, 1289, 1290, 1291, NHTSA Biomechanics Test Database, 2008
- Crandall et al., 2008a, ATD Thoracic Response Test Development, UVA1286, 1289, 1294, 1295, NHTSA Biomechanics Test Database, 2008
- Kent R., Shaw G., Lessley D., Crandall J., Kallieris D. and Svensson M.Y. (2003) Comparison of Belted Hybrid III, THOR, and Cadaver Thoracic Responses in Oblique Frontal and Full Frontal Sled Tests. SAE 2003 World Congress, Detroit, Michigan, USA, Society of Automotive Engineers, Inc., Warrendale, Pennsylvania, USA, SAE No. 2003-01-0160.
- Lessley D., Shaw G., Ash J. Crandall J. (2012) A methodology for assessing intrasegmental kinematics of the whole human spine during impacts, Japanese Society of Automotive Engineering Annual Congress, Yokohama, Japan, 2012.
- Ludewig P. M., Phadke V., Braman J., Hassett D. R., Cieminski C. J., and LaPrade R. E. (2009) The Journal of Bone and Joint Surgery, 91:378-89.
- Meskers C.C.M., Vermeulen H.M., de Groot J.H., van der Helm F.C.T., Rozing P.M. (1998) 3D shoulder position measurements using a six-degree-of-freedom electromagnetic tracking device, Clinical Biomechanics, 12:280-292
- Sahara W., Sugamoto K., Murai M., Yoshikawa H. (2007) Three-Dimensional Clavicular and Acromioclavicular Rotations during Arm Abduction Using Vertically Open MRI, Journal of Orthopaedic Research,

---

Schneider, L. W., Robbins, D. H., Pflüg, M. A. and Snyder, R. G. (1983) Development of Anthropometrically Based Design Specifications for an Advanced Adult Anthropomorphic Dummy Family. Vol. 1, Report UMTRI-83-53-1, U.S. Department of Transportation, National Highway Traffic Safety Administration.

Shaw G. and Lessley D. (2004) Evaluation of the THOR Advanced Frontal Crash Test Dummy, UVA950-957, NHTSA Biomechanics Test Database.

Shaw G., Parent D., Purtsezov S., Lessley D., Kerrigan J., Shin J., Crandall J., Zama Y., Ejima S., Kamiji K, Yasuki T. (2009a) Frontal Impact PMHS Sled Tests for FE Torso Model Development, Proceedings of the 2009 International IRCOBI Conference on the Biomechanics of Impact, September 7-10, York, UK, pp. 341-356.

Shaw G., Parent D., Purtsezov S., Lessley D., Crandall J., Kent R., Guillemot H., Ridella S., Takhouants E. and Martin P. (2009b) Impact response of restrained PMHS in frontal sled tests: skeletal deformation patterns under seat belt loading. 53rd Stapp Car Crash Conference, Savannah, Georgia, USA, 2-4 November, 2009. Paper number 2009-22-0001. Society of Automotive Engineers, Warrendale, PA, USA, pp. 1-48.

Törnvall F. V., Svensson M. Y., Davidsson J., Flogård A., Kallieris D. and Håland, Y. (2005a) Frontal Impact Dummy Kinematics in Oblique Frontal Collisions: Evaluation against Post Mortem Human Subject Test Data, *Traffic Injury Prevention* 6(4) pp. 340-50.

Törnvall F. V., Holmqvist K., Martinsson J. and Davidsson J. (2005b) Comparison of Shoulder Range-of-Motion and Stiffness between Volunteers, Hybrid III and THOR Alpha in Static Frontal Impact Loading, *International Journal of Crashworthiness*, Vol. 10, No. 2, pp. 151-160.

Törnvall F. V., Holmqvist K., Davidsson J., Svensson M. Y., Håland Y. and Öhrn H. (2007) A new THOR Shoulder Design: A Comparison of Shoulder with Volunteers, the Hybrid III and THOR NT. *Traffic Injury Prevention*, 8 (2) pp. 205-215.

Törnvall F. V. (2008) A New Shoulder for the THOR Dummy Intended for Oblique Collisions, PhD dissertation, Chalmers University of Technology, Göteborg, Sweden.

Törnvall F., Holmqvist K., Davidsson J., Svensson M., Gugler J., Steffan H. and Håland Y. (2008) Evaluation of Dummy Shoulder Kinematics in Oblique Frontal Collisions. Proceedings of the 2008 International IRCOBI Conference on the Biomechanics of Impact, September 17-19, Bern, Switzerland, pp. 195-210.

Veziñ P. (2002a) Human Thorax/Shoulder Behaviour during Frontal Impact with Airbag, FID Project, Work Package 2, D5 Part 1.

Veziñ P. (2002b) Human Thorax/Shoulder Behaviour during Frontal Impact without Airbag, FID Project, Work Package 2, D5 Part 2.

Veziñ P., Bruyere-Garnier K., Bermond F. Verriest J.P. (2002) Comparison of Hybrid III, Thor- $\alpha$  and PMHS Response in Frontal Sled Tests, Paper 2002-22-0001, STAPP Car Crash Conference, Vol. 46.

Wu, G., van der Helm, F.C.T., Veeger, H.E.J., Makhsouse, M., van Roy, P., Anglin, C., Nagels, J., Karduna, A., McQuade, K., Wang, X., Werner, F., Buchholz, B. (2005) ISB recommendation on definitions of joint coordinate systems of various joints for the reporting of human joint motion—Part II: shoulder, elbow, wrist and hand. *Journal of Biomechanics* 38.